NASA-TM-109848

AN HP-ADAPTIVE DISCONTINUOUS GALERKIN METHOD FOR HYPERBOLIC CONSERVATION LAWS

NASA
IN-67-TM
13734
140P

by

KIM S. BEY, B.S., M.S.

N94-34208
Unclas
G3/67 0013734

DISSERTATION

Presented to the Faculty of the Graduate School of
The University of Texas at Austin
in Partial Fulfillment
of the Requirements
for the Degree of

DOCTOR OF PHILOSOPHY

(NASA-TM-109848) AN HP ADAPTIVE DISCONTINUOUS GALERKIN METHOD FOR HYPERBOLIC CONSERVATION LAWS Ph.D. Thesis (Texas Univ.) 140 p

THE UNIVERSITY OF TEXAS AT AUSTIN
August 1994

AN HP-ADAPTIVE DISCONTINUOUS GALERKIN METHOD FOR HYPERBOLIC CONSERVATION LAWS

Approved by
Dissertation Committee:

Supervisor: _____

_____

_____

_____

_____

Acknowledgements

I wish to express my sincere gratitude to my advisor, Professor J. Tinsley Oden, for his invaluable guidance throughout this work. He has taught me many things, and this work would not have been possible without his patience and encouragement.

I would also like to thank Professors Eric Becker, Lyle Clark, Linda Hayes, and David Young for serving on my committee and for reviewing the work and the dissertation.

I would like to give special thanks to Mr. Abani Patra, a friend and colleague at TICAM, who generously gave his advice and assistance on implementing the adaptive and parallel strategies used in this work. Both were done in a remarkably short time thanks to his expertise and commitment.

Throughout the work on this dissertation, I have benefited from discussions with many colleagues to whom I express my sincere thanks. These include Professors Bernardo Cockburn, Joseph Flaherty, C. W. Shu, and Leszek Demkowicz, Dr. Mark Ainsworth, Dr. Weihan Wu, Dr. C.Y. Lee, and others.

The support of the NASA Langley Research Center, in particular my branch head Dr. Allan R. Wieting and my former division chief Dr. John B. Malone, is gratefully acknowledged.

Kim S. Bey

PRECEDING PAGE BLANK NOT FILMED

Table of Contents

Acknowledgements iii

List of Tables vi

List of Figures vii

Chapter 1. Introduction 1

1.1 Some Mathematical Preliminaries 3

1.2 Higher-Order Methods 6

1.3 *A Posteriori* Error Estimation and Adaptivity 11

1.4 Scope 12

Chapter 2. The Discontinuous Galerkin Method 15

2.1 A Linear Model Problem 15

2.2 Notation 16

2.3 Weak Formulation 20

2.4 *hp* Finite Element Approximation 26

2.5 *A Priori* Error Estimate 30

2.6 Implementation Issues 33

Chapter 3. *A Posteriori* Error Estimation 36

3.1 Element Residual Method 37

3.2 A Global Lower Bound on the Error 38

3.3 A Global Upper Bound on the Error 39

3.4 A Local Lower Bound on the Error 41

3.5 Approximation of the Local Problems 42

3.6 Remarks Concerning an Alternate Approach 43

Chapter 4. An hp-Adaptive Strategy **45**
4.1 The h-Refinement Step 48
4.2 The p-Enrichment Step 50
4.3 An hp-step as an Alternative to the p-Step 52
4.4 Selection of the Parameters 53

Chapter 5. Numerical Examples **54**
5.1 Example 1 54
5.2 Example 2 69
5.3 Example 3 76
5.4 Example 4 77

Chapter 6. Parallel Implementation **88**
6.1 Domain Decomposition for hp Meshes 89
6.1.1 Recursive Load Based Bisection of Coordinates (RLBBC) . . 90
6.1.2 Recursive Load Based Bisection of an Ordering (RLBBO) . . 92
6.2 Communications 94
6.3 Numerical Results 94

Chapter 7. Extensions to Nonlinear Hyperbolic Conservation Laws **99**
7.1 Discontinuous Galerkin Spatial Approximation 100
7.2 Runge-Kutta Time Discretization 103
7.3 Enforcing the Maximum Principle 107
7.3.1 The Projection $P : Q^p(K) \to Q^1(K)$ 108
7.3.2 The Local Projection $\Pi_K : Q^1(K) \to Q^1(K)$ 109
7.4 Numerical Results for Burger's Equation 112

Chapter 8. Concluding Remarks **120**
8.1 Summary 120
8.2 Conclusions and Future Work 121

Bibliography **124**

Vita **132**

List of Tables

5.1 Example 1 - Error using uniform hp meshes. 56

5.2 Example 1 - Error using quasi-uniform h and uniform p meshes. 56

5.3 Example 1 - Effect of the approximation of the local problem for the lower bound on the effectivity index. 59

5.4 Example 1 - Effect of the approximation of the local problem for the upper bound on the effectivity index. 61

5.5 Example 1 - Error history for an adaptive hp solution. 70

5.6 Example 2 - Error history for an adaptive hp solution starting from a uniform 4×4 mesh, $p = 2$. 70

5.7 Example 2 - Error history for an adaptive hp solution starting with a uniform 8×8 mesh, $p = 1$. 71

5.8 Example 3 - Error estimate obtained by approximating the upper bound local problem in $Q^{p_K+1}(K) \setminus Q^{p_K}(K)$. 78

5.9 Example 3 - Error history for an adaptive hp solution starting from a uniform 8×8 mesh, $p = 1$. 78

5.10 Example 4 - Error history for an adaptive hp solution. 84

6.1 Error history for an hhp-adaptive solution starting from a uniform 8×8 mesh, $p = 1$. 95

7.1 Parameters for the TVBM Runge-Kutta scheme 105

List of Figures

2.1 The affine map of the master element $\hat{K}$ to a typical element $K \in \mathcal{P}_h$. 18

5.1 Quadrilateral element mesh used for quasi-uniform refinements. 55

5.2 Example 1- Rate of convergence of error for fixed p. 57

5.3 Example 1- Rate of convergence of error for fixed h. 58

5.4 Example 1- Rate of convergence of error with number of unknowns. 60

5.5 Example 1 - Rate of convergence of the estimated error with uniform h-refinements. 62

5.6 Example 1 - Rate of convergence of the estimated error with uniform p-enrichments. 63

5.7 Example 1 - Local effectivity index for error estimate based on the upper bound local problem. (8×8 mesh, $p = 1$) 64

5.8 Example 1 - Local effectivity index for error estimate based on the upper bound local problem. (8×8 mesh, $p = 2$) 65

5.9 Example 1 - Local effectivity index for error estimate based on the upper bound local problem. (16×16 mesh, $p = 1$) 65

5.10 Example 1 - Error distribution on initial mesh. 66

5.11 Example 1 - Mesh and error distribution after the h-step. 67

5.12 Example 1 - Mesh and error distribution after the p-step. 68

5.13 Example 2 - Rate of convergence of the error with respect to the total number of unknowns. 72

5.14 Example 2 - Estimated error on initial 8×8 mesh, $p = 1$. 73

5.15 Example 2 - Local effectivity index for error estimate on initial 8×8 mesh, $p = 1$. 73

5.16 Example 2 - Estimated error on h-adapted mesh. 74

5.17 Example 2 - Local effectivity index for error estimate on h-adapted mesh. 74

5.18 Example 2 - Adaptive p-enriched mesh. 75

5.19 Example 2 - Estimated error on adaptive p-enriched mesh. . . . 75

5.20 Example 2 - Local effectivity index on adaptive p-enriched mesh. 76

5.21 Example 3 - Estimated error on initial 8×8 mesh, $p = 1$. 79
5.22 Example 3 - Local effectivity index on initial 8×8 mesh, $p = 1$. 79
5.23 Example 3 - Estimated error on h-adapted mesh. 80
5.24 Example 3 - Local effectivity index on h-adapted mesh. 80
5.25 Example 3 - Final p-adapted mesh. 81
5.26 Example 3 - Estimated error on adaptive p-enriched mesh. . . . 81
5.27 Example 3 - Local effectivity index on adapive p-enriched mesh. 82
5.28 Example 3 - Rate of convergence of the error with respect to the number of unknowns. 82
5.29 Example 4 - Estimated error on initial mesh, $p = 1$. 84
5.30 Example 4 - Local effectivity index on initial mesh, $p = 1$. . . . 85
5.31 Example 4 - Estimated error on h-adapted mesh. 85
5.32 Example 4 -Local effectivity index on h-adapted mesh. 86
5.33 Example 4 - p-adapted mesh. 86
5.34 Example 4 - Estimated error on p-adapted mesh. 87
5.35 Example 4 - Local effectivity index on p-adapted mesh. 87

6.1 Rate of convergence of the error with respect to the total number of unknowns. 96
6.2 Final mesh using the hhp-adaptive strategy. 97
6.3 Parallel speedup for the hp mesh. 98

7.1 Evolution of the exact solution to (7.30). 113
7.2 Discontinuous Galerkin solution to (7.30) at $t = 0.1$. Solutions obtained on an 8×8 mesh of uniform p-elements. 116
7.3 Rate of convergence of the error with h-refinements at $t = 0.1$. . 117
7.4 Rate of convergence of the error with the total number of unknowns at $t = 0.1$. 117
7.5 Discontinuous Galerkin solutions at $t = 0.45$. 118
7.6 Rate of convergence of the error in smooth regions at $t = 0.45$. ($\Omega_s = [-0.2, 0.4] \times [-0.2, 0.4]$) 119

Chapter 1

Introduction

Both the practitioner using computational fluid dynamics in engineering design calculations and the scientist grappling with gaps in the theoretical foundations are aware that much remains to be done before the subject can be put on firm ground. This is particularly true in the theory and numerical analysis of hyperbolic conservation laws, vital in gas dynamics and compressible fluid mechanics and a fundamental component in the resolution of solutions of the Navier-Stokes equations for compressible flow. There the numerical solution of hyperbolic systems is confronted with a list of major difficulties and questions that have been under study for many years.

These include classical problems of numerically resolving shocks and discontinuities, characteristic of solutions of hyperbolic problems, while simultaneously producing high-order, non-oscillatory results near shocks and elsewhere in the solution domain. Moreover, the basic issue of quality of numerical solutions is fundamentally important: how accurate are the numerical simulations and how does one obtain the most accurate results for a fixed computational resource? These questions lie at the core of modern adaptive methods that aim to control the error in the computed solution and to optimize the computational process. In addition, methodologies that attempt to address these issues

cannot be limited to one-dimensional cases; they must be extendable to problems involving realistic geometries, boundary and initial conditions in arbitrary domains in two- and three-dimensions. Finally, there is the issue of computational efficiency. Modern numerical schemes for large-scale applications should be readily parallelizable for implementation in emerging multi-processor architectures.

This dissertation addresses these issues for model classes of hyperbolic conservation laws. The basic approach developed in this work employs a new family of adaptive, *hp*-version, finite element methods based on a special discontinuous Galerkin formulation for hyperbolic problems. The discontinuous Galerkin formulation admits high-order local approximations on domains of quite general geometry, while providing a natural framework for finite element approximations and for theoretical developments. The use of *hp*-versions of the finite element method makes possible exponentially convergent schemes with very high accuracies in certain cases; the use of adaptive *hp*-schemes allows *h*-refinement in regions of low regularity and *p*-enrichment to deliver high accuracy, while keeping problem sizes manageable and dramatically smaller than many conventional approaches. The use of discontinuous Galerkin methods is uncommon in applications, but the methods rest on a reasonable mathematical basis for low-order cases and has local approximation features that can be exploited to produce very efficient schemes, especially in a parallel, multiprocessor environment.

The place of this work is to first and primarily focus on a model class of linear hyperbolic conservation laws for which concrete mathematical results, methodologies, error estimates, convergence criteria, and parallel adap-

tive strategies can be developed, and to then briefly explore some extensions to more general cases. Next, we provide preliminaries to the study and a review of some aspects of the theory of hyperbolic conservation laws. We also provide a review of relevant literature on this subject and on the numerical analysis of these types of problems.

1.1 Some Mathematical Preliminaries

The broad aim of this work is to lay mathematical foundations and to develop new numerical schemes which will aid in understanding and solving general systems of hyperbolic conservation laws of the form

$$\mathbf{U}_{,t} + \mathbf{F}^i(\mathbf{U})_{,x_i} = \mathbf{S}, \mathbf{x} = (x_1, x_2) \in \Omega \subset \Re^d, t > 0 \tag{1.1}$$

where $\mathbf{U}$ is a vector consisting of m components to be conserved in Ω and $\mathbf{S}$ is a vector-valued source term. The flux vectors $\mathbf{F}^i, i = 1, \cdots, d$ are, in general, a nonlinear function of $\mathbf{U}$. The subscript t denotes differentiation with respect to time and the subscripts x_i denote differentiation with respect to the spatial coordinate x_i, and in which summation convention for repeated indices is employed. Alternatively, (1.1) can be written in the quasi-linear form

$$\mathbf{U}_{,t} + \mathbf{A}^i(\mathbf{U})\mathbf{U}_{,x_i} = \mathbf{S} \tag{1.2}$$

where the flux Jacobian matrices

$$\mathbf{A}^i = \frac{\partial \mathbf{F}^i}{\partial \mathbf{U}} \tag{1.3}$$

have real eigenvalues. To complete the initial-boundary value problem, one must specify initial conditions of the form

$$\mathbf{U}(\mathbf{x}, 0) = \mathbf{U}_0(\mathbf{x}) \tag{1.4}$$

and appropriate boundary conditions.

Most of this investigation focuses on a simpler and restricted class of hyperbolic problems for which concrete results can be obtained and for which it is possible to treat some specific numerical issues in more detail than is possible for the general case.

The first difficulty encountered in developing numerical methods for hyperbolic systems of conservation laws in multiple space dimensions is the absence of a general mathematical theory. Hence, many popular numerical schemes for multi-dimensional systems are based on existence and uniqueness results for scalar hyperbolic conservation laws of the form

$$\begin{aligned} u_{,t} + f^i(u)_{,x_i} &= 0 \; ; \quad \mathbf{x} \in \Re^d, \; t > 0 \\ u(\mathbf{x}, 0) &= u_0(\mathbf{x}) \end{aligned} \tag{1.5}$$

where the fluxes f^i, $i = 1, \cdots, d$ are Lipschitz continuous functions of u and the initial data $u_0 \in L^\infty(\Re^d) \cap L^1(\Re^d)$ have compact support.

Historically, existence and uniqueness proofs have relied upon compactness arguments for sequences of solutions generated by the vanishing viscosity method, see Kružkov [32], or low-order finite difference approximations, see Glimm [22] and Crandall and Majda [15]. More recently, uniqueness results have been generalized using the concept of measure-valued solutions (see DiPerna [20]) providing a new tool for convergence proofs for a variety of numerical methods [14], [31]. Here some well-known results for scalar conservation laws are summarized.

Solutions to (1.5) develop discontinuities in finite time, even if the initial data is smooth. Thus, (1.5) must be interpreted in the sense of distributions,

or equivalently, weak solutions are sought which satisfy

$$\int_0^T \int_{\Re^d} \left(u\phi_t + \sum_{i=1}^{d} f^i(u)\phi_{x_i} \right) d\mathbf{x}\ dt + \int_{\Re^d} u_0\ \phi\ d\mathbf{x} = 0 \tag{1.6}$$

for all test functions $\phi \in C^\infty(\Re^d \times [0,T))$ with compact support. There are an infinite number of weak solutions satisfying (1.6) for given initial data u_0; however, the physically relevant solution satisfies an additional constraint, namely an entropy condition. The entropy condition takes into account the fact that physical processes are dissipative and that (1.5) models a physical process in the limit as the dissipation tends to zero. This solution, the so-called entropy solution, satisfies

$$\int_0^T \int_{\Re^d} |u-c|\phi_t + sign(u-c)(f^i(u) - f^i(c))\phi_{x_i} d\mathbf{x}\ dt \geq 0 \tag{1.7}$$

for all nonnegative test functions $\phi \in C_0^\infty(\Re^d \times [0,T))$ and all $c \in \Re$.

The following lemma summarizes some basic properties of solutions to (1.5) or (1.6).

Lemma 1 (Crandall and Majda [15]) *For every choice of initial data $u_0 \in L^\infty(\Re^d) \cap L^1(\Re^d)$, there exists a unique entropy solution $u \in C([0,\infty) : L^1(\Re^d))$ of (1.5) with $u(\mathbf{x},0) = u_0(\mathbf{x})$. Denoting $u(\mathbf{x},t)$ by $E(t)u_0$, we have*

(i) $||E(t)u_0 - E(t)v_0||_{L^1(\Re^d)} \leq ||u_0 - v_0||_{L^1(\Re^d)}$

(ii) $u_0 \leq v_0$ *a.e.* $\rightarrow E(t)u_0 \leq E(t)v_0$ *a.e.*

(iii) $u_0 \in [a,b]$ *a.e.* $\rightarrow E(t)u_0 \in [a,b]$ *a.e.*

(iv) If $u_0 \in BV(\Re^d)$, $t \rightarrow E(t)u_0$ *is Lipschitz continuous into* $L^1(\Re^d)$ *and* $||E(t)u_0||_{BV(\Re^d)} \leq ||u_0||_{BV(\Re^d)}$

The functions in the space $BV(\Re^d) \subset L^1_{loc}(\Re^d)$ have bounded variation and distributional derivatives that are locally measures. The variation of a function $v \in BV(\Re^d)$ for $d = 2$ is defined as

$$\begin{aligned} ||v||_{BV(\Re^2)} &= \sup_{\delta \in \Re \setminus \{0\}} \int_{\Re^2} \frac{|v(x+\delta, y) - v(x,y)|}{|\delta|} dx\ dy \\ &+ \sup_{\delta \in \Re \setminus \{0\}} \int_{\Re^2} \frac{|v(x, y+\delta) - v(x,y)|}{|\delta|} dx\ dy \end{aligned}$$

These results are typical of the mathematical theory that has influenced the development of many numerical schemes over the past decade: they apply to unbounded domains, scalar-valued solutions, and characterize the solutions as among function classes of low regularity. Our goal is to consider problems in bounded domains with specific inflow conditions, since these are the types of problems encountered in realistic application of the theory. Moreover, when there exist portions of the domain over which the solution is smooth, we wish to take advantage of that smoothness by exploiting higher-order methods which can exhibit high local accuracies. These types of considerations suggest discontinuous Galerkin methods as an approach worthy of study and set the present work apart from most conventional approaches to this subject.

1.2 Higher-Order Methods

A major challenge in designing higher-order methods for the numerical solution of hyperbolic conservation laws over the last decade has been to prevent nonphysical oscillations from occuring near discontinuities without destroying accuracy in smooth regions. These oscillations can pollute the solution globally and can lead to numerical instabilities not revealed by traditional stability

analysis applied to a linearized equation. One should also note that the notion of the "order" of a numerical scheme is not always defined consistently in the literature. In classical finite-difference literature, the order of a scheme refers to the order of the truncation error in the time-step Δt, and this may be quite different from the actual order of the error in, say, the L^2-norm. In discussing the order of various schemes in the literature on this subject, we generally refer to the truncation error, since this use is prevelent, albeit imprecise. In subsequent Chapters, we develop error estimates in well-defined norms so that the question of order of accuracy is clearly resolved.

The classical remedy for controlling oscillations, namely, regularizing the conservation law by adding an "artificial" diffusive term (e.g. [28], [34], and [34]), is easily applied to methods of arbitrarily high order [18], [49]. Unfortunately, this approach is not completely effective at eliminating oscillations and may destroy accuracy in smooth regions. The most successful methods for solving realistic problems are typically second-order accurate and attack oscillations directly by simply preventing them from occuring. These schemes, such as those based on the Flux-Corrected Transport (FCT) ideas of Boris and Book [8], or the Total Variation Diminishing (TVD) ideas of Harten [25], and the monotone reconstruction ideas of Van Leer [51], use a form of flux or solution limiting to enforce the discrete counterpart of properties (iii) or (iv) in Lemma 1 onto the approximate solution. Unfortunately, this limiting is based on one-dimensional concepts which are heuristically extended to multidimensional systems. Often these extensions result in a loss of accuracy in smooth regions [24].

Higher-order accurate (greater than second-order) methods for discon-

tinuous solutions of hyperbolic conservation laws are primarily in a developmental stage. Spectral methods have been combined with FCT ideas [10] and filtering methods [50] to control oscillations, but much of the work is for one space dimension and lacks the geometric flexibilty needed for adaptivity. Essentially NonOscillatory (ENO) schemes introduced by Harten, Enquist, Osher and Chakravarthy [26] produce high-order approximations for hyperbolic problems by using high-order polynomial interpolation of solution mean values. Oscillations are controlled by using a solution dependent stencil which avoids interpolation across discontinuities. To date, a full theoretical basis for these schemes is not available beyond one dimensional cases.

Cockburn, Shu, and collaborators [12], [13] developed one of the first high-order numerical schemes for hyperbolic conservation laws in two space dimensions. This work employed Runge-Kutta schemes for advancing the solution in time and an elaborate projection strategy that guaranteed that the total variation of the solutions remained bounded throughout the evolution process. Their TVB (total variation bounded) schemes thus generalized the TVD schemes of Harten and others. Goodman and LeVeque [24] showed that TVD schemes are at most first-order accurate in dimensions greater than one and hence, are not justified mathematically in two- or more dimensions. The TVB schemes, however, provide a basis for the development of high-order schemes on spatial domains of dimensions two and three. The Cockburn and Shu TVB methods are constructed using discontinuous Galerkin methods and, thus, extend these methods to nonlinear conservation laws. However, the emphasis of their work was in treating the discontinuous Galerkin method as a higher-order finite volume method, that is, focusing on the accuracy of solution mean values.

Moreover, these TVB schemes, thusfar, have delivered only second-order methods on non-cartesian meshes in multiple space dimensions. This work inspired some of the developments discussed in Chapter 7.

Among the earliest work on finite element approximations of hyperbolic problems is the classical paper of Lesaint and Raviart [33] which introduced the discontinuous Galerkin method for linear scalar hyperbolic problems. This work contained the first *a priori* error estimates for h-version methods based on elements of arbitrary, but uniform, polynomial order p. In their work, sub-optimal error estimates, with a loss in global accuracy of $O(h)$ in the L^2-norm, were obtained.

A detailed analysis of discontinuous Galerkin methods for h-version methods was contributed by Johnson and his collaborators [29], [30]. There quasi-optimal *a priori* estimates showed a global accuracy of $O(h^{p+\frac{1}{2}})$ in mesh-dependent norms. This work provided a general approach to the mathematical analysis of these methods that proved to be invaluable in the present work. Among the results established in the present study are developments of new *a priori* and *a posteriori* error estimates for hp-version discontinuous Galerkin finite element approximations of linear, scalar hyperbolic conservation laws. Thus, this study extends and generalizes the results of Johnson and others to p- and hp-version finite elements and provides, for the first time, *a posteriori* error estimates for such problems using extensions of the element residual method (see [1], [2]).

One reason for renewed interest in discontinuous Galerkin methods is the advent of parallel computations. The decomposition of large-scale problems into several computational components that can be handled simultane-

ously by multiple processors makes possible significant improvements in the efficiency with which large hyperbolic systems can be resolved. Some progress in parallelizations of high-order schemes for hyperbolic problems in one- and two-dimensions has been made by Biswas, Devine, and Flaherty [7]. In their work, extensions of the ideas of Cockburn and Shu [12], [13] are presented which make use of higher moments of the solutions over an element in defining a broader class of projections for imposing TVB behavior on the entire solution in an element and not just the mean values. At present, however, moment limiting is restricted to cartesian grids. A component of the work reported here is concerned with parallel computing methods for hp-finite element approximations of scalar conservation laws. The fact that discontinuous Galerkin methods involve very localized approximations over individual elements makes our techniques particularly amenable to element-by-element decomposition and parallel processing.

To a great extent, the present work represents a significant departure from conventional methods for the numerical solution of hyperbolic problems. Several fundamental issues are addressed: the use of discontinuous hp-methods, to provide high-order local approximation to deliver high accuracy when possible but also allowing mesh refinement to resolve irregularities in the solutions; the development of *a priori* error estimates to establish proofs of convergence and qualitative information on the performance of the method; the development of *a posteriori* error estimates to monitor the performance of the calculation and to estimate quality of the solution; the development of new adaptive strategies to control error and optimize meshes; and the development of parallel computing strategies to exploit the local character of discontinuous approximations

and to increase the speed with which solutions can be obtained. In addition to these developments, applications to nonlinear conservation laws are also presented.

1.3 *A Posteriori* Error Estimation and Adaptivity

The power of adaptivity to efficiently improve solution accuracy was recognized early on in the development of unstructured grid methods for hyperbolic conservation laws. These h-adaptive methods, based on refinement and derefinement of an initial mesh [35], [36], [16] or a complete remeshing of the domain [43], continue to be the preference for realistic flow simulations. With an emphasis on resolving certain features of the solution, many refinement indicators have been proposed which are based on some a priori knowledge of the solution behavior associated with certain phenomena. Typically, these indicators are loosely based on interpolation error estimates applied to key variables and can be grossly in error. While this approach may provide some relative measure of the local error in the solution, it does not in general provide a reliable estimate of the actual error in the approximate solution.

While the bulk of previous work has concentrated on h-adaptive methods combined with low-order approximations, the effectiveness of p-adaptive [7] and hp-adaptive [18] methods has been demonstrated for certain classes of hyperbolic problems. As noted earlier, the present study extends existing adaptive strategies to discontinuous approximations of hyperbolic conservation laws.

1.4 Scope

Following this introduction, a new formulation of the discontinuous Galerkin method is given for a model class of steady-state, scalar, linear hyperbolic problems in two dimensions. There a notion of hp-dependent norms is introduced which generalizes to hp-methods the idea of mesh-dependent norms used by Johnson and Pitkaranta [30]. Conceptually, one considers a partition of a domain $\Omega \subset \Re^2$ into finite elements and assigns to each element K a positive number p_K which is designed to appear in coefficients of a mesh-dependent norm in a way to optimize subsequent estimated convergence rates. The numbers p_K are identified with the maximum spectral orders of the shape functions used in approximations over K. *A priori* error estimates are derived in these norms.

In Chapter 3, the subject of *a posteriori* error estimates for the model problem is investigated. An extension of the element residual method to hyperbolic conservation laws is described. In the present investigation, two types of estimates are produced, one which delivers an upper bound to the global error in a suitable mesh-dependent norm and a lower bound in another related norm. Theorems are proven which establish that these estimates are indeed valid bounds on appropriate measures of the approximation error.

The availability of both *a priori* and *a posteriori* error estimates provides a powerful basis for developing adaptive strategies to control the error. In Chapter 4, an extension of the 3-step adaptive strategy for hp-finite element methods is presented. This work extends the development in [39] to hyperbolic conservation laws and represents, we believe, the first hp-adaptive methodology ever developed for this class of problem.

Chapter 5 is devoted to numerical experiments and testing of the theoretical results developed in earlier chapters. Several model problems in two dimensions are studied, including examples in non-rectangular domains. The numerical results exhibit significant features of the theory and the methodologies developed: 1) the asymptotic rates of convergence predicted by our theory of *a priori* estimates are fully confirmed by the computed rates; 2) exponential rates of convergence or super algebraic rates are observed, justifying finally the decision to use nonuniform hp-meshes for these types of problems; 3) the *a posteriori* estimation methods produce very good estimates of the actual error, with effectivity indices near unity in many cases, and with remarkably good local error indicators in most of the cases considered; 4) the 3-step adaptive strategy works surprisingly well and delivers a targeted error level quite regularly in around 3 steps; the significant accuracy with which the 3-step scheme was able to produce a mesh with a prescribed global error was unexpected.

In Chapter 6, issues of parallelization of the adaptive methods are investigated. There the local character of discontinuous Galerkin methods is exploited when possible. A parallel algorithm designed for implementation on the Intel iPSC860 computer with 16 processors is described and the results of numerical tests are presented. A major issue in the parallel implementation of hp-adaptive schemes is the design of domain decomposition strategies which result in a balanced work load on all processors. Two domain decomposition strategies recently developed by Patra [40] are used and nearly linear increases in speed are observed for certain cases.

Chapter 7 is devoted to some preliminary results on extensions of the work to nonlinear conservation laws. A model problem involving the solu-

tion of Burgers' equation on a two-dimensional domain is investigated. The exploratory results suggest that the methods developed here could be very effective for problems of this type. The local projection developed in this work is extremely effective at controlling oscillations at discontinuities without destroying accuracy in smooth regions. The projection strategy is a simple one designed with the idea of combining low-order approximations at shocks with higher-order approximations in smooth regions.

Finally, in Chapter 8, the major conclusions of the study are given together with suggestions for future work.

Chapter 2

The Discontinuous Galerkin Method

The methods presented in this chapter are valid for hyperbolic systems of conservation laws in multiple space dimensions. For clarity of presentation and for the purposes of analysis, however, we limit the discussion to a scalar linear hyperbolic conservation law. We begin with a detailed description of the method for a linear model problem and prove some important properties. Next we describe a finite element approximation and derive *a priori* error estimates for an *hp*-version of the discontinuous Galerkin method.

2.1 A Linear Model Problem

We consider a linear scalar hyperbolic conservation law on a convex polygonal domain Ω. Let $\boldsymbol{\beta} = (\beta_1, \beta_2)^T$ denote a constant unit velocity vector. The domain boundary $\partial\Omega$ with an outward unit normal vector $\mathbf{n}(x)$ consists of two parts: an inflow boundary $\Gamma_- = \{\mathbf{x} \in \partial\Omega \mid \boldsymbol{\beta} \cdot \mathbf{n}(x) < 0\}$ and an outflow boundary $\Gamma_+ = \partial\Omega \setminus \Gamma_-$. Let u denote the quantity that is to be conserved in Ω and consider the following hyperbolic boundary-value problem:

$$\boldsymbol{\beta} \cdot \boldsymbol{\nabla} u + au = f \quad \text{in } \Omega \subset \mathcal{R}^2 \tag{2.1}$$

$$\boldsymbol{\beta} \cdot \mathbf{n}\, u \;=\; \boldsymbol{\beta} \cdot \mathbf{n}\, g \quad \text{on } \Gamma_- \tag{2.2}$$

where $f \in L^2(\Omega)$, $g \in L^2(\Gamma_-)$, and $a = a(\mathbf{x})$ is a bounded measurable function on Ω such that $0 < a_0 \leq a(\mathbf{x})$. While this is the simplest of hyperbolic conservation laws, solutions to (2.1) may contain discontinuities along characteristic lines $\mathbf{x}(s)$ defined by $\frac{\partial \mathbf{x}}{\partial s} = \boldsymbol{\beta}$. Solutions to (2.1) belong to the space of functions $V(\Omega) = \{v \in L^2(\Omega) \mid v_\beta \in L^2(\Omega)\}$ where $v_\beta = \boldsymbol{\beta} \cdot \boldsymbol{\nabla} v$.

2.2 Notation

Throughout this work, notations and conventions standard in the literature on the mathematics and application of finite elements are used. Particularly, $H^s(\Omega)$ denotes the usual Sobolev space of functions with distributional derivatives of order s in $L^2(\Omega)$, equipped with the norm,

$$||u||_{s,\Omega} = \left\{ \int_\Omega \sum_{|\boldsymbol{\alpha}| \leq s} |D^{\boldsymbol{\alpha}} u|^2 dx \right\}^{\frac{1}{2}}$$

Other notations and norms are defined in this section and where they first appear in the text.

The starting point for the discontinuous Galerkin method is (2.1) defined on a partition of Ω. Let $\mathcal{P}_h$ denote a partition of Ω into $N = N(\mathcal{P}_h)$ subdomains K with boundaries ∂K such that

(i) $N(\mathcal{P}_h) < \infty$

(ii) $\bar{\Omega} = \bigcup\{\bar{K} : K \in \mathcal{P}_h\}$

(iii) For any pair of elements $K, L \in \mathcal{P}_h$ such that $K \neq L$, $K \cap L = 0$

(iv) K are Lipschitzian domains with piecewise smooth boundaries. The outward unit norm to ∂K is denoted by $\mathbf{n}_K$.

(v) $\partial K_- = \{\mathbf{x} \in \partial K | \ \boldsymbol{\beta} \cdot \mathbf{n}_K < 0\}$ and $\partial K_+ = \partial K \setminus \partial K_-$ and no boundary ∂K coincides with a streamline, $\mathbf{n}_K \cdot \boldsymbol{\beta} \neq 0$

(vi) $\Gamma_-^h = \bigcup_{K=1}^{N_K} \partial K \cap \Gamma_-$ coincides with Γ_- for every $h > 0$

(vii) $\Gamma_{KL} = \partial K \cap \partial L$ is an entire edge of both K and L

(viii) The elements $K \in \mathcal{P}_h$ are affine maps of a master element $\hat{K} = [-1,1] \times [-1,1]$, $K = F_K(\hat{K})$ as illustrated in Fig. 2.1.

(ix) $\mathcal{P}_h \in \mathcal{F}$ where $\mathcal{F}$ is a family of quasi-uniform refinements. Let $h_K = \text{diam}(K)$ and ρ_K denote the supremum of all spheres contained in K; then for all $\mathcal{P}_h \in \mathcal{F}$, there exist positive constants σ and τ, independent of $h = \max_{K \in \mathcal{P}_h} h_K$, such that

$$\frac{h}{h_K} \leq \tau \quad \text{and} \quad \frac{h_K}{\rho_K} \leq \sigma \tag{2.3}$$

∎

We extend $V(\Omega)$ to the partition using the broken space

$$\begin{aligned} V(\mathcal{P}_h) &= \prod_{K \in \mathcal{P}_h} V(K) \\ V(K) &= \{v \in L^2(K) | \ v_\beta \in L^2(K)\} \end{aligned}$$

which admits discontinuities across element interfaces and use the following notations concerning functions $v, w \in V(\mathcal{P}_h)$:

$$v^{\text{int } K} = v|_K(\mathbf{x}), \quad \mathbf{x} \in \partial K$$

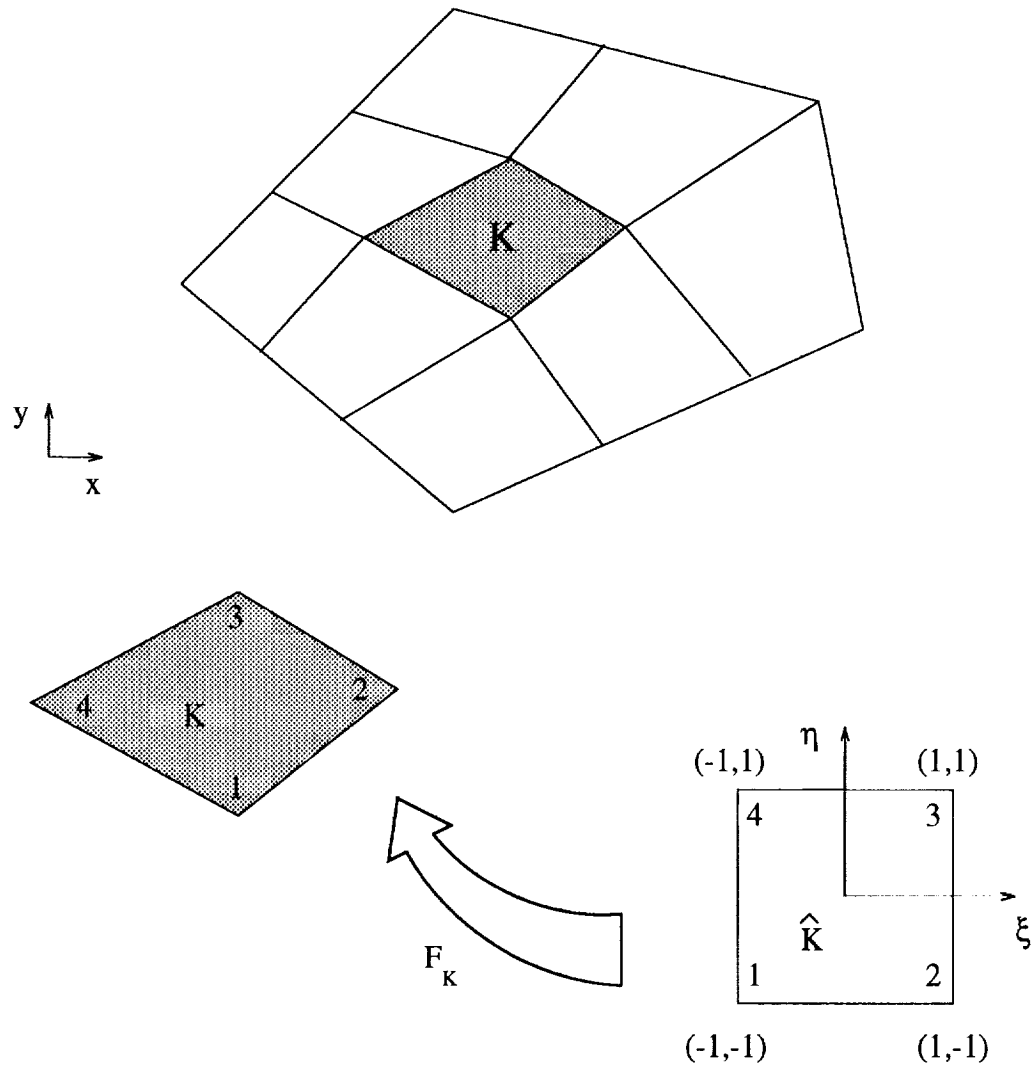

Figure 2.1: The affine map of the master element $\hat{K}$ to a typical element $K \in \mathcal{P}_h$.

$$
\begin{aligned}
v^{\text{ext } K} &= v|_L(\mathbf{x}), \quad \mathbf{x} \in \partial K \cap \partial L \\
v^{\pm} &= \lim_{\epsilon \to 0} v(\mathbf{x} \pm \epsilon \boldsymbol{\beta}) \\
\langle v, w \rangle_\gamma &= \int_\gamma vw|\boldsymbol{\beta} \cdot \mathbf{n}_\gamma| \, ds, \quad \gamma \subset \partial K \\
\langle\langle v \rangle\rangle_\gamma^2 &= \langle v, v \rangle_\gamma \\
(v, w)_K &= \int_K vw d\mathbf{x} \qquad (2.4) \\
||v||_K &= (v, v)_K
\end{aligned}
$$

We define the following norms for functions $v \in V(\mathcal{P}_h)$:

$$
\begin{aligned}
|||v|||_{B,K} &\stackrel{\text{def}}{=} \left\{ ||v_\beta||_K^2 + ||v||_K^2 + \langle\langle v \rangle\rangle_{\partial K}^2 \right\}^{\frac{1}{2}} \\
&= \left\{ ||v_\beta||_K^2 + ||v||_K^2 + \langle\langle v^+ \rangle\rangle_{\partial K_-}^2 + \langle\langle v^- \rangle\rangle_{\partial K_+}^2 \right\}^{\frac{1}{2}} \\
|||v|||_{1,\beta,K} &\stackrel{\text{def}}{=} \left\{ ||v_\beta||_K^2 + ||v||_K^2 + \langle\langle v^+ - v^- \rangle\rangle_{\partial K_- \setminus \Gamma_-}^2 + \langle\langle v \rangle\rangle_{\partial K \cap \partial\Omega}^2 \right\}^{\frac{1}{2}} \\
|||v|||_B &\stackrel{\text{def}}{=} \left\{ \sum_{K \in \mathcal{P}_h} |||v|||_{B,K}^2 \right\}^{\frac{1}{2}} \\
|||v|||_- &\stackrel{\text{def}}{=} \left\{ \sum_{K \in \mathcal{P}_h} \left[||v||_K^2 + \left(1 + \delta \frac{h_K}{p_K^2}\right) \langle\langle v^+ \rangle\rangle_{\partial K_-}^2 \right] \right\}^{\frac{1}{2}} \\
|||v|||_+ &\stackrel{\text{def}}{=} \left\{ \sum_{K \in \mathcal{P}_h} \left[||v||_K^2 + \left(1 + \delta \frac{h_K}{p_K^2}\right) \langle\langle v^- \rangle\rangle_{\partial K_+}^2 \right] \right\}^{\frac{1}{2}} \\
|||v|||_{\theta,\beta} &\stackrel{\text{def}}{=} \left\{ \sum_{K \in \mathcal{P}_h} \left[\theta_K ||v_\beta||_K^2 + ||v||_K^2 \right. \right.
\end{aligned}
$$

$$+ \quad (1+\delta\frac{h_K}{p_K^2})\left(\langle\langle v^+ - v^-\rangle\rangle^2_{\partial K_-\setminus\Gamma_-} + \langle\langle v\rangle\rangle^2_{\partial K\cap\partial\Omega}\right)\Bigg]\Bigg\}^{\frac{1}{2}} \qquad (2.5)$$

where θ is used to indicate the value of the parameter θ_K.

$$\begin{aligned}
\text{If } \theta &= \delta hp \text{ then } \theta_K = \delta\frac{h_K}{p_K^2} \\
\text{If } \theta &= hp \text{ then } \theta_K = \frac{h_K}{p_K^2} \\
\text{If } \theta &= h \text{ then } \theta_K = h_K \\
\text{If } \theta &= 0 \text{ then } \theta_K = 0 \\
\text{If } \theta &= 1 \text{ then } \theta_K = 1
\end{aligned}$$

The parameter p_K appearing in the definition of θ_K in the mesh-dependent norm (2.5) will later represent the spectral order of the polynomial approximation in K. The case in which the coefficient $\theta_K = \frac{h_K}{p_K^2}$ in (2.5) plays an important role in the stability and error of the method, as we show later. Throughout C is used to denote a generic positive constant, not necessarily the same at each occurence.

2.3 Weak Formulation

Property (v) of the partition implies that solutions $u \in V(\Omega)$ to (2.1) are continuous across element interfaces. Since the broken space admits discontinuities along element interfaces, we have the following problem corresponding to (2.1)

on the partition $\mathcal{P}_h$:

$$\left.\begin{aligned} \text{Find } u &\in V(\mathcal{P}_h) \text{ such that for every } K \in \mathcal{P}_h, \\ u_\beta + au &= f \quad \text{in } K \\ u^{\text{int } K}\boldsymbol{\beta}\cdot\mathbf{n}_K &= u^{\text{ext } K}\boldsymbol{\beta}\cdot\mathbf{n}_K \quad \forall \mathbf{x} \in \partial K_- \setminus \partial\Omega \\ u^{\text{int } K}\boldsymbol{\beta}\cdot\mathbf{n}_K &= g\,\boldsymbol{\beta}\cdot\mathbf{n}_K \quad \forall \mathbf{x} \in \partial K_- \cap \Gamma_- \end{aligned}\right\} \tag{2.6}$$

for which weak solutions are sought satisfying

$$\left.\begin{aligned} \text{Find } u &\in V(\mathcal{P}_h) \text{ such that for every } K \in \mathcal{P}_h, \\ (u_\beta + au, w)_K &= (f, w)_K \quad \forall w \in V(K) \\ \langle u^{\text{int } K}, v\rangle_{\partial K_-\setminus\partial\Omega} &= \langle u^{\text{ext } K}, v\rangle_{\partial K_-\setminus\partial\Omega} \quad \forall v \in V(K) \\ \langle u^{\text{int } K}, v\rangle_{\partial K_-\cap\Gamma_-} &= \langle g, v\rangle_{\partial K_-\cap\Gamma_-} \quad \forall v \in V(K) \end{aligned}\right\} \tag{2.7}$$

where we have taken the absolute value of $\boldsymbol{\beta}\cdot\mathbf{n}_K$ for convenience. Next, we introduce a global parameter δ which has a value of either 0 or 1. Recall that for any $v \in V(K)$ we have that $v_\beta \in L^2(K)$ so that we can set $w = v + \delta\frac{h_K}{p_K^2}v_\beta$ in (2.7) and then add the boundary integral equations multiplied by any constant. It will be convenient to choose this constant to be $(1 + \delta\frac{h_K}{p_K^2})$ and to write the method in the following abstract form. Let

$$\begin{aligned} B_K(u,v) &\stackrel{\text{def}}{=} (u_\beta + au, v + \delta\frac{h_K}{p_K^2}v_\beta)_K + (1 + \delta\frac{h_K}{p_K^2})\langle u^+ - u^-, v^+\rangle_{\partial K_-\setminus\Gamma_-} \\ &+ (1 + \delta\frac{h_K}{p_K^2})\langle u^+, v^+\rangle_{\partial K_-\cap\Gamma_-} \end{aligned} \tag{2.8}$$

$$L_K(v) \stackrel{\text{def}}{=} (f, v + \delta\frac{h_K}{p_K^2}v_\beta)_K + (1 + \delta\frac{h_K}{p_K^2})\langle g, v\rangle_{\partial K_-\cap\Gamma_-} \tag{2.9}$$

where, by definition, $u^+ = u^{\text{int } K}$ and $u^- = u^{\text{ext } K}$ on ∂K_-. Summing over all the elements in the partition yields the variational boundary value problem for weak solutions to (2.1) on the partition:

Find $u \in V(\mathcal{P}_h)$ such that

$$B(u,v) = L(v) \ , \ \text{for every } v \in V(\mathcal{P}_h) \tag{2.10}$$

where

$$B(u,v) \stackrel{\text{def}}{=} \sum_{K \in \mathcal{P}_h} B_K(u,v) \tag{2.11}$$

$$L(v) \stackrel{\text{def}}{=} \sum_{K \in \mathcal{P}_h} L_K(v) \tag{2.12}$$

Remarks:

(i) The case $\delta = 0$ in (2.8) is referred to as the "standard" discontinuous Galerkin method which can be viewed as a standard Galerkin method for a single element with weakly imposed boundary conditions for elements lying on the inflow boundary and weakly imposed continuity for elements on the interior of the domain.

(ii) The case $\delta = 1$ in (2.8) is the hp extension of the so-called "streamline upwind" discontinuous Galerkin method [29]. The modification of the test function is important when approximating solutions with sharp gradients as the additional term in the test function adds diffusion in the streamline direction without modifying the conservation law, i.e., without destroying accuracy in regions where the solution is smooth. ∎

Lemma 2 *Let the bilinear form $B(\cdot,\cdot)$ be defined by (2.11) and (2.8). Then there exists positive constants α, M_1, and M_2, independent of h_K and p_K, such*

that

$$B(v,v) \geq \alpha |||v|||^2_{\delta hp,\beta} \tag{2.13}$$

$$\begin{aligned} B(w,v) &\leq M_1 \left\{ \sum_{K\in\mathcal{P}_h} \left(1+\delta\frac{h_K}{p_K^2}\right) |||w|||^2_{1,\beta,K} \right\}^{\frac{1}{2}} \\ &\times \left\{ |||v|||^2_- + \delta \sum_{K\in\mathcal{P}_h} \frac{h_K}{p_K^2} \left[||v_\beta||^2_K + \langle\langle v^+\rangle\rangle^2_{\partial K_-} \right] \right\}^{\frac{1}{2}} \end{aligned} \tag{2.14}$$

$$\begin{aligned} B(w,v) &\leq M_1 \left\{ \sum_{K\in\mathcal{P}_h} |||w|||^2_+ + \delta \sum_{K\in\mathcal{P}_h} \frac{h_K}{p_K^2} \left[||w_\beta||^2_K + \langle\langle w^-\rangle\rangle^2_{\partial K_+} \right] \right\}^{\frac{1}{2}} \\ &\times \left\{ \sum_{K\in\mathcal{P}_h} \left(1+\delta\frac{h_K}{p_K^2}\right) |||v|||_{1,\beta,K} \right\}^{\frac{1}{2}} \end{aligned} \tag{2.15}$$

$$\begin{aligned} B(w,v) &\leq M_2 \left\{ \sum_{K\in\mathcal{P}_h} \left(1+\delta\frac{h_K}{p_K^2}\right) |||w|||^2_{B,K} \right\}^{\frac{1}{2}} \\ &\times \left\{ \sum_{K\in\mathcal{P}_h} \left(1+\delta\frac{h_K}{p_K^2}\right) |||v|||^2_{B,K} \right\}^{\frac{1}{2}} \end{aligned} \tag{2.16}$$

for every $w, v \in V(\mathcal{P}_h)$.

Proof: (i) From the definition of $B(\cdot,\cdot)$,

$$\begin{aligned} B(v,v) \geq\ & \min(1, \min_{\mathbf{x}\in\Omega} a(\mathbf{x})) \sum_{K\in\mathcal{P}_h} \left\{ \left(1+\delta\frac{h_K}{p_K^2}\right)(v,v_\beta)_K + \delta\frac{h_K}{p_K^2}||v_\beta||^2_K + ||v||^2_K \right. \\ &+ \left. \left(1+\delta\frac{h_K}{p_K^2}\right) \left(\langle\langle v^+\rangle\rangle^2_{\partial K_-\setminus\Gamma_-} - \langle v^-, v^+\rangle_{\partial K_-\setminus\Gamma_-} + \langle\langle v\rangle\rangle^2_{\partial K_-\cap\Gamma_-} \right) \right\} \end{aligned}$$

Equation (2.13) follows by substituting the results of applying Green's formula to the term $(v, v_\beta)_K$, that is,

$$\sum_{K\in\mathcal{P}_h} (v,v_\beta)_K = \frac{1}{2} \sum_{K\in\mathcal{P}_h} \left(\langle\langle v^-\rangle\rangle^2_{\partial K_-\setminus\Gamma_-} + \langle\langle v^+\rangle\rangle^2_{\partial K_-\setminus\Gamma_-} + \langle\langle v\rangle\rangle^2_{\partial K\cap\partial\Omega} \right) \tag{2.17}$$

into the above and choosing $\alpha = \frac{1}{2}\min(1, \min_{\mathbf{x}\in\Omega} a(\mathbf{x}))$.

(ii) Applying the Schwarz inequality to $B(\cdot,\cdot)$ as defined in (2.11) and (2.8) yields

$$\begin{aligned}
B(w,v) &\leq ||a||_{\infty,\Omega} \sum_{K\in\mathcal{P}_h} \Bigg[||w_\beta||_K ||v||_K + \delta \frac{h_K}{p_K^2} ||w_\beta||_K ||v_\beta||_K + ||w||_K ||v||_K \\
&+ \delta \frac{h_K}{p_K^2} ||w||_K ||v_\beta||_K + \left(1 + \delta \frac{h_K}{p_K^2}\right) \langle\langle w^+ - w^- \rangle\rangle_{\partial K_- \setminus \Gamma_-} \langle\langle v^+ \rangle\rangle_{\partial K_- \setminus \Gamma_-} \\
&+ \left(1 + \delta \frac{h_K}{p_K^2}\right) \langle\langle w^+ \rangle\rangle_{\partial K_- \cap \Gamma_-} \langle\langle v^+ \rangle\rangle_{\partial K_- \cap \Gamma_-} \Bigg] \\
&\leq ||a||_{\infty,\Omega} \Bigg\{ \sum_{K\in\mathcal{P}_h} \left(1 + \delta \frac{h_K}{p_K^2}\right) \Big[||w_\beta||_K^2 + ||w||_K^2 \\
&+ \langle\langle w^+ - w^- \rangle\rangle_{\partial K_- \setminus \Gamma_-}^2 + \langle\langle w \rangle\rangle_{\partial K \cap \partial\Omega}^2 \Big] \Bigg\}^{\frac{1}{2}} \\
&\times \Bigg\{ \sum_{K\in\mathcal{P}_h} \left[2\delta \frac{h_K}{p_K^2} ||v_\beta||_K^2 + 2||v||_K^2 + \left(1 + \delta \frac{h_K}{p_K^2}\right) \langle\langle v^+ \rangle\rangle_{\partial K_-}^2 \right] \Bigg\}^{\frac{1}{2}}
\end{aligned}$$

Equation (2.14) follows by selecting $M_1 = \sqrt{2}||a||_{\infty,\Omega}$.

(iii) Equation (2.15) is obtained by applying Greens formula to the term $(w, v_\beta)_K$ and $(w_\beta, v)_K$ in (2.11), and applying the Cauchy-Schwarz inequality.

(iv) Equation (2.16) is obtained by adding (2.14) and (2.15), applying the Cauchy-Schwarz inequality to the result, and selecting $M_2 = \frac{3}{2}||a||_{\infty,\Omega}$. ∎

Corollary 1 *Let $\delta = 1$ in (2.8). Then*

$$B(v,v) \geq \alpha |||v|||_{hp,\beta}^2 \tag{2.18}$$

and there exists a constant r_0 such that if $\frac{h_K}{p_K^2} \leq r_0 \; \forall K \in \mathcal{P}_h$,

$$B(w,v) \leq M_1' |||w|||_{1,\beta} \left\{ |||v|||_-^2 + \sum_{K\in\mathcal{P}_h} \frac{h_K}{p_K^2} ||v_\beta||_K^2 \right\}^{\frac{1}{2}} \tag{2.19}$$

$$B(w,v) \leq M_1' \left\{ |||w|||_+^2 + \sum_{K\in\mathcal{P}_h} \frac{h_K}{p_K^2} ||w_\beta||_K^2 \right\}^{\frac{1}{2}} |||v|||_{1,\beta} \tag{2.20}$$

$$B(w,v) \leq M_2(1+r_0)|||w|||_B |||v|||_B \tag{2.21}$$

Proof: Set $\delta = 1$ in (2.13)-(2.16) and choose $M_1' = M_1\sqrt{1+r_0}\max(1,\sqrt{r_0})$. ∎

Corollary 2 *Let $\delta = 0$ in (2.8). Then*

$$B(v,v) \geq \alpha |||v|||_{0,\beta}^2 \tag{2.22}$$

$$B(w,v) \leq M_1 |||w|||_{1,\beta} |||v|||_- \tag{2.23}$$

$$B(w,v) \leq M_1 |||w|||_+ |||v|||_{1,\beta} \tag{2.24}$$

$$B(w,v) \leq M_2 |||w|||_B |||v|||_B \tag{2.25}$$

∎

Remark:

Note that modified test function for the streamline upwind discontinuous Galerkin method results in improved stability of the bilinear form when compared to the standard Galerkin method (see (2.18) and (2.22)). The coercivity of the bilinear form for the streamline upwind discontinuous Galerkin method contains $||v_\beta||_K$ terms which do not appear in the coercivity condition for the standard Galerkin method. The significance of this additional stability is less important as $\frac{h_K}{p_K^2}$ approaches zero. ∎

2.4 *hp* Finite Element Approximation

We seek approximate solutions to (2.10) in the finite dimensional subspace $V_p(\mathcal{P}_h) \subset V(\mathcal{P}_h)$ defined as follows:

$$V_p(\mathcal{P}_h) = \{v \in L^2(\Omega) : v|_K = \hat{v}|_K \circ F_K \in Q^{p_K}(K)\} \tag{2.26}$$

where $Q^{p_K}(K)$ is the space of tensor products of polynomials of degree p_K defined on the master element. The basis for $Q^{p_K}(K)$ is formed by tensor products of Legendre polynomials. We use the notation $v_K \in Q^{p_K}(K)$ to mean $\hat{v}_K \in Q^{p_K}(\hat{K})$ and $v_K = \hat{v}_K \circ F_K$. We have the following inverse estimates for polynomials on a single element:

Lemma 3 *Let $K \in \mathcal{R}^2$ be an affine map of a master element $\hat{K} = [-1,1] \times [-1,1]$; that is $K = F_K(\hat{K})$. Let γ denote any edge of ∂K which is an affine map of a master edge $\hat{\gamma} = [-1,1]$. Let $\hat{w}_K$ be a polynomial of degree p_K defined on the master element. Let $w_K = \hat{w}_K \circ F_K$ denote the image of $\hat{w}_K$ under the transformation F_K. Then $\boldsymbol{\beta} \cdot \boldsymbol{\nabla} w_K$ satisfies the following:*

$$||\boldsymbol{\beta} \cdot \boldsymbol{\nabla} w_K||_K \leq C\frac{p_K^2}{h_K}||w_K||_K \tag{2.27}$$

$$\langle\langle \boldsymbol{\beta} \cdot \boldsymbol{\nabla} w_K \rangle\rangle_\gamma \leq C\frac{p_K^4}{h_K^2}\langle\langle w_K \rangle\rangle_\gamma^2 \tag{2.28}$$

where the constants C are independent of h_K, p_K, and w_K.

Proof: For polynomials of degree p_K on the master element (see Dorr [21]):

$$|\hat{w}_K|_{s,\hat{K}} \leq ||\hat{w}_K||_{s,\hat{K}} \leq Cp_K^{2s}||\hat{w}_K||_{\hat{K}} \tag{2.29}$$

$$|\hat{w}_K|_{s,\hat{\gamma}} \leq ||\hat{w}_K||_{s,\hat{\gamma}} \leq Cp_K^{2s}||\hat{w}_K||_{\hat{\gamma}} \tag{2.30}$$

where the constants $C > 0$ depends on s, but not on p_K or $\hat{w}_K$.

For affine mappings F_K, a standard scaling argument (see Ciarlet [11]) yields that for an integer $s \geq 0$, there exist constants $C > 0$ such that

$$|w_K|_{s,K} \leq C h_K^{1-s} |\hat{w}_K|_{s,\hat{K}} \tag{2.31}$$

$$|w_K|_{s,\gamma} \leq C h_K^{\frac{1}{2}-s} |\hat{w}_K|_{s,\hat{\gamma}} \tag{2.32}$$

$$|\hat{w}_K|_{s,\hat{K}} \leq C h_K^{s-1} |w_K|_{s,K} \tag{2.33}$$

$$|\hat{w}_K|_{s,\hat{\gamma}} \leq C h_K^{s-\frac{1}{2}} |w_K|_{s,\gamma} \tag{2.34}$$

where C depends on s, σ, and τ (see (2.3)), but not on h_K, p_K, or w_K.

The first estimate (2.27) follows by combining (2.31), (2.29), and (2.33). The second estimate (2.28) follows from (2.32), (2.30), and (2.34). ∎

Lemma 4 (Babuška and Suri [3]) *Let $K \in \mathcal{P}_h$, γ denote any edge of ∂K, and $u \in H^s(K)$. Then there exists a constant $C = C(s, \tau, \sigma)$ independent of u, p_K, and h_K, and a sequence $z_h^p \in Q^{p_K}(K), p_K = 1, 2, \ldots$, such that for every $0 \leq r \leq p_K$,*

$$||u - z_h^p||_{r,K} \leq C \frac{h_K^{\nu - r}}{p_K^{s-r}} ||u||_{s,K}, \ s \geq 0 \tag{2.35}$$

$$||u - z_h^p||_{0,\gamma} \leq C \frac{h_K^{\nu - \frac{1}{2}}}{p_K^{s-\frac{1}{2}}} ||u||_{s,K}, \ s \geq \frac{1}{2} \tag{2.36}$$

where $\nu = \min(p_K + 1, s)$. ∎

The approximate solution to (2.10) is obtained by replacing the exact solution $u \in V(\mathcal{P}_h)$ by $u_h^p \in V_p(\mathcal{P}_h)$ and the test function $v \in V(\mathcal{P}_h)$ by $v_h^p \in V_p(\mathcal{P}_h)$:

Find $u_h^p \in V_p(\mathcal{P}_h)$ such that

$$B(u_h^p, v_h^p) = L(v_h^p) \ , \ \forall v_h^p \in V_p(\mathcal{P}_h) \tag{2.37}$$

The improved stability of the streamline upwind discontinuous Galerkin method, $\delta = 1$ in (2.8), is recovered by the standard discontinuous Galerkin method, $\delta = 0$ in (2.8), on the finite dimensional space $V_p(\mathcal{P}_h)$.

Lemma 5 *Let $\delta = 0$ in (2.8). Then for every $v_h^p \in V_p(\mathcal{P}_h)$ there exists a $w_h^p \in V_p(\mathcal{P}_h)$ such that*

$$B(v_h^p, w_h^p) \geq \alpha' |||v_h^p|||_{hp,\beta}^2 \tag{2.38}$$

and

$$|||w_h^p|||_{hp,\beta} \leq C |||v_h^p|||_{hp,\beta} \tag{2.39}$$

where the positive constants α' and C are independent of h_K, p_K, and v_h^p.

Proof: Define the restriction of $w_h^p \in V_p(\mathcal{P}_h)$ to an element $K \in \mathcal{P}_h$ as

$$w_h^p|_K = v_h^p|_K + \gamma \frac{h_K}{p_K^2} \boldsymbol{\beta} \cdot \boldsymbol{\nabla} v_h^p|_K \tag{2.40}$$

where $\gamma \in (0, 1]$ is defined later in the proof. Dropping the h, p, and K scripts for ease in notation, we have

$$\begin{aligned}
B_K(v, w) &= \int_K (v_\beta + av)(v + \gamma \frac{h_K}{p_K^2} v_\beta) \, d\mathbf{x} \\
&+ \int_{\partial K_- \setminus \Gamma_-} (v^+ - v^-)(v^+ + \gamma \frac{h_K}{p_K^2} v_\beta{}^+) |\boldsymbol{\beta} \cdot \mathbf{n}_K| \, ds \\
&+ \int_{\partial K_- \cap \Gamma_-} v^+ (v^+ + \gamma \frac{h_K}{p_K^2} v_\beta{}^+) |\boldsymbol{\beta} \cdot \mathbf{n}_K| \, ds \\
&\geq a_0 ||v||_K^2 + \gamma \frac{h_K}{p_K^2} ||v_\beta||_K^2 + \int_K v v_\beta \, d\mathbf{x}
\end{aligned}$$

$$
\begin{aligned}
&+ \quad \gamma\frac{h_K}{p_K^2}\int_K vv_\beta \, d\mathbf{x} + \langle\langle v^+\rangle\rangle^2_{\partial K_-\cap\Gamma_-} + \langle\langle v^+\rangle\rangle^2_{\partial K_-\setminus\Gamma_-} \\
&- \quad \int_{\partial K_-\setminus\Gamma_-} v^+v^-|\boldsymbol{\beta}\cdot\mathbf{n}_K| \, ds + \gamma\frac{h_K}{p_K^2}\int_{\partial K_-\setminus\Gamma_-}(v^+ - v^-){v_\beta}^+|\boldsymbol{\beta}\cdot\mathbf{n}_K| \, ds \\
&+ \quad \gamma\frac{h_K}{p_K^2}\int_{\partial K_-\cap\Gamma_-} v^+{v_\beta}^+|\boldsymbol{\beta}\cdot\mathbf{n}_K| \, ds
\end{aligned}
$$

where $a_0 = \min_{\mathbf{x}\in\Omega} a(\mathbf{x})$. Noting that

$$
\int_K vv_\beta \, d\mathbf{x} = \frac{1}{2}\int_{\partial K_+}(v^-)^2|\boldsymbol{\beta}\cdot\mathbf{n}_K| \, ds - \frac{1}{2}\int_{\partial K_-}(v^+)^2|\boldsymbol{\beta}\cdot\mathbf{n}_K| \, ds \tag{2.41}
$$

and that from Lemma 3

$$
\begin{aligned}
|\int_K vv_\beta \, d\mathbf{x}| &\leq c_1\frac{p_K^2}{h_K}||v||_K^2 \\
|\int_{\partial K_-} v^+{v_\beta}^+|\boldsymbol{\beta}\cdot\mathbf{n}_K| \, ds| &\leq c_2\frac{p_K^2}{h_K}\langle\langle v^+\rangle\rangle^2_{\partial K_-}
\end{aligned}
$$

we have

$$
\begin{aligned}
B_K(v,w) &\geq (a_0 - c_1\gamma)||v||_K^2 + \gamma\frac{h_K}{p_K^2}||v_\beta||_K^2 \\
&+ \quad \frac{1}{2}\langle\langle v^+\rangle\rangle^2_{\partial K_-\setminus\Gamma_-} + (\frac{1}{2} - c_2\gamma)\langle\langle v\rangle\rangle^2_{\partial K_-\cap\Gamma_-} \\
&- \quad \int_{\partial K_-\setminus\Gamma_-} v^+v^-|\boldsymbol{\beta}\cdot\mathbf{n}_K| \, ds + \gamma\frac{h_K}{p_K^2}\int_{\partial K_-\setminus\Gamma_-}(v^+ - v^-){v_\beta}^+|\boldsymbol{\beta}\cdot\mathbf{n}_K| \, ds
\end{aligned}
$$

Using the Schwarz inequality and the previous inequalities, one can show that

$$
\begin{aligned}
|\gamma\frac{h_K}{p_K^2}\int_{\partial K_-\setminus\Gamma_-}(v^+ - v^-){v_\beta}^+|\boldsymbol{\beta}\cdot\mathbf{n}_K| \, ds| &\leq \frac{3c_2}{2}\gamma(\langle\langle v+\rangle\rangle^2_{\partial K_-\setminus\Gamma_-} \\
&+ \quad \langle\langle v^-\rangle\rangle^2_{\partial K_-\setminus\Gamma_-})
\end{aligned}
$$

Now summing over all the elements $K \in \mathcal{P}_h$ and realizing that

$$
\sum_{K\in\mathcal{P}_h}\{\frac{1}{2}\langle\langle v^-\rangle\rangle^2_{\partial K_-\setminus\Gamma_-} - \frac{3c_2}{2}\gamma\langle\langle v^-\rangle\rangle^2_{\partial K_-\setminus\Gamma_-}
$$

$$+ \quad (\frac{1}{2} - \frac{3c_2}{2}\gamma)\langle\langle v^+\rangle\rangle^2_{\partial K_-\setminus\Gamma_-} - \int_{\partial K_-\setminus\Gamma_-} v^+v^-|\boldsymbol{\beta}\cdot\mathbf{n}_K|\, ds\}$$

$$\geq \quad \frac{1}{2}\langle\langle v\rangle\rangle^2_{\Gamma_+} + \min(1, \frac{1}{2} - \frac{3c_2}{2}\gamma) \sum_{K\in\mathcal{P}_h} \langle\langle v^+ - v^-\rangle\rangle^2_{\partial K_-\setminus\Gamma_-}$$

results in

$$B(v_h^p, w_h^p) \quad \geq \quad (a_0 - c_1\gamma)||v||^2_\Omega + \gamma \sum_{K\in\mathcal{P}_h} \frac{h_K}{p_K^2}||v_\beta||^2_K$$

$$+ \quad (\frac{1}{2} - c_2\gamma)\langle\langle v\rangle\rangle^2_{\Gamma_-} + \frac{1}{2}\langle\langle v\rangle\rangle^2_{\Gamma_+}$$

$$+ \quad \min(1, \frac{1}{2} - \frac{3c_2}{2}\gamma) \sum_{K\in\mathcal{P}_h} \langle\langle v^+ - v^-\rangle\rangle^2_{\partial K_-\setminus\Gamma_-}$$

Choosing $\gamma = \min(\frac{1}{4}, \frac{a_0}{2c_1}, \frac{1}{6c_2})$ yields the first inequality.

The second inequality easily follows from the definition of w_h^p and Lemma 3.

∎

2.5 *A Priori* Error Estimate

The discontinuous Galerkin method (2.37) was first analyzed by Lesaint and Raviart [33] for a given fixed value of p_K, i.e. for the case in which $p_K = p$ for every element $K \in \mathcal{P}_h$. The error in a solution u_h to (2.37) approximating an exact solution $u \in H^s(\Omega)$ to (2.10) was shown to be

$$||u - u_h||_\Omega \leq Ch^{s-1}||u||_{s,\Omega}$$

This estimate is not optimal in the sense of interpolation error estimates and was improved by Johnson and Pitkaranta [30]. Using a mesh-dependent norm, they showed that

$$|||u - u_h|||_{h,\beta} \leq Ch^{s-\frac{1}{2}}||u||_{s,\Omega}$$

While this estimate is not optimal in the sense of interpolation error estimates for $||e||_\Omega = ||u - u_h||_\Omega$, it is optimal with respect to $\sqrt{h_K}||e_\beta||_K$ and $\langle\langle e^+ - e^-\rangle\rangle_{\partial K_- \setminus \Gamma_-}$. We shall derive estimates similar to Johnson and Pitkaranta [30] taking into account that p_K is not constant.

Theorem 1 *Let $u \in H^s(\Omega)$ be a solution to (2.10) and let u_h^p be a solution to (2.37). Then there exists a positive constant C, independent of h_K, p_K, and u, such that the error, $e = u - u_h^p$, satisfies the following estimate*

$$|||e|||_{hp,\beta} \leq C \left\{ \sum_{K \in \mathcal{P}_h} \left[\frac{h_K^{2\nu_K - 1}}{p_K^{2s-2}} \max\left(1, \frac{h_K}{p_K^2}\right) ||u||_{s,K}^2 \right] \right\}^{\frac{1}{2}} \tag{2.42}$$

where $\nu_K = \min(p_K + 1, s)$.

Proof: Let $\Pi_h^p u \in V_p(\mathcal{P}_h)$ be an approximation of u that satisfies the estimates in Lemma 4 and write

$$e = u - u_h^p = u - \Pi_h^p u + \Pi_h^p u - u_h^p \tag{2.43}$$

which implies that

$$\begin{aligned} |||e|||_{hp,\beta} &\leq |||u - \Pi_h^p u|||_{hp,\beta} + |||u_h^p - \Pi_h^p u|||_{hp,\beta} \\ &\stackrel{\text{def}}{=} |||\eta|||_{hp,\beta} + |||w|||_{hp,\beta} \end{aligned} \tag{2.44}$$

where, to simplify the notation, we set $\eta = u - \Pi_h^p u$ and $w = u_h^p - \Pi_h^p u$. Realizing that

$$|||v|||_{hp,\beta} \leq C \left\{ \sum_{K \in \mathcal{P}_h} \left[\frac{h_K}{p_K^2} ||v_\beta||_K^2 + ||v||_K^2 + \left(1 + \delta \frac{h_K}{p_K^2}\right) \langle\langle v \rangle\rangle_{\partial K}^2 \right] \right\}^{\frac{1}{2}}, \forall v \in V(\mathcal{P}_h)$$

combined with Lemma 4 yields bounds for the first term in (2.44):

$$
\begin{aligned}
|||\eta|||_{hp,\beta} &\leq C\left\{\sum_{K\in\mathcal{P}_h}\left[\frac{h_K^{2\mu_K-1}}{p_K^{2s}}+\frac{h_K^{2\mu_K}}{p_K^{2s}}+\frac{h_K^{2\mu_K-1}}{p_K^{2s-1}}+\delta\frac{h_K^{2\mu_K}}{p_K^{2s+1}}\right]||u||_{s,K}^2\right\}^{\frac{1}{2}} \\
&\leq C\left\{\sum_{K\in\mathcal{P}_h}\frac{h_K^{2\mu_K-1}}{p_K^{2s-2}}\max\left(\frac{1}{p_K},\frac{h_K}{p_K^2}\right)||u||_{s,K}^2\right\}^{\frac{1}{2}} \qquad (2.45)
\end{aligned}
$$

where $\mu_K = \min(p_K+1, s)$. Bounds for the second term in (2.44) follow from the orthogonality condition which is obtained by subtracting (2.37) from (2.10):

$$
B(e, v_h^p) = B(\eta, v_h^p) - B(w, v_h^p) = 0 \ , \ \forall v_h^p \in V_p(\mathcal{P}_h) \qquad (2.46)
$$

We choose $v_h^p = v^\delta$ in (2.46) where the particular choice for v^δ depends on the parameter δ in (2.8). For $\delta = 0$, we choose v^δ to be the function which satisfies Lemma 5. For $\delta = 1$, we choose $v^\delta = w$ and combine (2.46) with Corollary 1. The result for either case is

$$
C|||w|||_{hp,\beta}^2 \leq B(w, v^\delta) = B(\eta, v^\delta) \qquad (2.47)
$$

Integrating the terms $(\eta_\beta, v^\delta)_K$ and $(\eta, v_\beta^\delta)_K$ by parts in the definition of $B(\cdot,\cdot)$ in (2.11) yields

$$
\begin{aligned}
B(\eta, v^\delta) &\leq ||a||_{\infty,\Omega}\sum_{K\in\mathcal{P}_h}\Bigg[||\eta||_K||v^\delta||_K+\frac{p_K}{\sqrt{h_K}}||\eta||_K\cdot\frac{\sqrt{h_K}}{p_K}||v_\beta^\delta||_K \\
&+ \delta\frac{h_K}{p_K^2}||\eta_\beta||_K||v_\beta^\delta||_K+\delta\frac{h_K}{p_K^2}||\eta_\beta||_K||v^\delta||_K \\
&+ \left(1+\delta\frac{h_K}{p_K^2}\right)\langle\langle\eta^-\rangle\rangle_{\partial K_+\setminus\Gamma_+}\langle\langle v^{\delta+}-v^{\delta-}\rangle\rangle_{\partial K_+\setminus\Gamma_+} \\
&+ \left(1+\delta\frac{h_K}{p_K^2}\right)\langle\langle\eta^-\rangle\rangle_{\partial K_+\cap\Gamma_+}\langle\langle v^{\delta-}\rangle\rangle_{\partial K_+\cap\Gamma_+}\Bigg] \\
&\leq ||a||_{\infty,\Omega}(1+\delta)\left\{\sum_{K\in\mathcal{P}_h}\left[\left(1+\frac{p_K^2}{h_K}\right)||\eta||_K^2\right.\right.
\end{aligned}
$$

$$
\begin{aligned}
&+ \quad \delta\frac{h_K}{p_K^2}\left(1+\delta\frac{h_K}{p_K^2}\right)||\eta_\beta||_K^2 \\
&+ \quad \left(1+\delta\frac{h_K}{p_K^2}\right)\langle\langle\eta^-\rangle\rangle_{\partial K_+}^2\Bigg]\Bigg\}^{\frac{1}{2}} |||v^\delta|||_{hp,\beta} \qquad (2.48)
\end{aligned}
$$

Recall that for our choice of v^δ we have $|||v^\delta|||_{hp,\beta} = |||w|||_{hp,\beta}$ when $\delta = 1$ and $|||v^\delta|||_{hp,\beta} \leq C|||w|||_{hp,\beta}$ when $\delta = 0$. Equations (2.48), (2.47), and the estimates in Lemma 4 imply that

$$
\begin{aligned}
|||w|||_{hp,\beta} &\leq C\Bigg\{\sum_{K\in\mathcal{P}_h}\frac{h_K^{2\mu_K-1}}{p_K^{2s-2}}\Bigg[\frac{h_K}{p_K^2}\left(1+\frac{p_K}{h_K}\right)+\delta\left(1+\delta\frac{h_K}{p_K^2}\right) \\
&+ \frac{1}{p_K}\left(1+\delta\frac{h_K}{p_K^2}\right)\Bigg]||u||_{s,K}^2\Bigg\}^{\frac{1}{2}} \\
&\leq C\Bigg\{\sum_{K\in\mathcal{P}_h}\frac{h_K^{2\mu_K-1}}{p_K^{2s-2}}\max\left(\frac{h_K}{p_K^2},1,\frac{1}{p_K},\delta\frac{h_K^2}{p_K^4}\right)||u||_{s,K}^2\Bigg\}^{\frac{1}{2}} \qquad (2.49)
\end{aligned}
$$

Combining (2.49), (2.45), and (2.44) completes the proof. ∎

Remarks:

(i) For $\frac{h_K}{p_K^2} \leq 1$, the estimate becomes $|||e|||_{hp,\beta} \leq C\{\sum_{K\in\mathcal{P}_h}\frac{h_K^{2\nu_K-1}}{p_K^{2s-2}}||u||_{s,K}^2\}^{\frac{1}{2}}$

(ii) For p_K =constant, the *a priori* error estimate reduces to the one derived by Johnson and Pitkaranta[30].

(iii) Let $h = \max_{K\in\mathcal{P}_h} h_K$ and $p = \min p_K$, then $|||e|||_{hp,\beta} \leq \frac{h^{\mu-\frac{1}{2}}}{p^{s-1}}||u||_{s,\Omega}$.

∎

2.6 Implementation Issues

In the preceeding sections of this Chapter, the discontinuous Galerkin methods were represented as global methods for the purpose of analysis. The approxi-

mate problem is actually a local one since the approximate solution in an element is independent of the solution in the neighboring elements with the only coupling between elements occuring weakly through the fluxes on the element inflow boundary. Assume that u_h^{p-} is known on ∂K_-, then the approximate solution in element K satisfies

$$\tilde{B}_K(u_h^p|_K, v_h^p|_K) = \tilde{L}_K(v_h^p|_K) \ , \ \forall \ v_h^p|_K \in Q^{p_K}(K) \tag{2.50}$$

where

$$\tilde{B}_K(u_h^p, v_h^p) \stackrel{\text{def}}{=} (u_{h\beta}^p + a u_h^p, v_h^p + \delta \frac{h_K}{p_K^2} v_{h\beta}^p)_K \tag{2.51}$$

$$+ \quad (1 + \delta \frac{h_K}{p_K^2}) \langle u_h^{p+}, v_h^{p+} \rangle_{\partial K_-} \tag{2.52}$$

$$\tilde{L}_K(v_h^p) \stackrel{\text{def}}{=} (f, v_h^p + \delta \frac{h_K}{p_K^2} v_{h\beta}^p)_K + (1 + \delta \frac{h_K}{p_K^2}) \langle u_h^{p-}, v_h^{p+} \rangle_{\partial K_- \setminus \Gamma_-}$$

$$+ \quad (1 + \delta \frac{h_K}{p_K^2}) \langle g, v_h^{p+} \rangle_{\partial K_- \cap \Gamma_-} \tag{2.53}$$

In order to solve (2.37) in this fashion, one must define an ordering of elements that starts at the domain inflow boundary and sweeps through the partition in such a way that u_h^{p-} is known on ∂K_- prior to solving (2.50). Such an ordering always exists (see [33]) and is fairly straightforward to construct. This is the optimal solution technique for solving the linear model problem where element inflow boundaries can be identified a priori. However, an alternate approach is needed for solving the conservation law (1.5) where the fluxes depend on the solution, and thus, element inflow boundaries cannot be identified a priori.

With the aim of solving more general problems in mind, we will solve the linear model problem in a way that is easily extendable to the nonlinear case,

that takes full advantage of the discontinuous approximation, and is amenable to parallel computations; that is, by solving the time-dependent conservation law for the steady-state solution. Since time accuracy is not important in obtaining the steady solution, we use the classical forward or backward Euler time marching with a truncation error of $O(\Delta t^2)$. Let $u^{n+1} = u_h^p(\cdot, t_{n+1})$ where $t_{n+1} = (n+1)\Delta t$ and Δt is the time step increment. Assuming the solution at time t_n is known, then the forward Euler version of the scheme is given by

$$\sum_{K\in\mathcal{P}_h} (u^{n+1}, v)_K = \sum_{K\in\mathcal{P}_h} (u^n, v)_K + \Delta t\,[L(v) - B(u^n, v)] \tag{2.54}$$

and the backward Euler version is given by

$$\sum_{K\in\mathcal{P}_h} (u^{n+1}, v)_K + \Delta t \sum_{K\in\mathcal{P}_h} \tilde{B}_K(u^{n+1}, v) = \sum_{K\in\mathcal{P}_h} (u^n, v)_K + \Delta t \sum_{K\in\mathcal{P}_h} \tilde{L}_K(v) \tag{2.55}$$

To preserve the local character of the method, the inflow boundary terms appearing in the definition of $\tilde{L}_K(v)$ (see 2.53) are evaluated at time level t_n. The initial data, $u^0 = u_h^p(\cdot, 0)$, needed to complete the initial-boundary-value problem is taken to be a uniform field with a value associated with the inflow boundary conditions.

A time-accurate Runge-Kutta time marching scheme for nonlinear conservation laws is described in detail in Chapter 7. It can essentially be written as a sequence of steps in the same form as (2.54). Parallel implementation of the time marching discontinuous Galerkin methods for general hp meshes is described in Chapter 6.

Chapter 3

A Posteriori Error Estimation

The *a priori* estimates derived in the previous chapter are useful for predicting how the error in numerical solutions behaves with h-refinement or p-enrichment. Unfortunately, their usefulness in assessing the accuracy of a given numerical solution is limited since the estimate involves unknown constants and the exact solution we are approximating. Nevertheless, *a priori* error estimates such as (2.42) and interpolation error estimates such as (2.45) have been used extensively as error indicators to drive adaptive methods for hyperbolic problems [16], [43], [36]. Typically the unknown constant is set to unity and some post-processing of the approximate solution is used in place of the exact solution. While the element contributions to these global estimates may provide some relative measure of the local error, this approach in general fails to provide a reliable estimate of the actual error in a particular numerical solution and can be grossly in error.

In this chapter, we derive error estimates which are computed locally on a single element and contribute to a global error estimate which is accurate enough to provide a reliable assessment of the quality of the approximate solution.

3.1 Element Residual Method

The estimates derived here, based on the element residual method, are similiar to those proposed by Bank and Weiser [4] for elliptic problems and Oden, Demkowicz, Strouboulis, and Devloo [38] for solid and fluid mechanics problems. The element residual method was extended to hp-approximations for elliptic problems by Oden, Demkowicz, Rachowicz, and Westerman [37]. A global estimate of the error is obtained by summing element indicators which are the solutions to a local problem with the element residual as data. In references [38] and [37] , the local problem is of the same form as the global problem.

For continuous finite element approximations, the element residual involves fluxes on the boundary of an element. Since the fluxes are multi-valued, an averaged flux is used. Recently, Ainsworth and Oden [1], [2] have shown that it is possible to use a self-equilibrating average flux that results in an error estimate which is equivalent to the actual error and can be asymptotically exact for certain elliptic problems. For a discontinuous approximation, the jump in the element boundary flux arises naturally in the residual, eliminating the need for flux balancing.

The main difficulty with our formulation for hyperbolic conservation laws is that the norms associated with the continuity and coercivity of the bilinear form are different. Therefore, use of different norms makes it impossible to construct a single local problem which results in an upper and lower bound of the error in the same (or an equivalent) norm.

In the following sections we show that it is possible, however, to construct one local problem with a solution that provides a lower bound on the

actual error and another local problem with a solution that provides an upper bound on the actual error. We also show that a local problem based on the original problem results in a local lower bound. Moreover, if the approximation of the solution to this local problem is limited to a certain class, then the estimate is equivalent to another commonly used approach: estimating the error as the difference between a newly contructed (and hopefully more accurate) solution and the approximate solution on hand.

3.2 A Global Lower Bound on the Error

We define a local problem which results in a lower bound on the error in a sense to be defined precisely later. Let $\hat{u}_K \in Q^{p_K}(K)$ denote the approximate solution in element K and $\varphi_K \in V(K)$ be the solution to the following local problem,

$$A_K^L(\varphi_K, v_K) = B_K(e_K, v_K) = L_K(v_K) - B_K(\hat{u}_K, v_K) \qquad \forall v_K \in V(K) \quad (3.1)$$

where

$$A_K^L(\varphi_K, v_K) \stackrel{\text{def}}{=} \frac{h_K}{p_K^2}(\boldsymbol{\beta} \cdot \boldsymbol{\nabla}\varphi_K, \boldsymbol{\beta} \cdot \boldsymbol{\nabla} v_K)_K + \bar{a}(\varphi_K, v_K)_K + \langle \varphi_K, v_K \rangle_{\partial K_-} \quad (3.2)$$

and $\bar{a} > 0$ is a constant. Then

$$A^L(\varphi, v) = \sum_{K \in \mathcal{P}_h} A_K^L(\varphi_K, v_K) \quad (3.3)$$

induces a norm on $V(\mathcal{P}_h)$ which will be referred to as the A^L-norm:

$$||v||_{A^L}^2 = A^L(v, v) \qquad \forall v \in V(\mathcal{P}_h) \quad (3.4)$$

The solution to the local problem (3.1) provides a lower bound on the error in the following sense:

Lemma 6 *Let $\varphi \in V(\mathcal{P}_h)$ be the solution to the following problem:*

$$A^L(\varphi, v) = B(e, v) \qquad \forall v \in V(\mathcal{P}_h) \tag{3.5}$$

There exist positive constants k_1 and r_0 such that if $\frac{h_K}{p_K^2} \leq r_0 \quad \forall K \in \mathcal{P}_h$ then

$$||\varphi||_{A^L} \leq k_1 |||e|||_{1,\beta} \tag{3.6}$$

Proof:

$$\begin{aligned}
||\varphi||^2_{A^L} = A^L(\varphi,\varphi) &= B(e,\varphi) \\
&\leq M_1 \left\{ \sum_{K\in\mathcal{P}_h} \left(1 + \delta \frac{h_K}{p_K^2}\right) |||e|||^2_{1,\beta,K} \right\}^{\frac{1}{2}} \\
&\times \left\{ \sum_{K\in\mathcal{P}_h} \left[\delta \frac{h_K}{p_K^2} ||\varphi_\beta||^2_K + ||\varphi||^2_K \right.\right. \\
&+ \left.\left. \left(1 + \delta \frac{h_K}{p_K^2}\right) \langle\langle \varphi^+ \rangle\rangle^2_{\partial K_-} \right] \right\}^{\frac{1}{2}} \quad \text{from (2.14)} \\
&\leq M_1 (1 + \delta r_0) \max(1, \frac{1}{\sqrt{\bar{a}}}) |||e|||_{1,\beta} ||\varphi||_{A^L}
\end{aligned}$$

The desired inequality (3.6) follows by choosing $k_1 = M_1(1 + \delta r_0)\max(1, \frac{1}{\sqrt{\bar{a}}})$.

∎

3.3 A Global Upper Bound on the Error

For simplicity, the estimates in this section are derived for the case when $\delta = 1$ in (2.8). We construct a local problem which results in an upper bound on the error. Let $\hat{u}_K \in Q^{p_K}(K)$ denote the approximate solution in element K and ψ_K be the solution to the following local problem,

$$A^U_K(\psi_K, v_K) = B_K(e_K, v_K) = L_K(v_K) - B_K(\hat{u}_K, v_K) \quad \forall\, v \in V(K) \tag{3.7}$$

where

$$A^U_K(\psi_K, v_K) \stackrel{\text{def}}{=} \frac{h_K}{p_K^2}(\boldsymbol{\beta} \cdot \boldsymbol{\nabla}\psi_K, \boldsymbol{\beta} \cdot \boldsymbol{\nabla} v_K)_K + \bar{a}(\psi_K, v_K)_K \tag{3.8}$$

and $\bar{a} > 0$ is a constant. Then the A^U-norm is defined as

$$||\psi||^2_{A^U} = A^U(\psi, \psi) = \sum_{K \in \mathcal{P}_h} A^U_K(\psi_K, \psi_K) \tag{3.9}$$

The solution to the local problem (3.7) provides an upper bound on the error in the following sense:

Lemma 7 *Let $\psi \in V(\mathcal{P}_h)$ be the solution to the following problem:*

$$A^U(\psi, v) = B(e, v) \qquad \forall v \in V(\mathcal{P}_h) \tag{3.10}$$

where $\delta = 1$ in the definition of $B(\cdot, \cdot)$ in (2.11). Then there exists a positive constant k_2 such that

$$||\psi||_{A^U} \geq k_2 |||e|||_{hp,\beta} \tag{3.11}$$

Proof: Using (2.18) of Corollary 1,

$$\begin{aligned}
\alpha |||e|||^2_{hp,\beta} \leq B(e,e) &= A^U(\psi, e) \\
&\leq ||\psi||_{A^U} ||e||_{A^U} \\
&= ||\psi||_{A^U} \{ \sum_{K \in \mathcal{P}_h} \frac{h_K}{p_K^2} ||e_\beta||^2_K + \bar{a}||e||^2_K \}^{\frac{1}{2}} \\
&\leq \max(1, \sqrt{\bar{a}}) ||\psi||_{A^U} \{ \sum_{K \in \mathcal{P}_h} \frac{h_K}{p_K^2} ||e_\beta||^2_K + ||e||^2_K \}^{\frac{1}{2}} \\
&\leq \max(1, \sqrt{\bar{a}}) ||\psi||_{A^U} |||e|||_{hp,\beta}
\end{aligned}$$

Choosing $k_2 = \frac{\alpha}{\max(1, \sqrt{\bar{a}})}$ completes the proof. ∎

3.4 A Local Lower Bound on the Error

Recall the bilinear form (2.50) which characterizes the space marching form of the discontinuous Galerkin method:

$$\begin{aligned}\tilde{B}_K(u_h^p, v_h^p) &\stackrel{\text{def}}{=} (u_{h\beta}^p + au_h^p, v_h^p + \delta\frac{h_K}{p_K^2}v_{h\beta}^p)_K \\ &+ (1+\delta\frac{h_K}{p_K^2})\langle u_h^{p+}, v_h^{p+}\rangle_{\partial K_-}\end{aligned}$$

Introducing a local norm,

$$\begin{aligned}||v_K||_{\tilde{B}_K} &\stackrel{\text{def}}{=} \Bigg[\delta\frac{h_K}{p_K^2}||v_{K,\beta}||_K^2 + ||v_K||_K^2 \\ &+ \frac{1}{2}\left(1+\delta\frac{h_K}{p_K^2}\right)\langle\langle v^+\rangle\rangle_{\partial K_-}^2 \\ &+ \frac{1}{2}\left(1+\delta\frac{h_K}{p_K^2}\right)\langle\langle v^-\rangle\rangle_{\partial K_+}^2\Bigg]^{\frac{1}{2}}\end{aligned} \tag{3.12}$$

and using Green's formula, it is easy to show that there exist a constant $C > 0$ such that

$$\tilde{B}_K(v_K, v_K) \geq C||v||_{\tilde{B}_K}^2 \quad \forall v_K \in V(K) \tag{3.13}$$

Now consider the following local problem:

Find $\varphi_K \in V(K)$ such that

$$\tilde{B}_K(\varphi_K, v_K) = B_K(e_K, v_K)\ ,\ \forall v_K \in V(K) \tag{3.14}$$

then φ_K provides a local lower bound on the error in the following sense.

Lemma 8 *Let $\varphi_K \in V(K)$ be the solution to (3.14). Then there exists a constant $k_3 > 0$ such that*

$$||\varphi_K||_{\tilde{B}_K} \leq k_3\left(1+\delta\frac{h_K}{p_K^2}\right)|||e|||_{1,\beta,K} \tag{3.15}$$

Proof: Setting $v_K = \varphi_K$ in (3.14) and using (3.13) yields

$$C||\varphi_K||^2_{\tilde{B}_K} \leq \tilde{B}_K(\varphi_K, \varphi_K) = B_K(e_K, \varphi_K) \tag{3.16}$$

Setting $M_K = \max(1, ||a||_{\infty,K})$ and applying Young's inequality, $ab \leq \frac{1}{4\epsilon}a^2 + \epsilon b^2$, $\epsilon > 0$, to each term in $B_K(e_K, \varphi_K)$ yields

$$B_K(e_K, \varphi_K) \leq \frac{M_K}{4\epsilon}\left(1 + \delta\frac{h_K}{p_K^2}\right)|||e|||^2_{1,\beta,K} + 2M_K\epsilon||\varphi_K||^2_{\tilde{B}_K} \tag{3.17}$$

Selecting $\epsilon < \frac{C}{2M_K}$ in (3.17) and combining with (3.16) completes the proof. ∎

3.5 Approximation of the Local Problems

An approximate solution to the local problem measured in the corresponding norm serves as a local error indicator for an element. Since the discontinuous Galerkin solution satisfies the orthogonality condition,

$$B_K(e, v) = 0 \quad \forall v \in Q^{p_K}(K) \tag{3.18}$$

we must approximate the error indicator with a polynomial of degree $p_K + \sigma_K$ where $\sigma_K \geq 1$ in order for the discrete local problem to have a non-trivial solution. If a complete polynomial of degree $p_K + \sigma_K$ (on the master element) is used to approximate the solution to the local problem, then the discrete local problem requires the solution of a system of order $(p_K + \sigma_K + 1)^2$. This system can be fairly large compared to the system of order $(p_K + 1)^2$ equations used to obtain the approximate solution for which we are estimating the error.

Since $(p_K + 1)^2$ terms on the right hand side of the discrete local problem (corresponding to (3.18)) are zero, we can make a simplification by approximating the solution to the local problem in the space $Q^{p_K+\sigma_K}(K) \setminus Q^{p_K}(K)$.

In other words, the solution to the local problem can be approximated with incomplete polynomials of degree $p_K + \sigma_K$ by neglecting the terms associated with polynomials of degree p_K. This simplification results in a system of $\sigma_K(\sigma_K + 2p_K + 2)$ equations for each element.

The size of the local problem can be further reduced by approximating its solution using only the "bubble" functions in the enriched space denoted by $Q_0^{p_K+\sigma_K}(K) \setminus Q_0^{p_K}(K)$. These are the polynomials in $Q^{p_K+\sigma_K}(K) \setminus Q^{p_K}(K)$ which are zero on the boundary of an element. This additional simplification results in a system of $\sigma_K(\sigma_K + 2p_K - 2)$ equations which is smaller than system of equations used to obtain the approximate solution.

3.6 Remarks Concerning an Alternate Approach

Suppose that an approximation U to the exact solution u can be constructed which is more accurate than the approximate solution on hand, u_h^p. Then a simple estimate of the error, $e = u - u_h^p = u - U + U - u_h^p$, is $\theta = ||U - u_h^p||$ where $||\cdot||$ is any suitable norm. Using the triangle inequality, we have

$$||e|| - ||u - U|| \leq \theta \leq ||e|| + ||u - U||$$

or equivalently

$$1 - \frac{||u - U||}{||e||} \leq \frac{\theta}{||e||} \leq 1 + \frac{||u - U||}{||e||}$$

If $||u - U|| << ||e|| = ||u - u_h^p||$, then $\theta = ||U - u_h^p||$ is a good error estimate with an effectivity index near unity. The main difficulty with this approach is to efficiently construct such a U. One obvious strategy for constructing a more accurate approximation, U, is to re-solve the approximate boundary-value problem on an enriched space.

For continuous finite element approximations, this leads to a global system of equations that is much larger, and therefore much more costly to solve, than the original problem. For a discontinuous approximation, re-solving the problem on an enriched space of complete polynomials is still more costly than the original problem, but is no more costly than solving the local problems in section 3.2-3.4 on the complete polynomial space.

The computational cost of this approach can be further reduced by "freezing" the lower-order solution and re-solving the problem on an incomplete polynomial space of bubble functions. In other words, let $U_K = u_h^p|_K + w_K$ where $w_K \in Q_0^{p_K+\sigma_K}(K) \setminus Q_0^{p_K}(K)$ satisfies

$$B_K(w_K, v) = L_K(v) - B_K(u_h^p, v) \quad \forall v \in Q_0^{p_K+\sigma_K}(K) \setminus Q_0^{p_K}(K) \tag{3.19}$$

In this case, the error estimate is $\theta = ||U - u_h^p|| = ||w||$. Note that this is equivalent to solving the local problem (3.14) on the space of bubble functions. We remark that Peraire and Morgan [44] simply post-process the approximate solution to obtain the degrees-of-freedom (higher-order derivatives) corresponding to the bubble functions.

Chapter 4

An hp-Adaptive Strategy

The hp-adaptive strategy used here is based on a 3-step strategy developed by Oden, Patra, and Feng [39]. The strategy was developed for a large class of elliptic problems and has been shown to yield exponential rates of convergence with respect to CPU time [39]. The hp-adaptive strategy is based on a reliable *a posteriori* error estimate for determining the error in the approximate solution and an *a priori* error estimate for determining how to modify the mesh to improve the solution accuracy to a specified level. The goal of the hp-strategy is to deliver a solution with a specified error in only three steps:

(i) Construct an initial partition $\mathcal{P}_0$ containing $N(\mathcal{P}_0)$ elements. The elements in $\mathcal{P}_0$ can be of uniform $p_K = p_0$ and essentially uniform in $h_K = h_0$. Solve the problem of interest on $V_{p_0}(\mathcal{P}_0)$ and estimate the error.

(ii) Construct a partition $\mathcal{P}_1$ by subdividing each element in $\mathcal{P}_0$ into the number of elements required to equally distribute the error and reduce it to a specified level. Solve the problem on $V_{p_0}(\mathcal{P}_1)$ and estimate the error.

(iii) Enrich the approximation space by increasing p_K for every $K \in \mathcal{P}_1$ in such a way to equally distribute the error in smooth regions and reduce it to the specified level. Solve the problem on the enriched space $V_{p_1}(\mathcal{P}_1)$ and estimate the error.

If the estimated error in the solution is larger than the specified error after the third step, then it is necessary to repeat steps (ii) and (iii) until the desired error is attained. For discontinuous solutions, p-enrichments in step (iii) are confined to elements in regions where the solution is smooth, since higher-order elements at discontinuities may result in oscillatory solutions. Moreover, p-enrichment of elements in regions where the solution is of low regularity does not improve the accuracy of the approximation, as indicated by the riori estimate (2.42).

The data structure used for the resulting hp-meshes is based on the work of Demkowicz, Oden, Rachowicz, and Hardy[19] for continuous finite element approximations. The data structure for the initial mesh consists of nodal coordinates, element connectivities, boundary conditions, a list of neighboring elements, and element orders based on the number of edge and interior degrees of freedom. Refinements are achieved via bisection of an element in the initial mesh and are added using a tree data structure. The data structure routines enforce a mesh irregularity index of 1 and enrich the order of an edge for an element with a neighboring element of higher-order. These two properties are necessary for maintaining continuity of the finite element approximation and are not needed when using the discontinuous Galerkin approximation. The data structure for the degrees of freedom for the discontinuous approximation consists of three arrays to store the vertex, edge, and interior degrees of freedom. For non-uniform p-meshes, the edge (and interior) degrees of freedom are

stored consecutively with integer arrays which provide the address of the first location of the edge (and interior) degrees of freedom in the global array.

We make some basic assumptions before describing the adaptive strategy in detail. First, recall that the norm used in the *a priori* estimate (2.42) includes jump terms on the element inflow boundaries:

$$\left\{ \sum_{K \in \mathcal{P}_h} \left[\frac{h_K}{p_K^2} ||e_\beta||_K^2 + ||e||_K^2 + \langle\langle e^+ - e^- \rangle\rangle_{\partial K_- \setminus \Gamma_-}^2 + \langle\langle e \rangle\rangle_{\partial K \cap \partial\Omega}^2 \right] \right\}^{\frac{1}{2}}$$

$$\leq C \left\{ \sum_{K \in \mathcal{P}_h} \left[\frac{h_K^{2\mu_K}}{p_K^{2\nu_K}} \max\left(1, \frac{h_K}{p_K^2}\right) ||u||_{r,K}^2 \right] \right\}^{\frac{1}{2}} \tag{4.1}$$

For the *a posteriori* estimate we have several choices: the solution to the local problem which yields a lower bound (3.1), the solution to the local problem which yields an upper bound (3.7), and the simple estimate obtained by re-solving the problem on an enriched polynomial space (3.14). Since the norm induced by the lower bound local problem contains the error on the element inflow boundary, and not the jump in the error as in (2.42), we cannot use this estimate to drive our adaptive strategy. Fortunately, the norm induced by the upper bound local problem contains no element boundary terms and the simple estimate can be measured in any norm desired. We will use the norm induced by upper bound local problem with $\bar{a} = 1$ and assume that the meshes at each step in the adaptive procedure are such that $\max\left(1, \frac{h_K}{p_K^2}\right) = 1$. Noting that (2.42) is valid if we drop the jump terms we can write

$$||e||_{AU} = \left\{ \sum_{K \in \mathcal{P}_h} \left[\frac{h_K}{p_K^2} ||e_\beta||_K^2 + ||e||_K^2 \right] \right\}^{\frac{1}{2}} \leq C \left\{ \sum_{K \in \mathcal{P}_h} \left[\frac{h_K^{2\mu_K}}{p_K^{2\nu_K}} ||u||_{r,K}^2 \right] \right\}^{\frac{1}{2}} \tag{4.2}$$

We assume that the *a posteriori* error estimate is a good enough approximation to the actual error to replace the left hand side of (2.42) and treat the inequality as an equality. Admittedly, this may not be a good assumption for coarse meshes and rough solutions, but it provides some means of predicting the structure of the new mesh.

Since the adaptive procedure is based on refinement and then enrichment of an initial mesh, the term $C||u||^2_{r,K}$ remains constant throughout the adaptive process and can be calculated from the estimated error on the initial mesh. Let θ_0 denote the estimated error for the solution $\hat{u}_0 \in V_{p_0}(\mathcal{P}_0)$ in step (i). Then,

$$\theta_0^2 = \sum_{K\in\mathcal{P}_0} \theta_{0,K}^2 = \sum_{K\in\mathcal{P}_0} \frac{h_K^{2\mu_K}}{p_0^{2\nu_K}} C||u||^2_{r,K} = \sum_{K\in\mathcal{P}_0} \frac{h_K^{2\mu_K}}{p_0^{2\nu_K}} \Lambda_K \tag{4.3}$$

or at the element level

$$\Lambda_K = \frac{p_0^{\nu_K}}{h_K^{\mu_K}} \theta_{0,K} \tag{4.4}$$

4.1 The h-Refinement Step

Let η_T denote the target error to be achieved by the entire 3-step strategy. We specify η_T as a percentage of the solution measured in the same norm as the error to assign it some physical relevance. For the h-step, we seek a partition which will deliver an intermediate target error $\eta_h = \alpha\eta_T$ where α is some constant chosen so that $\eta_T < \eta_h$. The partition $\mathcal{P}_1$ is constructed by subdividing each element $K \in \mathcal{P}_0$ into n_K elements such that the error $\theta_1 = \eta_h(||\hat{u}_0||_{AU} + \theta_0)$ is distributed equally among the elements in $\mathcal{P}_1$. Following (4.3), we have

$$\theta_1^2 = \sum_{K\in\mathcal{P}_0} \sum_{L=1}^{n_K} \theta_{1,L}^2 = \sum_{K\in\mathcal{P}_0} \sum_{L=1}^{n_K} \frac{h_L^{2\mu_K}}{p_0^{2\nu_K}} \Lambda_L^2 \tag{4.5}$$

where

$$
\begin{aligned}
h_L &= \frac{h_K}{\sqrt{n_K}} \\
\Lambda_K^2 &= \sum_{L=1}^{n_K} \Lambda_L^2
\end{aligned}
\tag{4.6}
$$

For a mesh which achieves an equally distributed error,

$$
\theta_{1,L} = \frac{\theta_1}{\sqrt{N(\mathcal{P}_1)}}, \; L = 1, \cdots, N(\mathcal{P}_1) \tag{4.7}
$$

where

$$
N(\mathcal{P}_1) = \sum_{K=1}^{N(\mathcal{P}_0)} n_K \tag{4.8}
$$

Combining (4.5),(4.6), and (4.7) yields

$$
n_K^{\mu_K+1} = \frac{h_K^{2\mu_K}}{p_0^{2\nu_K}} \frac{\Lambda_K^2}{\theta_1^2} N(\mathcal{P}_1); \; K = 1, \cdots N(\mathcal{P}_0) \tag{4.9}
$$

Equations (4.8) and (4.9) are solved iteratively to determine n_K for each element $K \in \mathcal{P}_0$.

Remarks:

(i) A value of $n_K \leq 0$ signals that de-refinement is needed to equidistribute the error. Although not implemented in this work, de-refinement significantly decreases the computational cost of the overall process.

(ii) The largest local errors will occur in elements which contain a discontinuity. These elements will receive the highest level of refinement.

(iii) For ease in implementation, the refinement of an element $K \in \mathcal{P}_0$ is limited to 2 levels.

(iv) The parameters $\mu_K = \min(p_0 + \frac{1}{2}, r - \frac{1}{2})$ and $\nu_K = r - 1$ are global constants dictated by the regularity of the exact solution $u \in V(\Omega)$. Formally, (2.42) is not valid when the solution contains a discontinuity on the interior of an element. However, numerical experiments suggest that (2.42) the rate of convergence of the error is $\mu_K = \frac{1}{2}$ when the solution contains a discontinuity which is not alligned with the element interfaces. This value of μ_K is consistent with the finite difference results of Sanders [47]. ∎

4.2 The p-Enrichment Step

Let θ_h denote the estimated error in the solution $\hat{u}_1 \in V_{p_0}(\mathcal{P}_1)$ obtained in step (ii). Treating the *a priori* estimate as an equality,

$$\theta_h^2 = \sum_{K \in \mathcal{P}_1} \theta_{h,K}^2 = \sum_{K \in \mathcal{P}_1} \frac{h_K^{2\mu_K}}{p_0^{2\nu_K}} \Lambda_K^2 \tag{4.10}$$

which gives the constants Λ_K on $\mathcal{P}_1$:

$$\Lambda_K = \frac{p_0^{\nu_K}}{h_K^{\mu_K}} \theta_{h,K}; \; K = 1, \cdots, N(\mathcal{P}_1) \tag{4.11}$$

The error is reduced by constructing a distribution of polynomial orders, p_1, where the polynomial order of each element in $\mathcal{P}_1$ is selected to equally distribute the target error. Setting $\theta_T = \eta_T(||\hat{u}_1||_{A^U} + \theta_h)$ and using the *a priori* estimate, we have

$$\theta_T^2 = \sum_{K \in \mathcal{P}_1} \theta_{T,K}^2 = \sum_{K \in \mathcal{P}_1} \frac{h_K^{2\mu_K}}{p_K^{2\nu_K}} \Lambda_K^2 \tag{4.12}$$

where for an equally distributed error

$$\theta_{T,K} = \frac{\theta_T}{\sqrt{N(\mathcal{P}_1)}} \tag{4.13}$$

Combining (4.11), (4.12), and (4.13) yields the new value p_K for each element in $\mathcal{P}_1$:

$$p_K^{\nu_K} = \frac{p_0^{\nu_K}\theta_{h,K}\sqrt{N(\mathcal{P}_1)}}{\theta_T} \tag{4.14}$$

For smooth solutions, the parameter μ_K in (4.12) depends on p_K which is unknown at this point. Here we use the value which is actually associated with p_0. More discussion on the parameters μ_K and nu_K is given in section 4.4.

For discontinuous solutions, p-enrichments are confined to regions where the solution is smooth since increasing p at discontinuities may result in oscillatory solutions and does not improve the accuracy of the approximation. The local regularity of the solution on each element $K \in \mathcal{P}_0$ is estimated by computing the rate of convergence, $\hat{\mu}_K$, of the local error in steps (i) and (ii):

$$\hat{\mu}_K = \frac{\log\theta_{0,K} - \log\sqrt{\sum_{L=1}^{n_K}\theta_{h,L}^2}}{\log h_K - \log\frac{h_K}{\sqrt{n_K}}}, \quad K = 1,\cdots,N(\mathcal{P}_0) \tag{4.15}$$

From the *a priori* estimate (2.42), the expected rate of convergence is $p_0 + \frac{1}{2}$ if the solution is smooth in $K \in \mathcal{P}_0$. To prohibit p-enrichments in discontinuous regions, we simply set $p_L = p_0, L = 1,\cdots,n_K$ if $\hat{\mu}_K < p_0 + \frac{1}{2}$ for the parent element. The contribution of these elements to the global error therefore remains fixed in the p-step of the adaptive strategy. If this contribution exceeds the target θ_T, then an additional h-step is required before the p-step in order to achieve the target error.

4.3 An hp-step as an Alternative to the p-Step

For smooth solutions or for solutions which contain mild discontinuities, the p-step should be adequate to reduce the global error to the specified level. For problems with strong discontinuities, however, the local error at discontinuities may be significantly large and dominate the global error obtained after the h-step, particularly in the current implementation where a maximum of 2 levels of refinement are permitted.

An alternative to the p-step of the adaptive strategy is an hp-step where h-refinement is performed at the discontinuity and p-enrichment is performed in smooth regions. In this case, the target error is specified as a reduction factor for the error in discontinuous regions and for the smooth region individually. Let η_D denote the normalized error in discontinuous regions and η_S denote the normalized error in smooth regions. Then the target error for the hp-step is specified by the reduction factors α_D and α_S as

$$\eta_T = \sqrt{(\alpha_D \eta_D)^2 + (\alpha_S \eta_S)^2} \tag{4.16}$$

The criteria of $\hat{\mu}_K < p_0 + \frac{1}{2}$, where $\hat{\mu}_K$ is given by (4.15), is used to distinguish discontinuous regions from smooth regions. Equations (4.8) and (4.9), with $N(\mathcal{P}_0)$ replaced by the number of elements in the discontinuous region, are used to determine the number of elements required to reduce the error in discontinuous regions to $\alpha_D \eta_D$. Equation (4.14), with $N(\mathcal{P}_1)$ replaced by the number of elements in the smooth region, is used to determine the values of p_K required to reduce the error in the smooth region to $\alpha_S \eta_S$. This approach is referred to as an hhp-adaptive strategy.

4.4 Selection of the Parameters

Formally, the parameters μ_K and ν_K depend on the global regularity of the solution. However, the rate of convergence of the local error depends on the local regularity of the solution. For piecewise continuous solutions, the rate of convergence of the local error varies greatly between the smooth regions of the solution and some small neighborhood around discontinuities. Using global values of these parameters based on an irregular solution results in over-refinement of smooth regions while using global values based on smooth solutions results in under-refinement of discontinuities. Here we use local values of μ_K and ν_K which are initially computed for a uniform h-refinement and a uniform p-enrichment of a coarse mesh. These local values are passed onto the initial mesh used for the adaptive strategy. Local values of μ_K are then re-computed after the h-step using (4.15). These are the values used in (4.12) for the p- or hp-step. While there is little theoretical justification for using local values, numerical results indicate that the approach works quite well for solutions with discontinuities.

Selection of the reduction factor α used to determine the intermediate target error for the h-step of the adaptive strategy is important in obtaining an optimal mesh. Specifying a value of α which gives an intermediate error which is closer to the target error than it is to the initial error will result in meshes with mostly h-refinement. Specifying a value of α which gives an intermediate target error which is closer to the initial error than it is to the target error leads to meshes with little h-refinement and elements with large values of p_K. Numerical experiments for elliptic problems suggest that the optimal choice is $\alpha = \frac{\mu}{\nu}$, where μ and ν are the rates of convergence of the global error. [41]

Chapter 5

Numerical Examples

The discontinuous Galerkin method is used to solve several examples to verify the *a priori* error estimates derived in Chapter 2, and to investigate the performance of the the *a posteriori* error estimates of Chapter 3 and the hp-adaptive strategy of Chapter 4. The reliability of the *a posteriori* error estimates is measured by the effectivity index which is the ratio of the estimated error to the exact error. A reliable estimate is one for which the effectivity index is close to one.

5.1 Example 1

We solve the linear model problem (2.1) with the following data:

(i) $\Omega = (-1,1) \times (-1,1)$

(ii) $\boldsymbol{\beta} = (0.8, 0.6)^T$

(iii) $a(\mathbf{x}) = 1.0$

(iv) $g = 1.0$

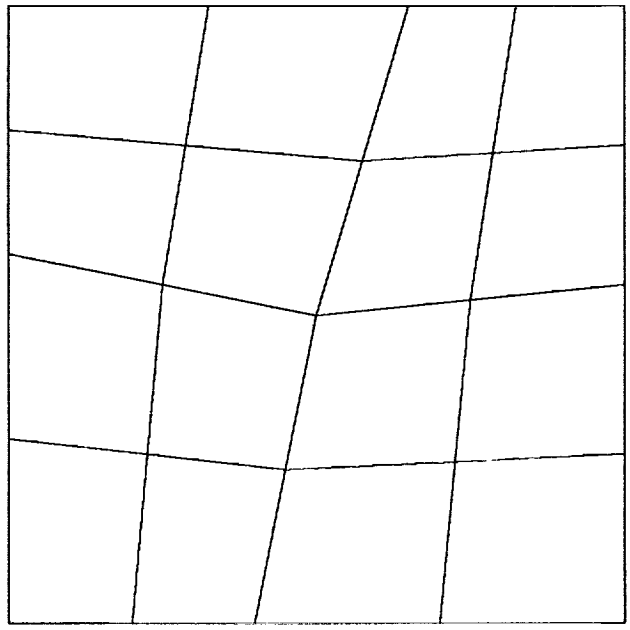

Figure 5.1: Quadrilateral element mesh used for quasi-uniform refinements.

The source term f is chosen so that the exact solution to (2.1) is the $C^\infty(\Omega)$ function,

$$u(x,y) = 1 + \sin\left(\frac{\pi}{8}(1+x)(1+y)^2\right) \tag{5.1}$$

The *a priori* error estimate (2.42) is verified by solving the problem for a sequence of uniform h-refinements and p-enrichments of a mesh of square elements and quasi-uniform h-refinements and p-enrichments of the mesh of quadrilateral elements shown in Fig. 5.1. The mesh-dependent norm of the actual error in the solution obtained with varying h and p is listed in Table 5.1 for the square element mesh and in Table 5.2 for the quadrilateral element mesh.

Mesh	$-\log h$	$-log\ \lvert\lvert\lvert u-u_h\rvert\rvert\rvert_{hp,\beta}$			
		$p=1$	$p=2$	$p=3$	$p=4$
2×2	0.000	——	——	1.8323	2.2787
4×4	0.301	0.5552	1.7066	2.5426	3.6065
8×8	0.602	0.9692	2.3909	3.5467	4.9612
16×16	0.903	1.4003	3.1163	4.5834	6.3047
32×32	1.204	1.8412	3.8574	——	——

Table 5.1: Example 1 - Error using uniform hp meshes.

Mesh	$-\log h$	$-log\ \lvert\lvert\lvert u-u_h\rvert\rvert\rvert_{hp,\beta}$			
		$p=1$	$p=2$	$p=3$	$p=4$
2×2	-0.2116	——	0.8586	1.7402	2.2831
4×4	0.0689	0.5153	1.5930	2.5395	3.4998
8×8	0.347	0.9571	2.3641	3.5814	4.9723
16×16	0.641	1.3913	3.0955	4.6208	6.3196
32×32	0.938	1.8129	3.7870	——	——

Table 5.2: Example 1 - Error using quasi-uniform h and uniform p meshes.

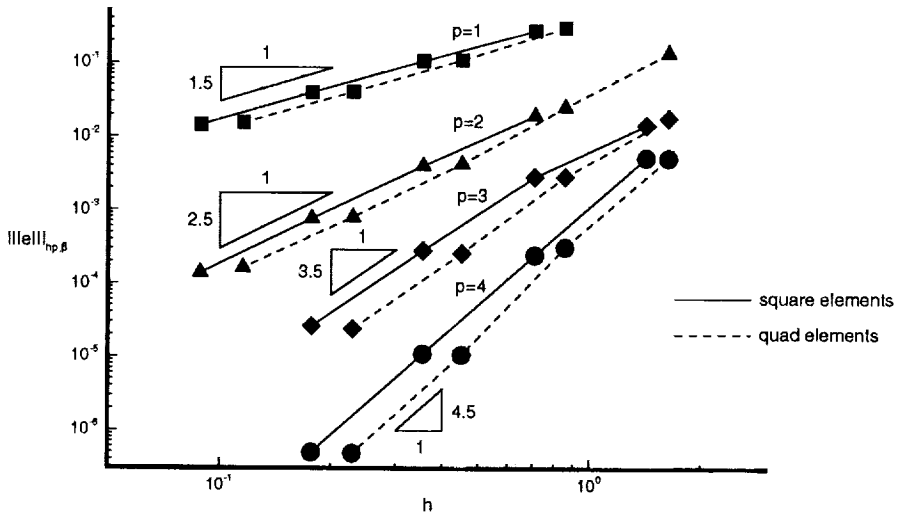

Figure 5.2: Example 1- Rate of convergence of error for fixed p.

To verify the estimate (2.42), first consider the case when p_K is fixed and h_K is varied. According to (2.42), $|||e|||_{hp,\beta} \leq Ch_K^{p_K+\frac{1}{2}}||u||_{r,\Omega}$. This is verified in Fig. 5.2 where $|||e|||_{hp,\beta}$ is shown as a function of h_K. On the log-log scale, the slope of the lines corresponding to a fixed value of p_K is indeed $p_K + \frac{1}{2}$ for both the uniform and quasi-uniform meshes. Next consider the case when h_K is fixed and p_K is varied. In this case, the estimate (2.42) reduces to $|||e|||_{hp,\beta} \leq C{p_K}^{-r+1}||u||_{r,\Omega}$. Since $u \in C^\infty(\Omega)$, exponential rates of convergence are expected. This is confirmed in Fig. 5.3 where the curves corresponding to $|||e|||_{hp,\beta}$ as a function of p_K have a slope on the log-log scale which increases as p_K increases. These results are combined in Fig. 5.4 where $|||e|||_{hp,\beta}$ is shown as a function of the total number of unknowns in the solution. The solid lines represent h-refinements for a fixed p and the dashed lines represent p-enrichment for a fixed h. Clearly for smooth solutions, higher-order accuracy

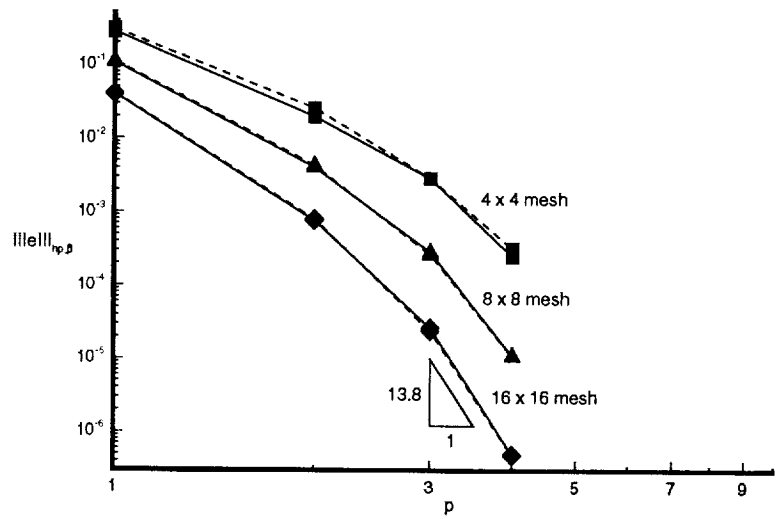

Figure 5.3: Example 1- Rate of convergence of error for fixed h.

is achieved for the same number of unknowns using higher-order elements.

Next we investigate the performance of the *a posteriori* error estimates in Chapter 3. Recall that the complete polynomial space $Q^{p_K+\sigma_K}(K)$ or the incomplete space $Q^{p_K+\sigma_K}(K)\setminus Q^{p_K}(K)$, $\sigma_K \geq 1$ may be used in approximating the solution to the local problem. The effect of approximating the local problem on the performance of the error estimate for the lower bound (3.1) is shown in Table 5.3. The effectivity indices listed in Table 5.3 are greater than one for all values of σ_K when the complete polynomial space is used and less than one for small values of σ_K when the incomplete polynomial space is used. Note that the effectivity index is closest to one for the complete polynomial space with $\sigma_K = 1$. The effect of approximating the local problem on the performance of the error estimate for the upper bound (3.7) is shown in Table 5.4. The effectivity indices for the upper bound estimate are significantly larger than

			$\hat{\varphi}_K \in Q^{p_K+\sigma_K}(K)$	$\hat{\varphi}_K \in Q^{p_K+\sigma_K}(K) \setminus Q^{p_K}(K)$
Mesh	p_K	σ_K	η_L	η_L
8×8	1	1	1.0938	0.7628
8×8	1	2	1.1272	0.8921
8×8	1	3	1.1347	0.9788
8×8	1	4	1.1372	1.0175
16×16	1	1	1.1765	0.7933
16×16	1	2	1.2229	0.9492
16×16	1	3	1.2340	1.0465
16×16	1	4	1.2378	1.0898
8×8	2	1	1.1224	0.9555
8×8	2	2	1.2009	1.0711

Table 5.3: Example 1 - Effect of the approximation of the local problem for the lower bound on the effectivity index.

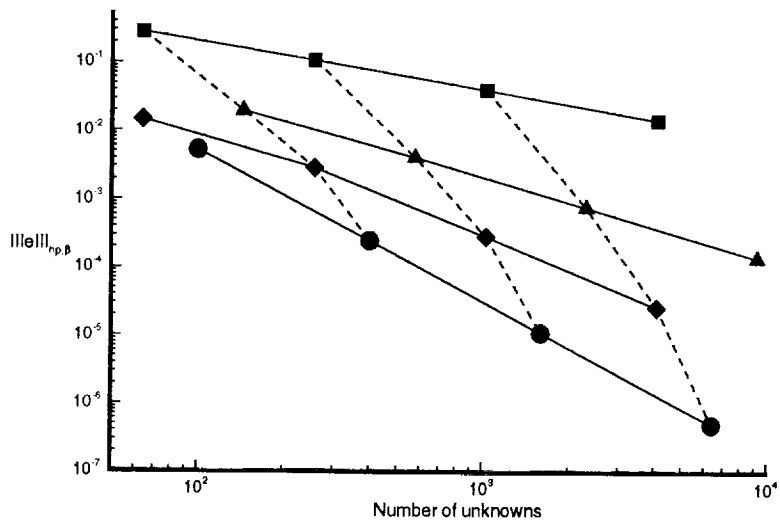

Figure 5.4: Example 1- Rate of convergence of error with number of unknowns.

one when the complete polynomial space is used and close to one when the incomplete polynomial space with $\sigma_K = 1$ is used to approximate the solution to the local problem.

Next we verify that the error estimate exhibits the same rates of convergence as the actual error with h-refinement or p-enrichment. Based on the results from above, the error is estimated by solving the lower bound local problem in $Q^{p_K+1}(K)$ and by solving the upper bound local problem in $Q^{p_K+1}(K) \setminus Q^{p_K}(K)$. The estimated error for a sequence of h-refinements of meshes with fixed p is shown as a function of the mesh size in Fig. 5.5. The slope of the lines is $p + \frac{1}{2}$ as in the case of the actual error (see Fig. 5.2). The estimated error for a sequence of p-enrichments of a uniform mesh is shown in Fig. 5.6 where the same behavior as the actual error (see Fig. 5.3) is observed.

			$\hat{\psi}_K \in Q^{p_K+\sigma_K}(K)$	$\hat{\psi}_K \in Q^{p_K+\sigma_K}(K) \setminus Q^{p_K}(K)$
Mesh	p_K	σ_K	η_U	η_U
8×8	1	1	4.1911	1.0536
8×8	1	2	4.3603	1.3551
8×8	1	3	5.1297	2.0930
8×8	1	4	5.3218	2.6803
16×16	1	1	6.4441	1.1238
16×16	1	2	6.6729	1.4980
16×16	1	3	7.9048	2.8298
16×16	1	4	8.1157	3.6008
8×8	2	1	2.6353	1.1957
8×8	2	2	3.7052	1.4012

Table 5.4: Example 1 - Effect of the approximation of the local problem for the upper bound on the effectivity index.

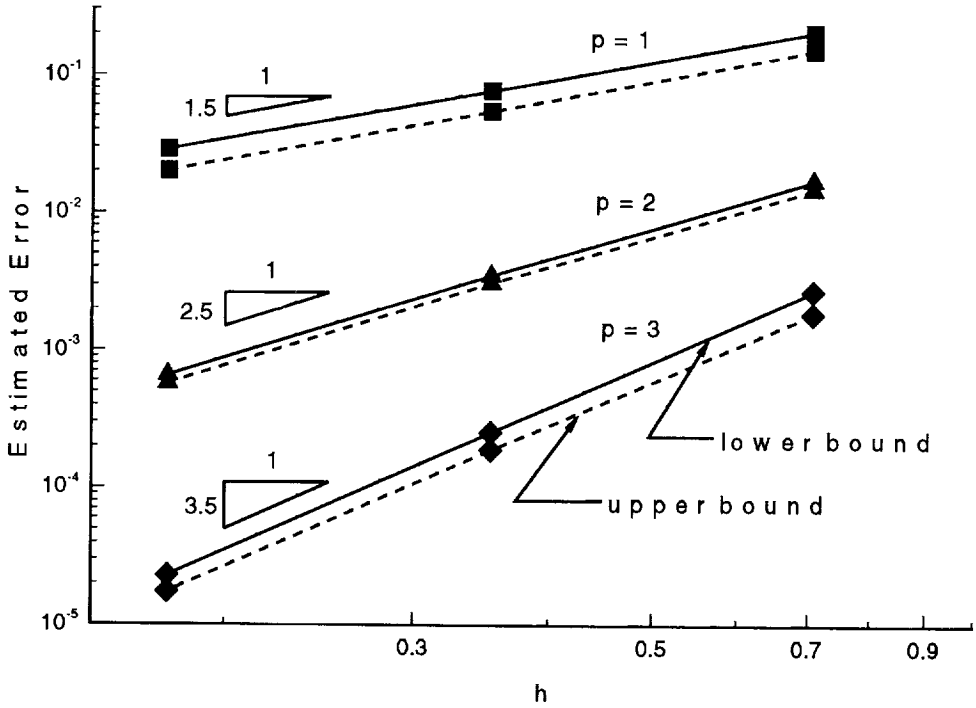

Figure 5.5: Example 1 - Rate of convergence of the estimated error with uniform h-refinements.

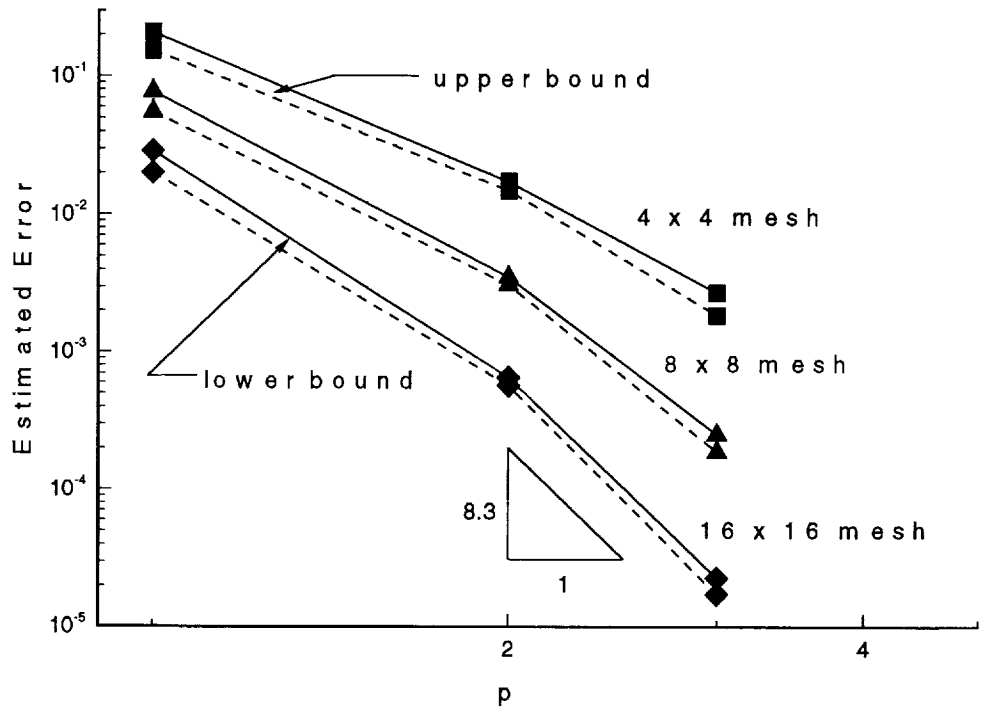

Figure 5.6: Example 1 - Rate of convergence of the estimated error with uniform p-enrichments.

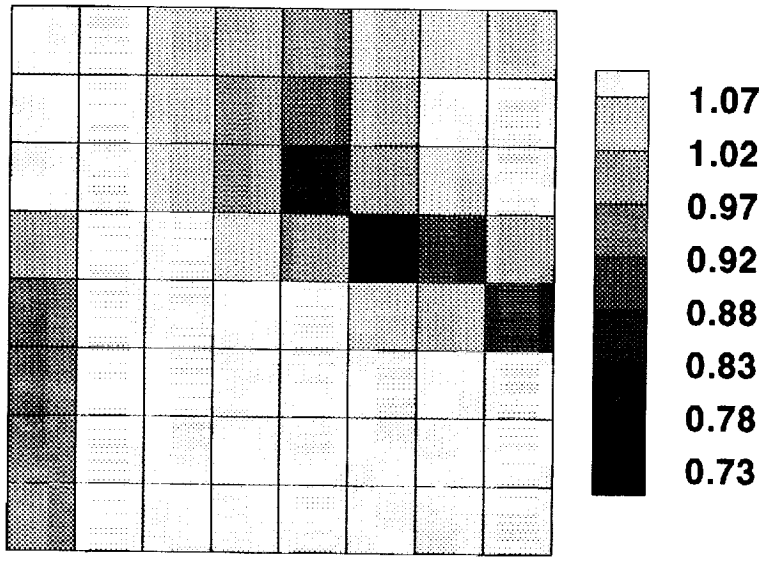

Figure 5.7: Example 1 - Local effectivity index for error estimate based on the upper bound local problem. (8×8 mesh, $p = 1$)

While the theory developed thusfar applies to global error estimates, local effectivity indices near unity are desired in order to use the estimate to drive an effective adaptive strategy. The local (element) effectivity index for the error estimate based on the upper bound local problem (3.7) using the incomplete polynomial space $Q^{p_K+1}(K) \setminus Q^{p_K}(K)$ is shown for a uniform 8×8 element $p = 1$ mesh in Fig. 5.7, for a uniform 8×8 element $p = 2$ mesh in Fig. 5.8, and for a uniform 16×16 element $p = 1$ mesh in Fig. 5.9. For all cases investigated, the local effectivity index is close to one except in a few isolated elements. This indicates that the error estimate is reliable enough to drive the hp-adaptive strategy. Therefore, the solution to the upper bound local problem on the incomplete polynomial space with $\sigma_K = 1$ will be used throughout to drive the hp-adaptive strategy.

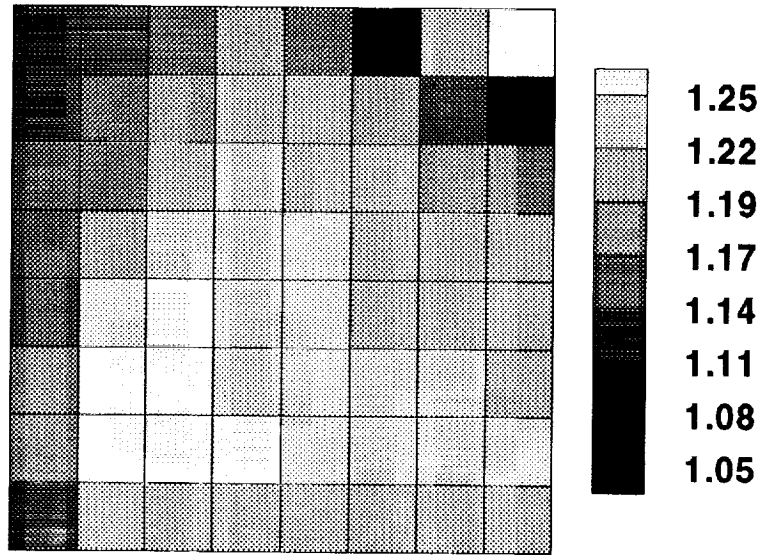

Figure 5.8: Example 1 - Local effectivity index for error estimate based on the upper bound local problem. (8×8 mesh, $p = 2$)

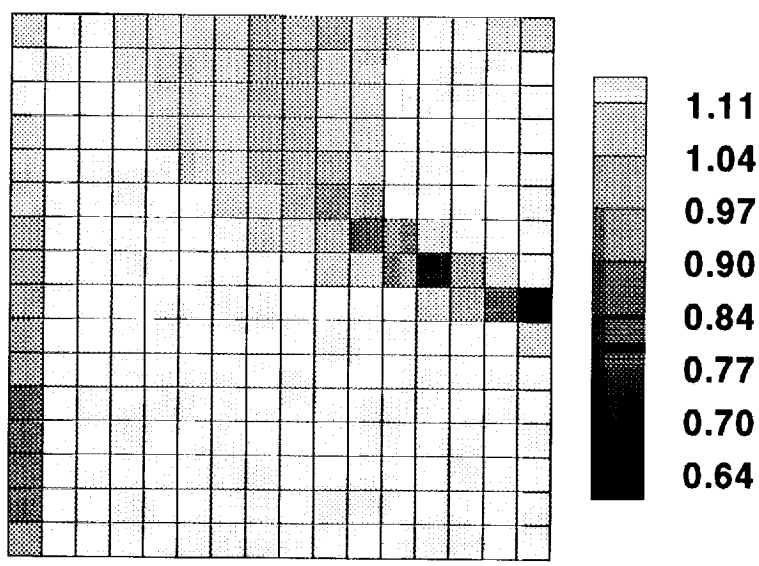

Figure 5.9: Example 1 - Local effectivity index for error estimate based on the upper bound local problem. (16×16 mesh, $p = 1$)

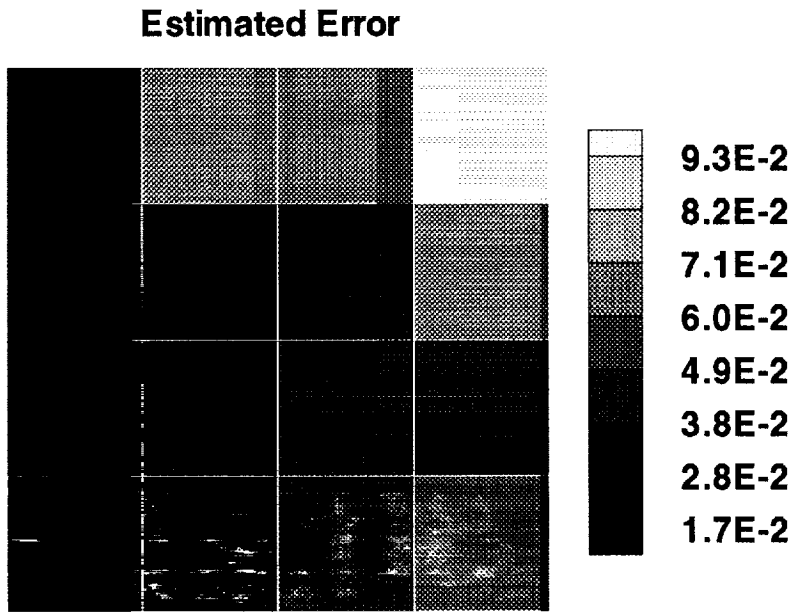

Figure 5.10: Example 1 - Error distribution on initial mesh.

The results of applying the adaptive strategy described in Chapter 4 to this problem are summarized in Table 5.5. The normalized error listed in the table is the ratio of the global error to the sum of the global solution and the error in the norm associated with the local problem. Starting with the estimated error on an initial mesh of 4×4 $p = 1$ elements, shown in Fig. 5.10, a target error of 1.5 percent is specified. An estimated error of 1.2 percent is actually achieved on the resulting h-adapted mesh (see Fig. 5.11). For the p-step of the adaptive strategy, a target error of 0.1 percent is specified. An estimated error of 0.11 percent is actually achieved on the p-adapted mesh (see Fig. 5.12). The distribution of the error on the adapted meshes, shown in Figs. 5.11 and 5.12, is also reduced by an order of magnitude at each adaptive step.

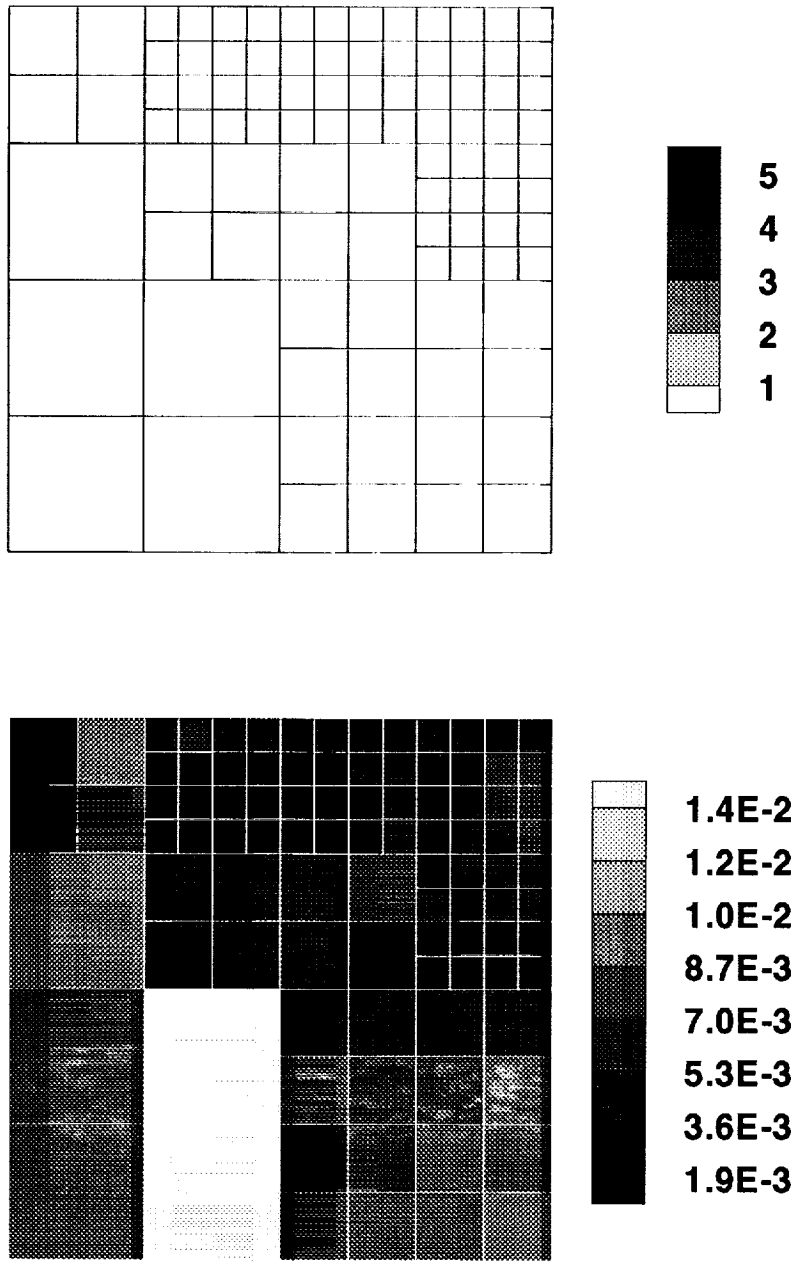

Figure 5.11: Example 1 - Mesh and error distribution after the h-step.

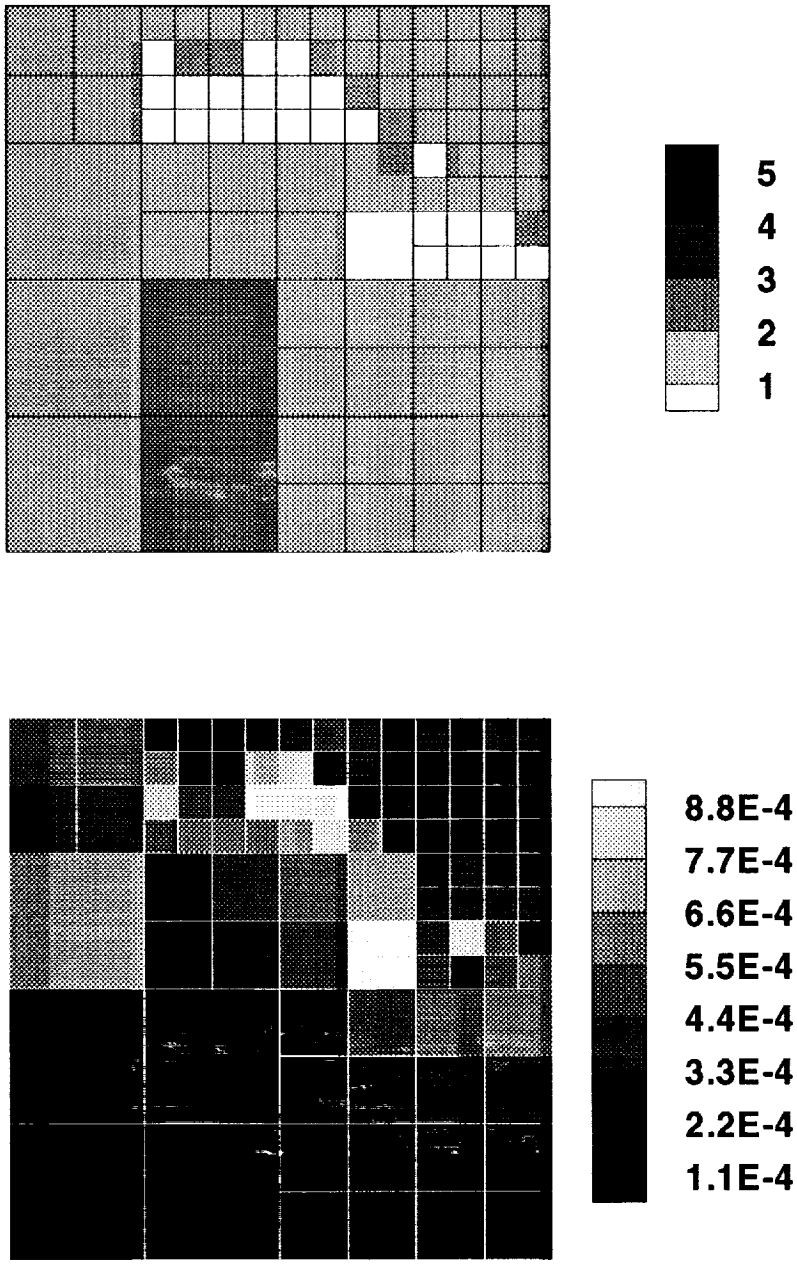

Figure 5.12: Example 1 - Mesh and error distribution after the p-step.

5.2 Example 2

We solve the linear model problem (2.1) with the following data:

(i) $\Omega = (-1,1) \times (-1,1)$

(ii) $\boldsymbol{\beta} = (1.0, 0.0)^T$

(iii) $a(\mathbf{x}) = 1.0$

(iv) $g = \begin{cases} 3e^{-5(1+y^2)} & \text{if } y < 0 \\ -3e^{-5(1+y^2)} & \text{otherwise} \end{cases}$

The source term f is chosen so that the exact solution to (2.1) is the discontinuous function,

$$u(x,y) = \begin{cases} 3e^{-5(x^2+y^2)} & \text{if } y < 0 \\ -3e^{-5(x^2+y^2)} & \text{otherwise} \end{cases} \tag{5.2}$$

The discontinuity is aligned with element interfaces at $y = 0$ to illustrate the advantage of using a discontinuous method to capture discontinuities, particularly if the adaptive scheme includes some shock fitting which aligns the grid with the discontinuity.

The problem was solved using a variety of uniform meshes with h-refinements, p-enrichments, and the hp-adaptive strategy with no special treatment at the shock. The error histories for two hp-adaptive solutions with different initial meshes are listed in Tables 5.6 and 5.7. For both cases, the target error was achieved at each step in the adaptive process. Note also that the global effectivity index is near unity for all steps.

The rate of convergence of the estimated and exact error is compared in Fig. 5.13. The exact error (denoted by a solid line in the figure) and the

Adaptive step	Target normalized error	Exact error $\|\|e\|\|_{A_U}$	Estimated error $\|\|\psi\|\|_{A_U}$	Achieved normalized estimated error $\frac{\|\|\psi\|\|_{A_U}}{\|\|\hat{u}\|\|_{A_U}+\|\|\psi\|\|_{A_U}}$
Initial 4×4 $p = 1$ mesh	——	0.1663	0.2078	0.03786
h-refinement	0.015	0.03619	0.03847	0.012105
p-enrichment	0.001	0.00377	0.00355	0.001116

Table 5.5: Example 1 - Error history for an adaptive *hp* solution.

Adaptive step	Target normalized error	Achieved normalized error	Estimated error $\|\|\psi\|\|_{A_U}$	Effectivity index
Initial 4×4 mesh, $p = 2$	——	0.091	0.371	1.055
h-refinement	0.05	0.031	0.127	1.073
p-enrichment	0.005	0.0029	0.012	1.424

Table 5.6: Example 2 - Error history for an adaptive *hp* solution starting from a uniform 4×4 mesh, $p = 2$.

Adaptive step	Target normalized error	Achieved normalized error	Estimated error $\|\|\psi\|\|_{A_U}$	Effectivity index
Initial 8×8 mesh, $p = 1$	——	0.154	0.616	0.998
h-refinement	0.075	0.033	0.137	0.996
p-enrichment	0.005	0.0055	0.023	0.901

Table 5.7: Example 2 - Error history for an adaptive hp solution starting with a uniform 8×8 mesh, $p = 1$.

estimated error (denoted by a dashed line) are in close agreement, indicating the reliablilty of the estimate. Note that with the discontinuity aligned with element interfaces, the error behaves as if the solution is smooth, that is, algebraic rates of convergence are achieved with respect to mesh refinements, and exponential rates of convergence are achieved with respect to p-enrichments. In this case, the most significant error reduction with fewest degrees of freedom will result by specifying a target error for the h-step which is closer to the initial error than to the final target error. This is verified by the two curves corresponding to the hp-adaptive solutions in Fig. 5.13. Results of the hp-adaptive solution from the initial 8×8 element $p = 1$ mesh are shown in Figs. 5.14 - 5.20. The estimated error in the solution on the initial mesh is shown in Fig. 5.14 with the corresponding effectivity index shown in Fig. 5.15.

For the h-step in the adaptive procedure, a normalized target error of 7.5 percent resulted in the mesh shown in Fig. 5.16. The estimated error in the solution obtained on the h-adapted mesh is also shown in Fig. 5.16 and the corresponding effectivity index is shown in 5.17. Poor local error estimates

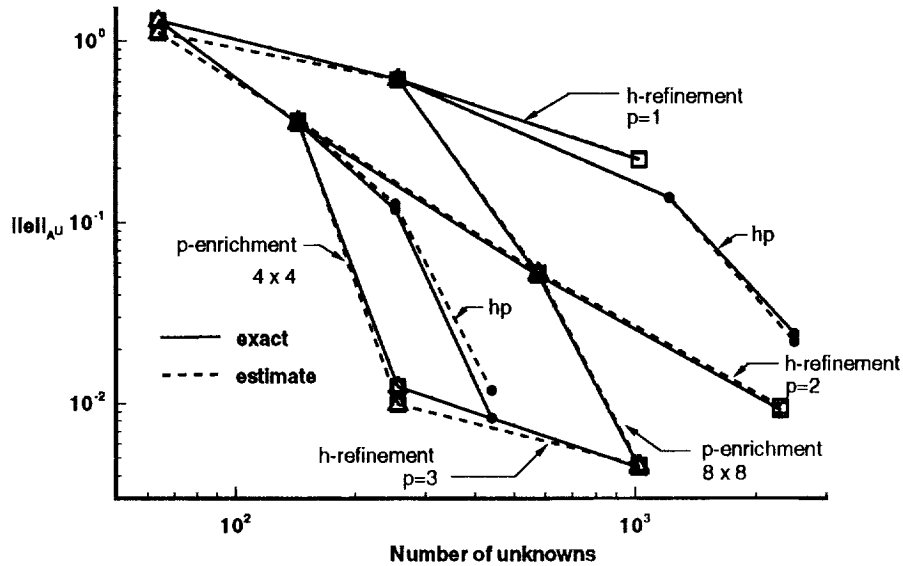

Figure 5.13: Example 2 - Rate of convergence of the error with respect to the total number of unknowns.

are observed in the two parallel vertical regions indicated by the darker shades in Fig. 5.17. Moreover, the local error is significantly underestimated in these regions, possibly due to a failure of the procedure to adequately handle the very high changes in gradients in these regions. The global effectivity indices, however, are quite satisfactory with effectivity indices very near unity.

For the p-step, a normalized target error of 0.5 percent resulted in the distribution of p shown in Fig. 5.18. The estimated error for the solution obtained on the hp-mesh and corresponding local effectivity index are shown in Figs. 5.19 and 5.20. The same degradation of the local effectivity indices are observed in the regions where u_β is large. Moreover, there is a slight decrease in the global effectivity index, however, the global value is still quite acceptable.

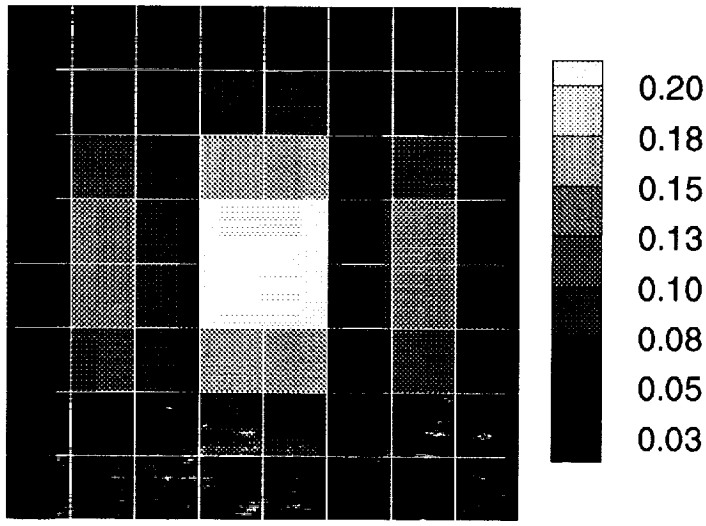

Figure 5.14: Example 2 - Estimated error on initial 8×8 mesh, $p = 1$.

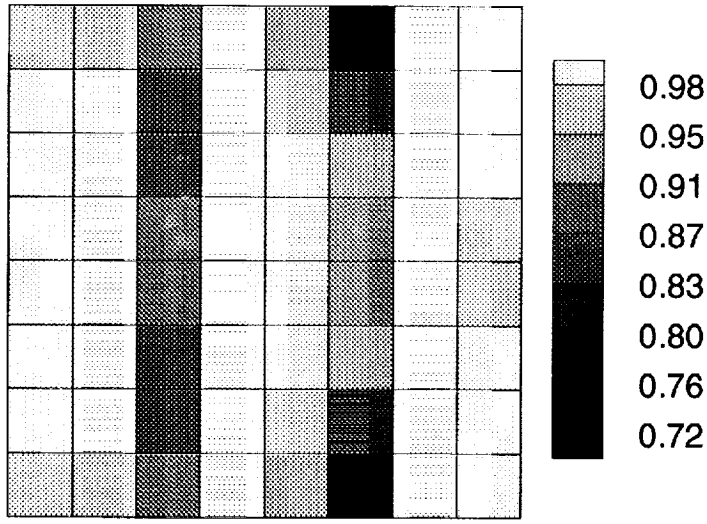

Figure 5.15: Example 2 - Local effectivity index for error estimate on initial 8×8 mesh, $p = 1$.

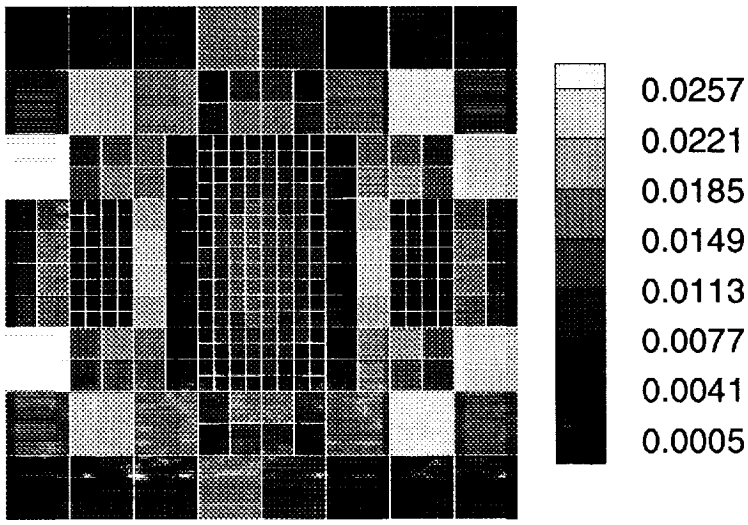

Figure 5.16: Example 2 - Estimated error on h-adapted mesh.

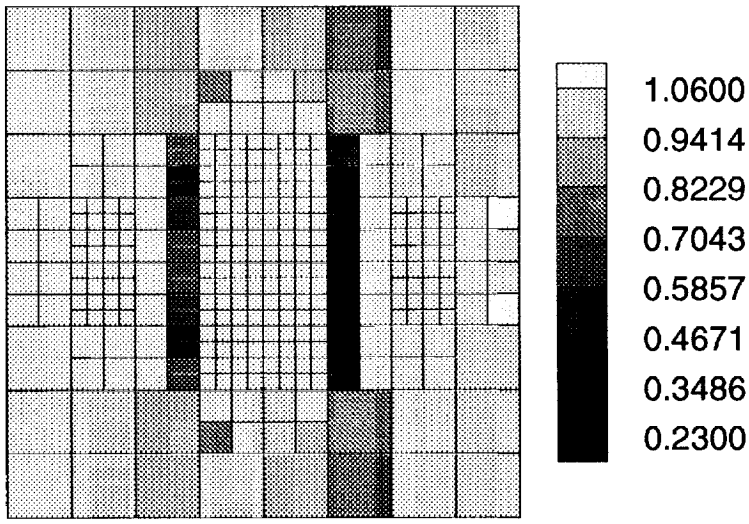

Figure 5.17: Example 2 - Local effectivity index for error estimate on h-adapted mesh.

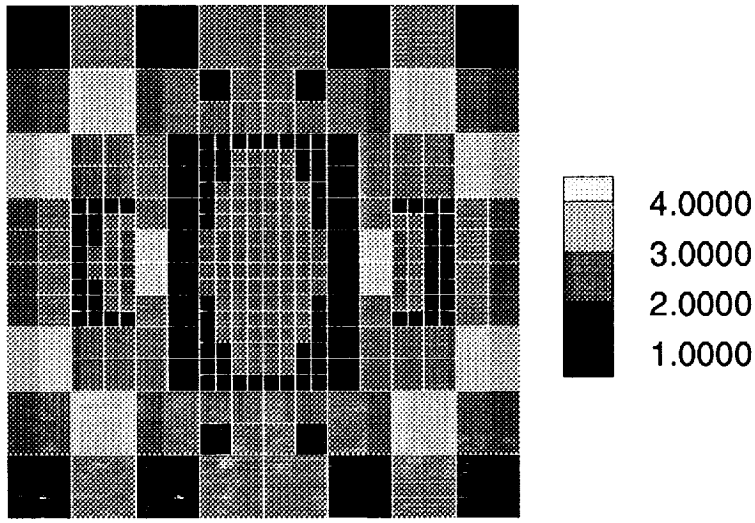

Figure 5.18: Example 2 - Adaptive p-enriched mesh.

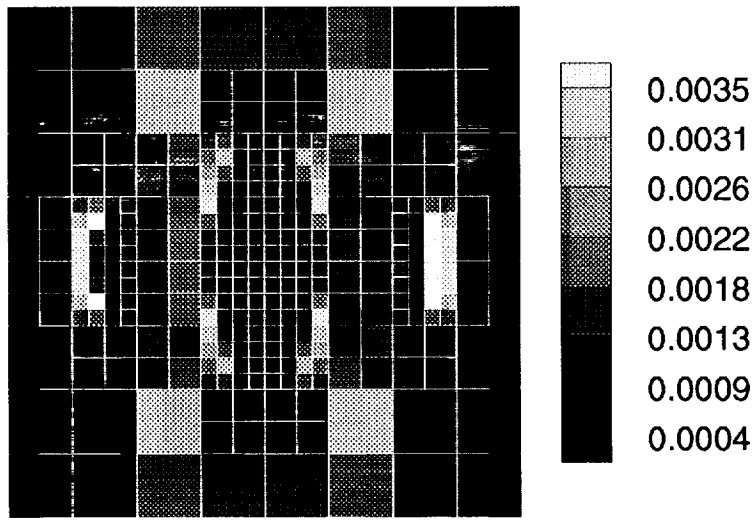

Figure 5.19: Example 2 - Estimated error on adaptive p-enriched mesh.

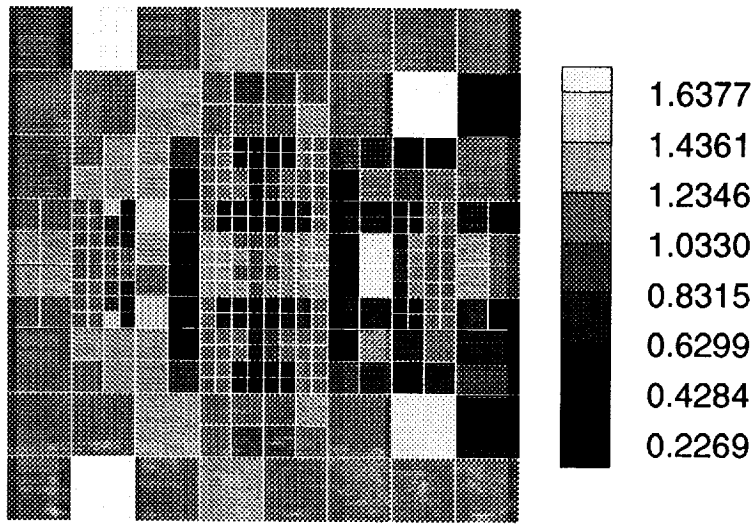

Figure 5.20: Example 2 - Local effectivity index on adaptive p-enriched mesh.

5.3 Example 3

The following data is used in (2.1):

(i) $\Omega = (-1,1) \times (-1,1)$

(ii) $\boldsymbol{\beta} = (\frac{\sqrt{2}}{2}, \frac{\sqrt{2}}{2})^T$

(iii) $a(\mathbf{x}) = 1.0$

(iv) $g(x,y) = \begin{cases} 5e^{-[\frac{1}{4}+y^2]} + 3e^{-[1+(y-\frac{1}{2})^2]} & x = -1 \\ -1 - 8e^{-5[(x-\frac{1}{2})^2+\frac{1}{4}]} & y = -1 \end{cases}$

The source term f in (2.1) is chosen so that the exact solution is a function which is discontinuous along the domain diagonal given by

$$u(x,y) = \begin{cases} 5e^{-[(x+\frac{1}{2})^2+y^2]} + 3e^{-[x^2+(y-\frac{1}{2})^2]} & \text{if } y > x \\ -1 - 8e^{-5[(x-\frac{1}{2})^2+(y+\frac{1}{2})^2]} & \text{otherwise} \end{cases} \tag{5.3}$$

The global effectivity index for the estimate obtained by solving the upper bound local problem in the space $Q^{p_K+1}(K)\backslash Q^{p_K}(K)$ for several uniform hp meshes is listed in Table 5.8 which shows that the global error is slightly under-estimated. Results at each step in the adaptive strategy, shown in Figs. 5.21 - 5.27, show that the under-estimation of the global error is primarily due to the under-estimation of the local error at the discontinuity. A summary of the hp-strategy is listed in Table 5.9. Note that while the adaptive strategy is able to reduce the error to the target value in the h-step, the achieved error after the p-step largely represents the remaining error in the discontinuity after the h-step.

The error achieved by the adaptive strategy is compared to uniform refinements of $p = 1$ and $p = 2$ meshes in Fig. 5.28. This plot shows that the rate at which the error is reduced in the p-step is much higher than is possible using $h-$refinements alone. Moreover, the main source of the error in the final solution is attributed to the discontinuity (see Fig. 5.26. In Chapter 6, we solve a similar problem on a parallel computer and use the hhp-adaptive strategy described in Chapter 4 to reduce the error in solution over the entire domain.

5.4 Example 4

The following data is used for (2.1):

(i) Ω is an equilateral triangle with side length of 2 and the base aligned with the x-axis

(ii) $\boldsymbol{\beta} = (\frac{\sqrt{2}}{2}, \frac{\sqrt{2}}{2})^T$

Mesh	p_K	$\|\|\hat{\psi}\|\|_{A^U}$	$\|\|e\|\|_{A^U}$	η_U
4×4	1	3.01325	3.81716	0.79
4×4	2	1.49536	1.97645	0.76
8×8	1	1.62507	2.10238	0.77
8×8	2	0.82209	1.35611	0.61
16×16	1	0.88158	1.37317	0.64
16×16	2	0.63044	1.00438	0.63
32×32	1	0.85472	1.01102	0.85

Table 5.8: Example 3 - Error estimate obtained by approximating the upper bound local problem in $Q^{p_K+1}(K) \setminus Q^{p_K}(K)$.

Adaptive step	Target normalized error	Achieved normalized error	Estimated error $\|\|\psi\|\|_{A_U}$	Effectivity index
Initial 8×8 element $p = 1$ mesh	—	0.118	1.625	0.77
h-refinement	0.05	0.048	0.673	0.63
p-enrichment	0.03	0.038	0.541	0.55

Table 5.9: Example 3 - Error history for an adaptive hp solution starting from a uniform 8×8 mesh, $p = 1$.

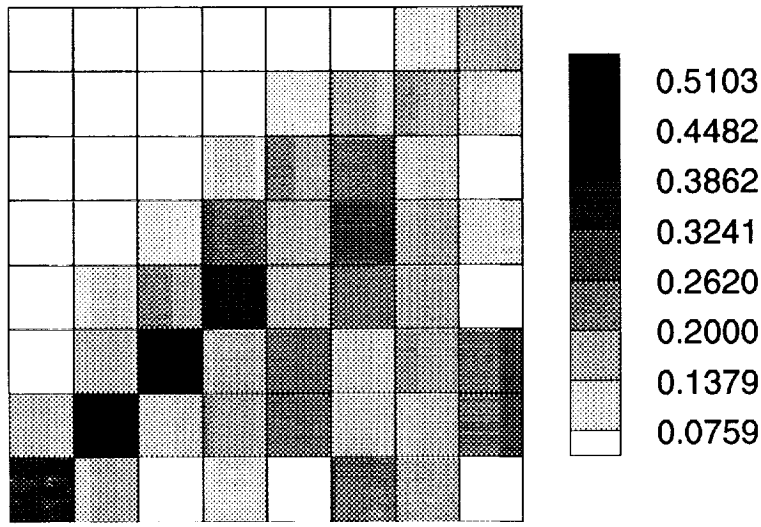

Figure 5.21: Example 3 - Estimated error on initial 8×8 mesh, $p = 1$.

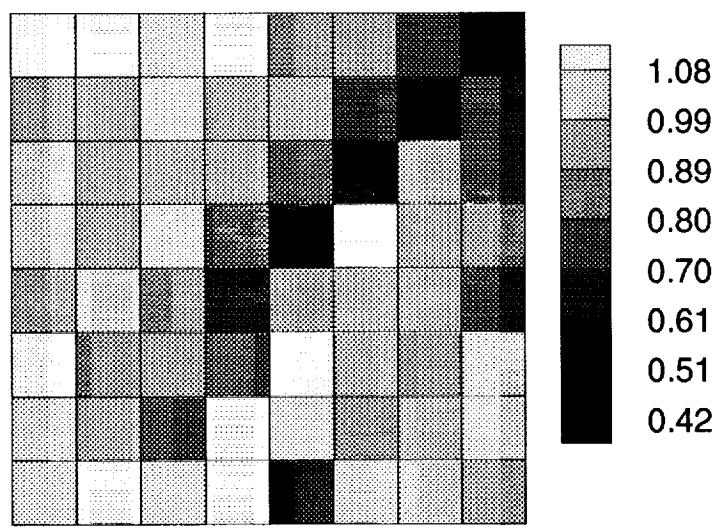

Figure 5.22: Example 3 - Local effectivity index on initial 8×8 mesh, $p = 1$.

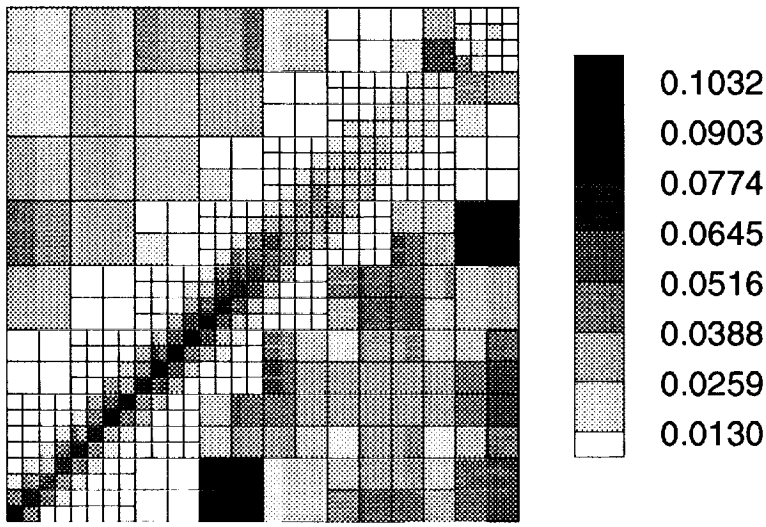

Figure 5.23: Example 3 - Estimated error on h-adapted mesh.

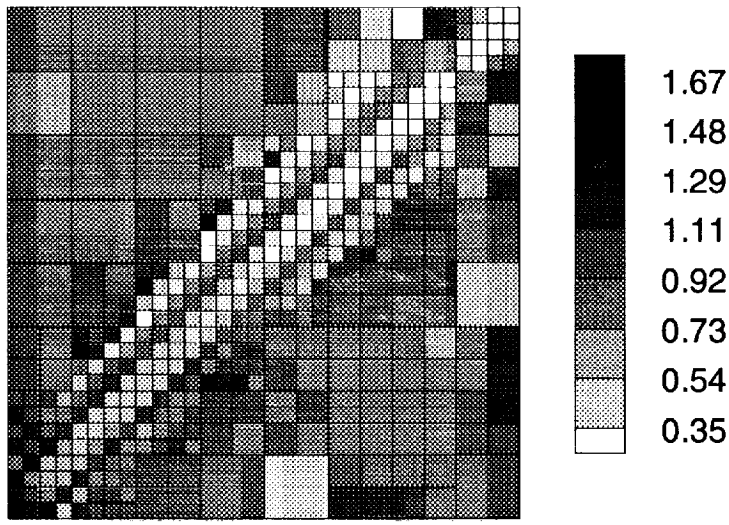

Figure 5.24: Example 3 - Local effectivity index on h-adapted mesh.

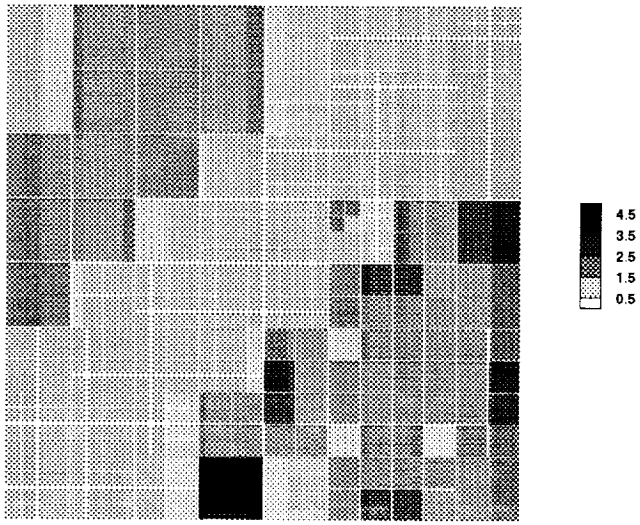

Figure 5.25: Example 3 - Final p-adapted mesh.

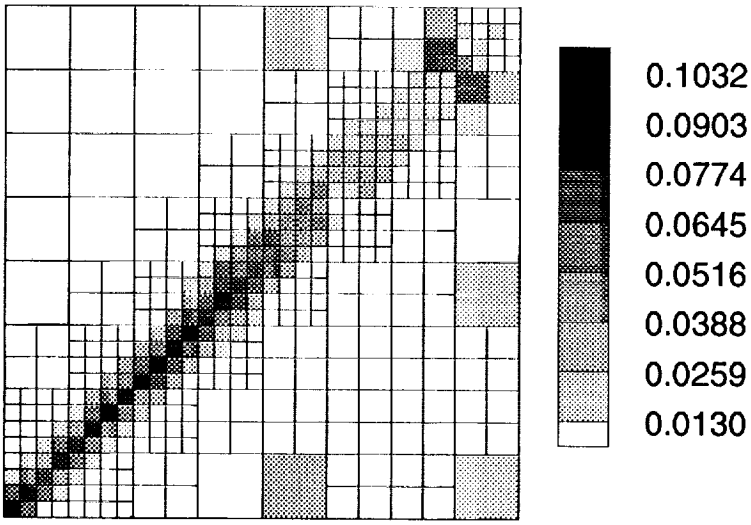

Figure 5.26: Example 3 - Estimated error on adaptive p-enriched mesh.

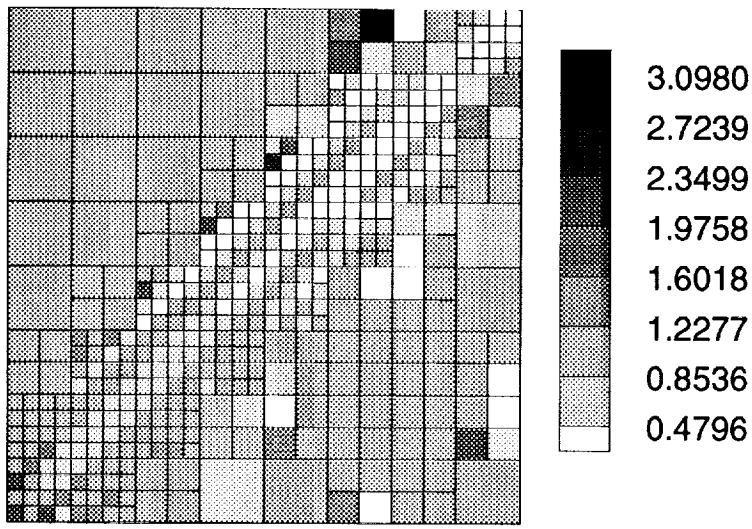

Figure 5.27: Example 3 - Local effectivity index on adapive p-enriched mesh.

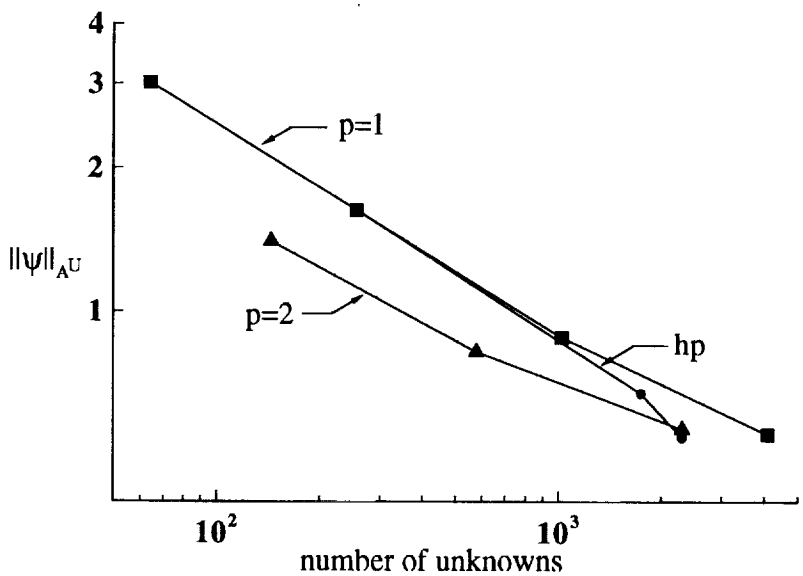

Figure 5.28: Example 3 - Rate of convergence of the error with respect to the number of unknowns.

(iii) $a(\mathbf{x}) = 1.0$

The source term f in (2.1) is chosen so that the exact solution is a

$$u(r) = \sin 5r\{\tan^{-1} 100 + \tan^{-1}[100(r-1)]\} \tag{5.4}$$

where

$$r^2 = (x+0.1)^2 + 4y^2$$

The inflow boundary conditions are obtained by evaluating the exact solution along the inflow boundary

$$g(r) = \begin{cases} u(r) & r^2 = (x+0.1)^2 & \text{on } y = 0 \\ u(r) & r^2 = (x+0.1)^2 + 4\tan^2(\frac{\pi}{3})x^2 & \text{on } y = \tan(\frac{\pi}{3})x \end{cases}$$

The error history for an hp-adaptive solution is listed in Table 5.10 and the resulting meshes, local error estimates, and local effectivity indices are shown in Figs. 5.29 - 5.35.

While the exact solution to this problem is continuous, it contains a very steep front which can be seen as the dark regions in Fig. 5.29. The global effectivity indices listed in Table 5.10 demonstrate the reliablility of the error estimate on non-rectangular meshes. The local effectivity indices for all the meshes are close to unity over most elements, however, there is some slight under-estimation of the error for the uniform p-meshes. Though it is difficult to see from the figure, the under-estimation of the error occurs in the region of the steep front. There is also some rather severe over-estimation of the error on the p-adapted mesh. This over-estimation occurs primarily in the $p = 5$ elements and does not have a significant effect on the global effectivity of the error estimate.

Adaptive step	Target normalized error	Achieved normalized error	Estimated error $\|\|\psi\|\|_{A_U}$	Effectivity index
Initial mesh $p = 1$	——	0.130	2.514	0.87
h-refinement	0.075	0.029	0.641	1.027
p-enrichment	0.003	0.0025	0.559	1.028

Table 5.10: Example 4 - Error history for an adaptive hp solution.

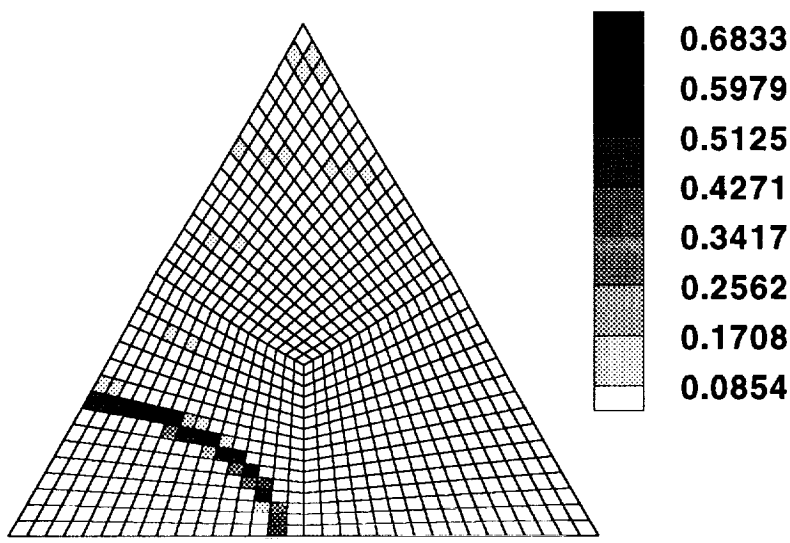

Figure 5.29: Example 4 - Estimated error on initial mesh, $p = 1$.

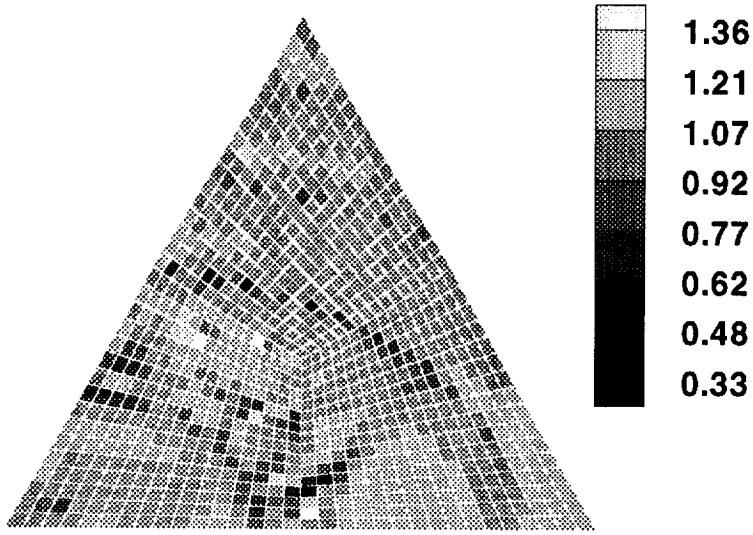

Figure 5.30: Example 4 - Local effectivity index on initial mesh, $p = 1$.

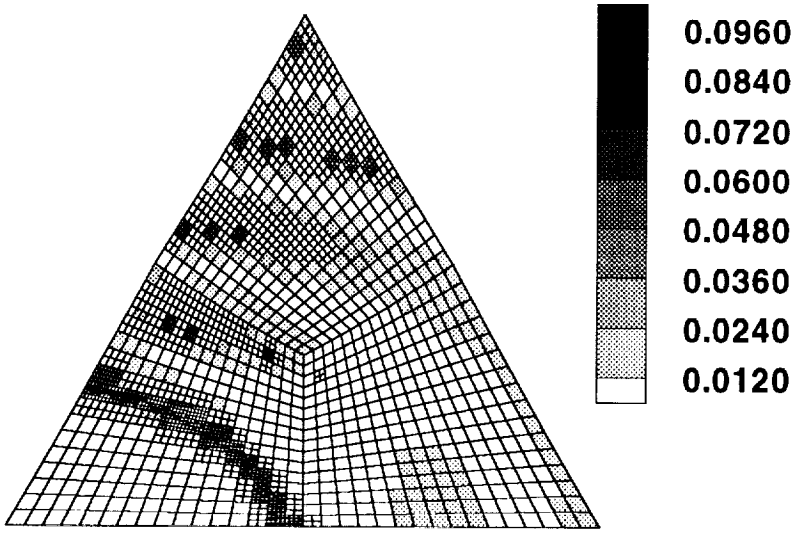

Figure 5.31: Example 4 - Estimated error on h-adapted mesh.

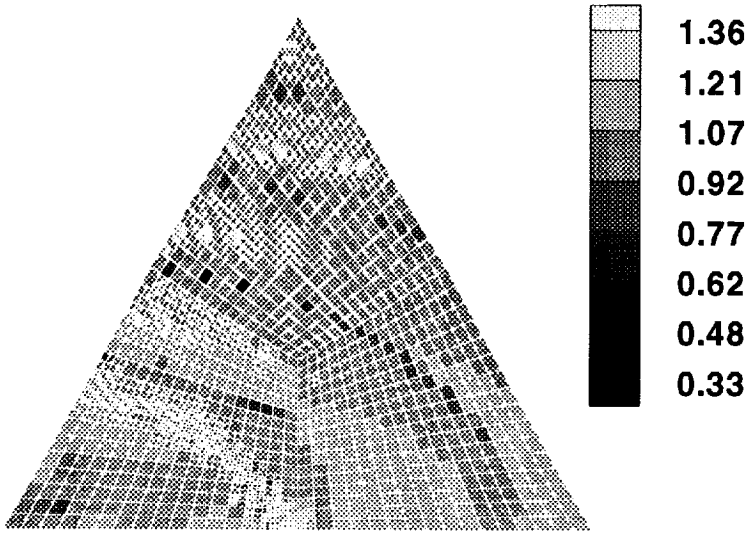

Figure 5.32: Example 4 -Local effectivity index on h-adapted mesh.

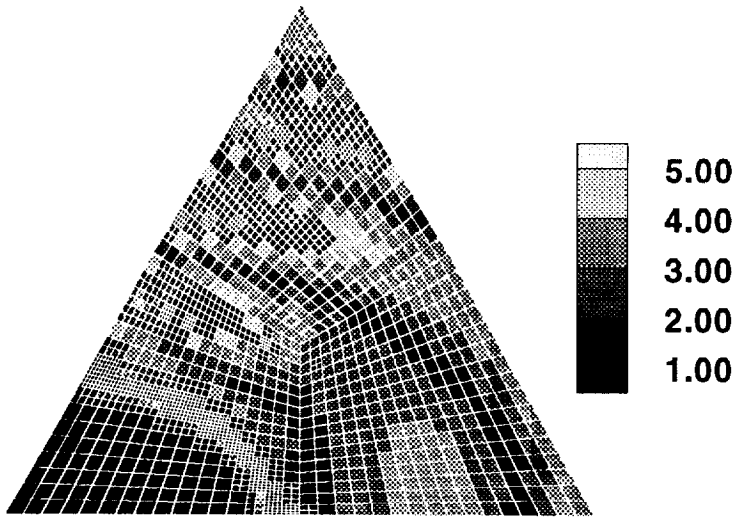

Figure 5.33: Example 4 - p-adapted mesh.

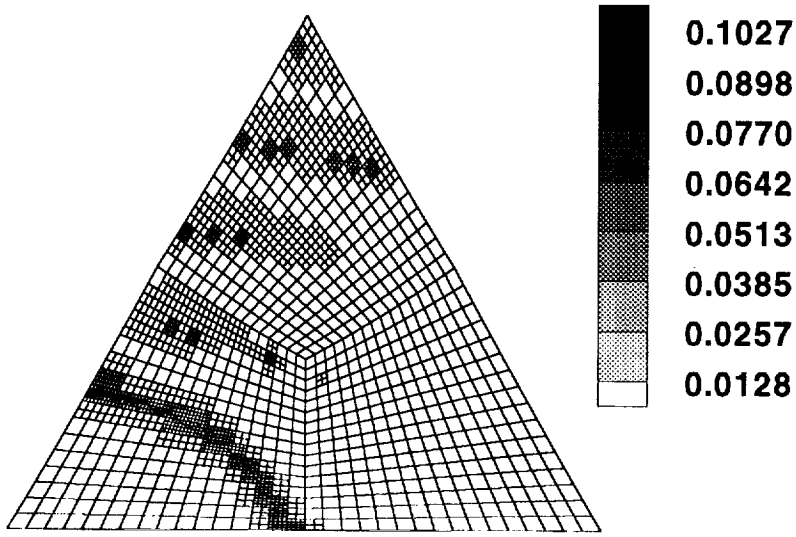

Figure 5.34: Example 4 - Estimated error on p-adapted mesh.

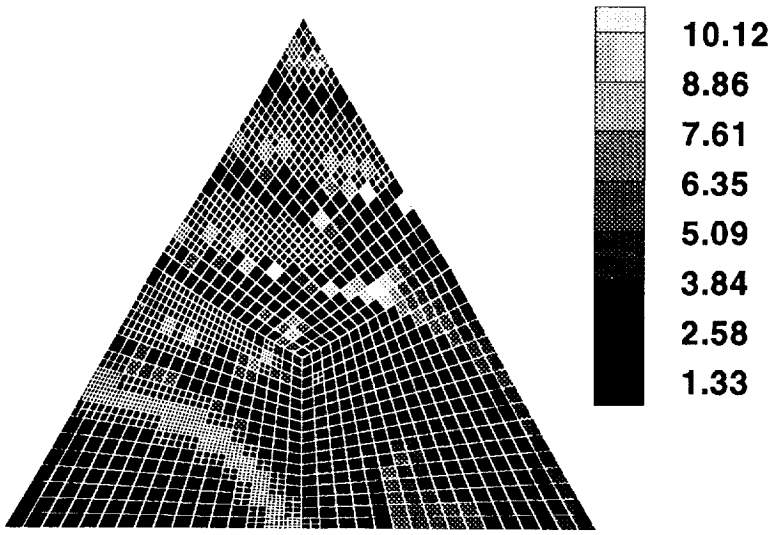

Figure 5.35: Example 4 - Local effectivity index on p-adapted mesh.

Chapter 6

Parallel Implementation

The time-marching versions of the discontinuous Galerkin methods, (2.54), (2.55), and the Runge-Kutta discontinuous Galerkin method described in the next Chapter, fall naturally into the class of single program multiple data (SPMD) parallel applications. Given the solution at time level t_n, the solution is advanced to time level t_{n+1} by solving a $(p_K + 1)^2 \times (p_K + 1)^2$ system of linear equations for the $(p_K + 1)^2$ degrees of freedom for every element K in the partition. The only coupling between elements in the partition arises in the evaluation of the boundary integrals in (2.8) where the solution along common edges of neighboring elements is needed. The evolution of the solution can be performed on all the elements simultaneously, once this information is available.

The primary issue in a parallel implementation of discontinuous Galerkin methods is to balance the workload among the available processors while minimizing the communication between processors, thereby optimizing the utilization of the multi-processor environment. For a machine with P processors, this is accomplished by dividing the partition into P subdomains and assigning the elements contained in a particular subdomain to a particular processor. In order to minimize communications, the interface of the subdomain boundaries should have as small a measure as possible. Moreover, the local nature

of the discontinuous Galerkin formulation requires communication of the solution only along subdomain boundaries at each time step. Since computations are performed at an element level, communications can be overlapped with the computation to further minimize the penalty of communicating between processors.

While the parallel implementation described in this Chapter is targeted for the Intel iPSC 860 computer which is a distributed memory machine with 32 processors arranged in a hypercube architecture, many concepts are general, and, therefore applicable to other multi-processor machines.

6.1 Domain Decomposition for *hp* Meshes

The goal of the domain decomposition strategy is to evenly distribute the workload among the processors while minimizing the size of the subdomain boundaries. Most domain decomposition methods have been developed and analyzed for h-type meshes where the number of degrees of freedom, and hence the computational effort, is the same for every element in the mesh. For these types of meshes, equally distributing the elements among the available processors will result in a balanced load.

The most successful domain decomposition methods in this situation are based on recursive bisectioning of either the physical domain or an ordering of the elements. In the recursive bisectioning of the physical domain, trial separators define possible subdomain configurations. The selection of a separator as a subdomain interface is based on the resulting load balance as well as interface size. Vavasis [52] has obtained theoretical bounds on the achievable load balance and interface size. One disadvantage of this approach is that it

can be computationally expensive for multiple space dimensions.

Recursive bisectioning methods based on an ordering of the elements have a computational advantage since the bisectioning is performed on a one-dimensional list of elements, regardless of the spatial dimension of the domain. One difficulty with this approach is constructing an ordering which preserves the locality of the elements in the mesh. A locality-preserving ordering is necessary to avoid multiply connected or disconnected subdomains and to minimize interface size. Pothen, Simon, and Liou [45] construct such an ordering by using the second eigenvector of the Laplacian matrix associated with the graph of the mesh.

For *hp* meshes, where the number of degrees of freedom (and hence the computational effort) vary from element to element, the domain decomposition must include some measure of the computational work for each element. Here we investigate two load-based recursive bisection methods developed by Patra [40] which seek to balance the load using some local measure of the computational work. In this study, the number of degrees of freedom in an element, $(p_K + 1)^2$, are used as a measure of its computational load.

6.1.1 Recursive Load Based Bisection of Coordinates (RLBBC)

An algorithm for this method which is based on recursive bisectioning of the physical domain is given below.

θ_K: computational effort estimate for element K, θ_K specified as *dof* in the description of the algorithm. It may be replaced by any alternate measure of computational effort.

D_I : list of elements in subdomain I.

n_l : number of trial separator surfaces.

q_i : quality index for a trial separator.

1. Compute maximum and minimum coordinates in any one of the dimensions of the entire domain $x1_{min}, x1_{max}$

   For i = 1 to n_l do

2. compute

   $x1_i = x1_{min} + \frac{(x1_{max} - x1_{min})}{n_i}$

   $q_i = \frac{dof_{left}}{dof_{right}} * dof_{tot} + dof_{inter}$

   where dof_{left} and dof_{right} are the degrees of freedom to the left and right of $x1_i$, respectively, and dof_{inter} is the degrees of freedom on the trial separator $x1_i$.

3. Choose as interface the separator corresponding to the lowest q_i.

4. If the center of mass of element has an x1 coordinate less than that of the interface then

   $D_1 \leftarrow D_1 \cup \{K\}$

   Else

   $D_2 \leftarrow D_2 \cup \{K\}$

   At this stage, the original domain has been split into two.

5. For the next level of decomposition apply steps 1-4 with D_1 and D_2 instead of the entire domain and with x_2 as the coordinate. This will result in

four subdomains. In three-dimensions, for the next level use 1-4 with these four subdomains and with x_3 as the coordinate. This process is recursively continued until the desired number of domains is attained. Clearly, for better shaped domains, equal numbers of splits in each coordinate must be made. Thus, for two dimensions, 4^n subdomains and in three dimensions, 8^n subdomains are obtained.

6.1.2 Recursive Load Based Bisection of an Ordering (RLBBO)

This method is based on recursive bisectioning of an ordering of the elements. The ordering is based on results of Peano[42] and Hilbert[27] concerning a class of continuous mappings of the unit interval onto a unit hypercube. The significance of their results is that one can construct a space filling curve which connects a set of points in n-dimensional space and uniqely maps them onto the unit interval. Applying this mapping to the set of points given by the element centroids, results in an ordering of the elements defined by its location on the unit interval. Complete details of the Peano-Hilert ordering and proof that it is locality-preserving can be found in Patra [40].

An algoritm for this method follows:

$h_n : \Re \rightarrow U_n$, where U_I is a the unit interval and U_n is the unit hypercube.

D_I : list of elements in subdomain I.

n_l : number of trial separator surfaces.

q_i : quality index for a trial separator.

1. Create an ordering of the elements by mapping the centroids of the ele-

ments onto a Peano-Hilbert curve. (See [40])

2. Let t_K be the distance of the centroid of element K along the space filling curve.

3. Compute maximum and minimum of t_K, t_max and t_min.

4. Compute n_l trial separator levels as

$$t_i = t_{min} + \frac{t_{max} - t_{min}}{n_l}$$

5. For each t_i compute a quality of interface index q_i

$$q_i = abs(\frac{dof_{left}}{dof_{right}} - 1) \cdot dof_{tot} + dof_{inter}$$

Replace dof by error or other load estimate as appropriate.

6. Choose as interface t_{int} the t_i that corresponds to lowest q_i

7. For K = 1 to the total number of elements

If $t_K \leq t_{int}$ then

$D_1 \leftarrow D_1 \cup \{K\}$

else

$D_2 \leftarrow D_2 \cup \{K\}$

end if

end for

At this stage, the original domain has been split into two.

8. Apply 1-7 recursively on each of the generated subdomains.

6.2 Communications

Communication between processors on distributed memory machines can significantly effect the overall performance of the parallel implementation, particularly if a processor must wait to receive information from another processor before proceeding with a calculation. To compute the solution at time level t_{n+1} on a particular subdomain, the solution at t_n is needed from interface elements on neighboring subdomains. Using synchronous communications, that is, requesting information from neighboring processors at the time that it is needed, leads to unnecessary waiting by all processors. Moreover, communication conflicts are likely to occur since two-way communication is required across interior subdomain boundaries. Asynchronous communications are used to minimize this wait time. When the solution for an interface element is computed on a processor, it is then sent to the processor containing the neighboring element.

6.3 Numerical Results

Results are presented for an *hhp*-adaptive solution to an example similar to example 3 in Chapter 5, except that the source term f is selected so that the exact solution is

$$u(x,y) = \begin{cases} 5e^{-[(x+\frac{1}{2})^2+y^2]} + 3e^{-[x^2+(y-\frac{1}{2})^2]} & \text{if } y > x \\ -1 - 5e^{-5[(x-\frac{1}{2})^2+(y+\frac{1}{2})^2]} & \text{otherwise} \end{cases} \tag{6.1}$$

The error history obtained with the *hhp*-adaptive strategy described in Chapter 4 is listed in Table 6.1 which shows that this approach is very effective at reducing the global error in the discontinuous solution. These results are compared graphically with results from Chapter 3 in Fig. 6.1. Note the significant decrease in the error due to the additional h-refinement at the shock.

Adaptive step	Target normalized error	Achieved normalized error	Estimated error $\|\|\psi\|\|_{A_U}$	Effectivity index
Initial 8×8 mesh, $p = 1$	——	0.126	1.391	0.72
h-refinement	0.0628	0.0759	0.861	0.69
p-enrichment	0.0558	0.0311	0.359	0.53

Table 6.1: Error history for an hhp-adaptive solution starting from a uniform 8×8 mesh, $p = 1$.

While this adaptive strategy leads to significantly more unknowns in the problem, the reduction in the error, when compared to error obtained by uniform h-refinements of a mesh of $p = 1$ or $p = 2$ elements, is orders of magnitude. The final hp mesh, shown in Fig. 6.2, is particularly demanding for a domain decomposition method because of the concentration of elements resulting from 4 levels of refinement in the lower left quadrant of the domain and the large p elements in the smooth regions.

We use the speedup as a measure of the effectiveness of the domain decomposition startegy at balancing the load. The speedup is defined here as the ratio of the CPU time required to obtain the solution using 4 processors to the CPU time required to obtain the solution using n processors, where $n \geq 4$. Ideal (also called linear) speedup implies that the work load is equally balanced among the processors and is indicated by a slope of two on a graph of the speedup as a function of the number of processors. The speedup obtained on the hp-mesh using the two decomposition strategies is shown in Fig. 6.3. Nearly optimal speedup of 1.8 is obtained using the RLBBC method when going

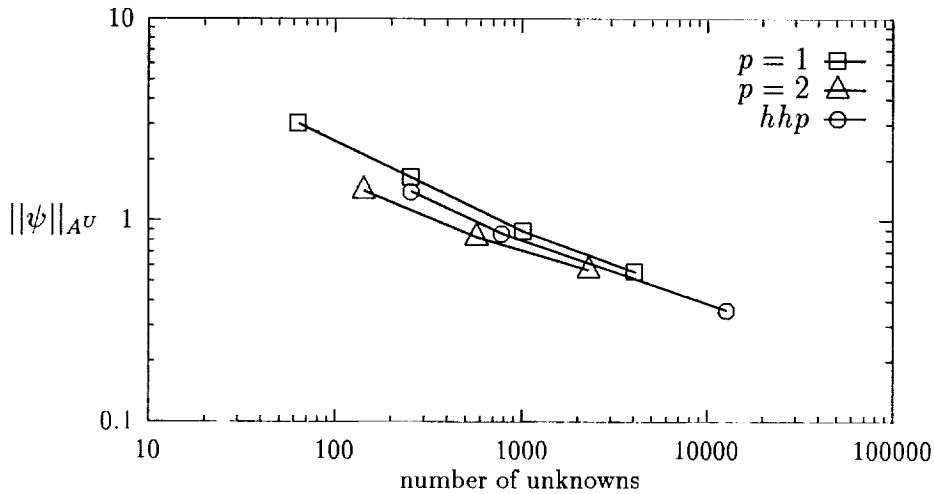

Figure 6.1: Rate of convergence of the error with respect to the total number of unknowns.

from 4 to 8 processors. The speedup drops off as the number of processors increases, indicating that the load is unbalanced. The speedup of 1.3 when going from 4 to 8 processors when using the RLBBO method indicates that the method yields very poor load balancing when only a few processors are used. Fortunately, the RLBBO method provides more balanced loads for a larger number of processors where a speedup of 1.85 is achieved when going from 8 to 16 processors.

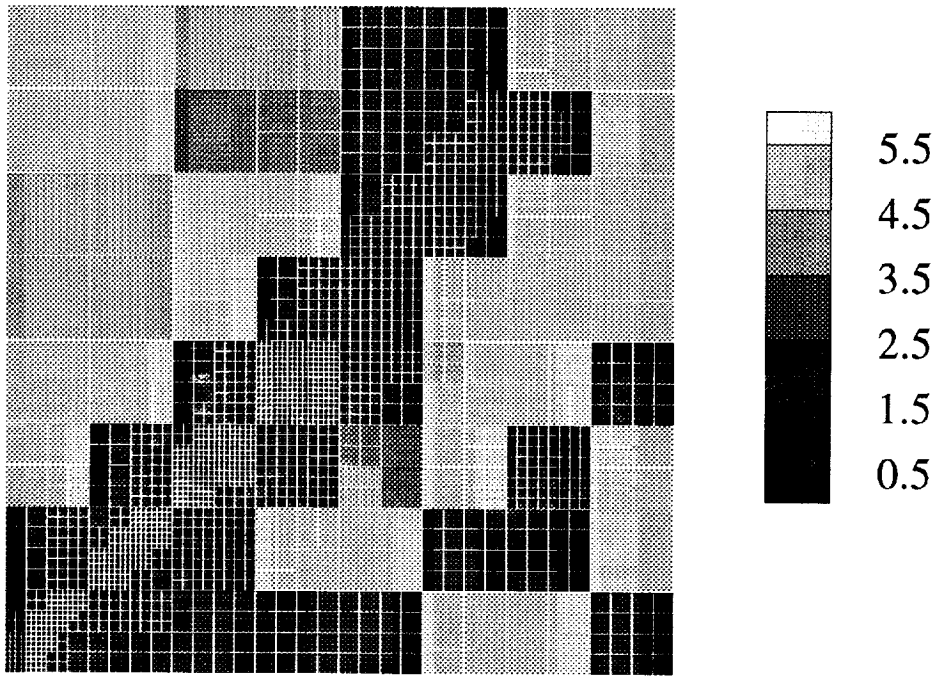

Figure 6.2: Final mesh using the *hhp*-adaptive strategy.

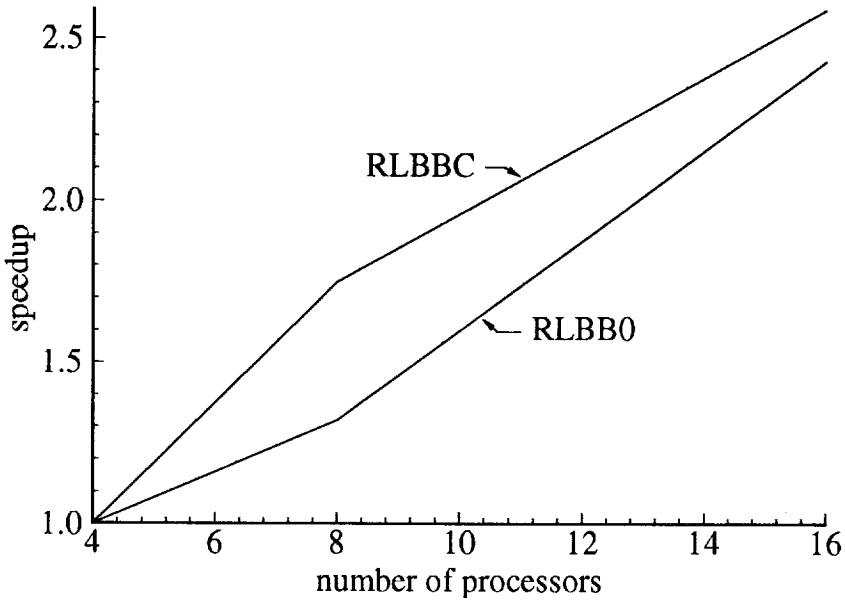

Figure 6.3: Parallel speedup for the *hp* mesh.

Chapter 7

Extensions to Nonlinear Hyperbolic Conservation Laws

In this chapter, we describe extensions of the discontinuous Galerkin method to nonlinear hyperbolic conservation laws of the form (1.5) on convex polygonal domains. For simplicity, the method is described for a two-dimensional scalar conservation law written as

$$u_t + \nabla \cdot \mathbf{q}(u) = 0 \ (x, y) \in \Omega \subset \Re^2, \ t > 0 \tag{7.1}$$

where $\mathbf{q}(u) = f^1(u)\ \mathbf{i} + f^2(u)\ \mathbf{j}$ denotes the flux vector. For a description of the method for hyperbolic systems of conservation laws, in particular, the Euler equations of gas dynamics, see Bey and Oden[6].

To complete the initial boundary-value problem, (7.1) is accompanied by initial conditions

$$u(x, y, 0) = u_0(x, y); \ (x, y) \in \Omega \tag{7.2}$$

and boundary conditions of the form

$$u(x, y, t) = d(t); \ (x, y) \in \Gamma^- \tag{7.3}$$

where Γ^- is the inflow boundary, $\Gamma^- = \{(x, y) \in \partial\Omega : \frac{\partial \mathbf{q}}{\partial u} \cdot \mathbf{n} < 0\}$, $\mathbf{n}$ is the outward unit normal to the boundary ($\partial\Omega = \Gamma^- \cap \Gamma^+$), and $d(t)$ is prescribed inflow data.

The version of the discontinuous Galerkin method used here, first proposed by Cockburn and Shu [13], [12], is based on the method of lines. The system of ordinary differential equations resulting from the discontinuous Galerkin spatial approximation is marched in time using a multi-stage Runge-Kutta scheme. A local projection is used at each stage to control oscillations and prevent nonlinear instabilities. In reference [13], a projection is constructed for $p = 1$ and $p = 2$ elements in one space dimension and possible extensions to higher-order elements are proposed. In reference [12], some important theoretical results are derived for multi-dimension problems, but a projection is constructed and verified only for linear $p = 1$ triangles. Moreover, the emphasis of their work is in predicting element mean values, and while the high-order solution is available, it is ignored in the presentation of numerical results. Here we construct a very simple projection for general quadrilateral (or triangular) elements of arbitrary order and take full advantage of the finite element approximation. For alternate projection strategies for quadrilaterals, we refer to Bey and Oden [6] and to Biswas, Devine, and Flaherty [7] for a general projection strategy on Cartesian grids.

7.1 Discontinuous Galerkin Spatial Approximation

The primary difference in the discontinuous Galerkin formulation for nonlinear conservation laws is the treatment of the boundary fluxes at element interfaces and the need for the projection to control oscillations. Recall that for the linear conservation law $\mathbf{q}(u) = \boldsymbol{\beta} u$ and hence $\frac{d\mathbf{q}}{du} \cdot \mathbf{n}_K = \boldsymbol{\beta} \cdot \mathbf{n}_K < 0$, which defines element inflow boundaries, is known a priori. For the nonlinear conservation law, $\frac{d\mathbf{q}}{du} \cdot \mathbf{n}_K$ is a function of u and is thus unknown.

The discontinuous Galerkin spatial approximation is defined on a partition of the domain satisfying the properties in Chapter 2 (except property (v) defining element inflow boundaries) and solutions are sought in the finite dimensional space $V_p(\mathcal{P}_h) = \{v \in L^1(\Omega) \mid v|_K \in Q^{p_K}(K)\}$. The weak form of (7.1) on a single element is obtained by multiplying by a test function $v(\mathbf{x})$ and integrating the first-order spatial term by parts:

$$\text{Find } u(\mathbf{x},t)|_K \in L^1(K) \times C^1(0,T) \text{ such that}$$

$$\int_K u(\mathbf{x},0)v(\mathbf{x})d\mathbf{x} = \int_K u_0(\mathbf{x})v(\mathbf{x})dx \text{ and} \tag{7.4}$$

$$\frac{d}{dt}(u,v)_K - \int_K \mathbf{q}(u)\cdot\nabla v d\mathbf{x} + \int_{\partial K} \mathbf{q}(u)\cdot\mathbf{n}_K v\, ds = 0 \tag{7.5}$$

for all admissible test functions $v(\mathbf{x})$.

The element boundary flux $\mathbf{q}(u)\cdot\mathbf{n}_K$ in (7.5) is not uniquely defined when replacing u by its approximation $u_h^p \in V_p(\mathcal{P}_h)$. Since u_h^p is discontinuous across element interfaces, $\mathbf{q}(u_h^p)\cdot\mathbf{n}_K$ has two values on ∂K, one associated with u_h^p on the interior of element K and one associated with u_h^p on the exterior of the element. The ambiguity in evaluating the boundary flux in (7.5) is eliminated by replacing it with a numerical flux function:

$$h_{K,e} = h_{K,e}(u_h^{p,int(K)}, u_h^{p,ext(K)})$$

$$\text{where} \quad u_h^{p,int(K)} = u_h^p(x,y,\cdot)|_{\text{edge } e \text{ of element } K}$$

$$u_h^{p,ext(K)} = \begin{cases} u_h^p(x,y,\cdot)|_{\text{edge } e \text{ of element } K_e}, & \partial K \cap \Gamma_- = 0 \\ d(t), & \partial K \cap \Gamma_- \neq 0 \end{cases}$$

The numerical flux function is required to have certain properties to enhance the convergence properties of the approximate solution:

1. $h_{K,e}(u_h^{p,int(K)}, u_h^{p,ext(K)})$ is a monotone flux function, i.e. $h_{K,e}$ is non-decreasing in $u_h^{p,int(K)}$ and non-increasing in $u_h^{p,ext(K)}$

2. $h_{K,e}(\cdot,\cdot)$ is consistent, i.e., $h_{K,e}(u,u) = \mathbf{q}(u)\cdot\mathbf{n}_{K,e}$

3. $h_{K,e}(u_h^{p,int(K)}, u_h^{p,ext(K)})$ is Lipschitz continuous

4. $h_{K,e}(u_h^{p,int(K)}, u_h^{p,ext(K)})$ is directionally consistent in the sense that

$$h_{K,e}(u_h^{p,int(K)}, u_h^{p,ext(K)}) = -h_{K_e,e}(u_h^{p,int(K_e)}, u_h^{p,ext(K_e)})$$

Note that this last property enforces continuity of the normal flux at element interfaces. Any function which satisfies the properties listed above can be used in this numerical scheme. Some examples of fluxes satisfying these conditions are the numerical fluxes of Godunov [23], Enquist-Osher [17], and Roe [46].

The semi-discrete problem which results from the discontinuous Galerkin approximation to (7.1) can now be written for a typical element $K \in \mathcal{P}_h$:

$$\text{Find } u_h^p(\mathbf{x},t)|_K \in Q^{p_K}(K) \times C^1(0,T] \text{ such that}$$

$$\begin{aligned}
\int_K u_h^p(\mathbf{x},0)|_K v(\mathbf{x})d\mathbf{x} &= \int_K u_0(\mathbf{x})v(\mathbf{x})d\mathbf{x} \qquad \text{and} \\
\frac{d}{dt}\int_K u_h^p(\mathbf{x},t)v(\mathbf{x})\,dx\,dy &= \int_K \mathbf{q}(u_h^p(\mathbf{x},t))\cdot\nabla v(\mathbf{x})d\mathbf{x} \\
&- \sum_{e\in\partial K\setminus\partial\Omega}\int_e h_{K,e}(u_h^{p,int(K)}, u_h^{p,ext(K)})v\,ds \\
&- \sum_{e\in\partial K\cap\Gamma^-}\int_e h_{K,e}(u_h^{p,int(K)}, d(t))v\,ds \\
&- \sum_{e\in\partial K\cap\Gamma^+}\int_e \mathbf{q}(u_h^p)\cdot\mathbf{n}_{K,e}v\,ds \qquad (7.6)
\end{aligned}$$

$$\text{for every } v(\mathbf{x}) \in Q^{p_K}(K)$$

Note that the integral over the element boundary is represented as the sum of integrals along element edges where $\mathbf{n}_{K,e}$ denotes the outward unit normal to edge e of element K. For the linear conservation law, (7.6) reduces to the methods (2.54) and (2.55) provided that the numerical flux reduces to

$$\begin{aligned} h_{K,e}(u_h^{p,int(K)}, u_h^{p,ext(K)}) &= \frac{1}{2}(u_h^{p,int(K)} + u_h^{p,ext(K)})\boldsymbol{\beta} \cdot \mathbf{n}_{K,e} \\ &- \frac{1}{2}|\boldsymbol{\beta} \cdot \mathbf{n}_{K,e}|(u_h^{p,ext(K)} - u_h^{p,int(K)}) \end{aligned}$$

when $\mathbf{q}(u) = \boldsymbol{\beta} u$.

7.2 Runge-Kutta Time Discretization

The system of ordinary differential equations in (7.6) can be discretized in time using one of many time marching schemes, e.g. forward Euler, backward Euler, or some predictor-corrector method. These schemes combined with acceleration techniques, e.g. local time-stepping or multigrid, are good choices for problems where only the steady-state solution is of interest. For truly time-accurate solutions, however, it is necessary to have the order of accuracy of the time discretization to be equal to the order of accuracy of the spatial approximation. Using classical interpolation-type error estimates, Cockburn et. al. [12] show that the Galerkin spatial approximation with uniform p elements satisfies the estimate

$$||L_h(u_h^p) + \nabla \cdot \mathbf{q}(u_h^p)||_{L^\infty(\Omega)} \leq Ch^{(p+1)}|\mathbf{q}(u)|_{W^{p+2,\infty}(\Omega)} \tag{7.7}$$

where we have used the abstract notation of Cockburn, Hou, and Shu [12] to represent (7.6),

$$\frac{d}{dt}u_h^p(\mathbf{x},t)|_K = L_h(u_h^p(\mathbf{x},t)|_K) \tag{7.8}$$

which formally requires the inversion of the $(p_K + 1) \times (p_K + 1)$ mass matrix in (7.6). Runge-Kutta methods can be used to obtain a time marching scheme for which the truncation error is of order $\Delta t^{(p_K+1)}$ for $u_h^p|_K \in Q^p(K)$.

Let Δt denote the time step increment and assume the approximate solution $u_h^p(\mathbf{x}, t_n)$, $t_n = n\Delta t$ is known. We use a special class of explicit Runge-Kutta schemes written in the classical form as

$$\begin{aligned} u_h^p(\mathbf{x}, t_{n+1}) &= u_h^p(\mathbf{x}, t_n) + \sum_{i=1}^{s} b_i k_i \\ \text{where } k_i &= \Delta t L_h(u_h^p(\mathbf{x}, t_n) + \sum_{j=1}^{i-1} a_{ij} k_j) \end{aligned} \tag{7.9}$$

which is represented by the Butcher-array [9]

$$\begin{array}{c|cccc} 0 & & & & \\ c_2 & a_{21} & & & \\ \vdots & \vdots & \ddots & & \\ c_s & a_{s1} & \cdots & a_{s,s-1} & \\ \hline & b_1 & \cdots & & b_s \end{array}$$

where $c_i = \sum_{j=1}^{i-1} a_{ij}$ define the abscissa $t_i = t_n + c_i \Delta t$ for a non-autonomous system which would result, for example, if the conservation law contained a time-dependent source term. The special class of schemes can be written in multi-stage form as

$$\begin{aligned} u^{(0)} &= u_h^p(\cdot, t_n) \\ u^{(i)} &= \Pi_h \sum_{k=0}^{i-1} [\alpha_{ik} u^{(k)} + \Delta t \beta_{ik} L_h(u^{(k)})], \; i = 1, ..., s \\ u_h^p(\cdot, t_{n+1}) &= u^{(s)} \end{aligned} \tag{7.10}$$

where α_{ik} and β_{ik} are free parameters and Π_h denotes a projection operator to be discussed later. For consistency, $\alpha_{ik} \geq 0$ and $\sum_{k=0}^{i-1} \alpha_{ik} = 1$. We use the

Order	δ	α_{ik}	β_{ik}	Classical form
2	1.0	$\begin{array}{ll} 1 & \\ \frac{1}{2} & \frac{1}{2} \end{array}$	$\begin{array}{ll} 1 & \\ 0 & \frac{1}{2} \end{array}$	$\begin{array}{c\|cc} 0 & & \\ 1 & 1 & \\ \hline & \frac{1}{2} & \frac{1}{2} \end{array}$
3	1.0	$\begin{array}{lll} 1 & & \\ \frac{3}{4} & \frac{1}{4} & \\ \frac{1}{3} & 0 & \frac{2}{3} \end{array}$	$\begin{array}{lll} 1 & & \\ 0 & \frac{1}{4} & \\ 0 & 0 & \frac{2}{3} \end{array}$	$\begin{array}{c\|ccc} 0 & & & \\ 1 & 1 & & \\ \frac{1}{2} & \frac{1}{4} & \frac{1}{4} & \\ \hline & \frac{1}{6} & \frac{1}{6} & \frac{1}{6} \end{array}$
4	1.5	$\begin{array}{llll} 1 & & & \\ \frac{1}{2} & \frac{1}{2} & & \\ \frac{1}{9} & \frac{2}{9} & \frac{2}{3} & \\ 0 & \frac{1}{3} & \frac{1}{3} & \frac{1}{3} \end{array}$	$\begin{array}{llll} \frac{1}{2} & & & \\ -\frac{1}{4} & \frac{1}{2} & & \\ -\frac{1}{9} & -\frac{1}{3} & 1 & \\ 0 & \frac{1}{6} & 0 & \frac{1}{6} \end{array}$	$\begin{array}{c\|cccc} 0 & & & & \\ \frac{1}{2} & \frac{1}{2} & & & \\ \frac{1}{2} & 0 & \frac{1}{2} & & \\ 1 & 0 & 0 & 1 & \\ \hline & \frac{1}{6} & \frac{1}{3} & \frac{1}{3} & \frac{1}{6} \end{array}$

Table 7.1: Parameters for the TVBM Runge-Kutta scheme

parameters listed in Table 7.1 which were derived by Shu [48] to result in a time discretization that is TVD (Total Variation Diminishing) when combined with finite difference schemes in one space dimension. For multiple space dimensions, the parameters listed in Table 7.1 result in a scheme which is TVBM (Total Variation Bounded in the Means) as defined in the following lemma.

Lemma 9 (Cockburn, Hou, and Shu [12])

$$\textit{Let } a_0 \quad = \quad \inf_{\mathbf{x}\in\Omega} u_0(\mathbf{x})$$

$$
\begin{aligned}
b_0 &= \sup_{\mathbf{x}\in\Omega} u_0(\mathbf{x}) \\
\bar{u}_K^n &\stackrel{\text{def}}{=} \frac{1}{|K|}\int_K u_h^p(\mathbf{x}, t_n)|_K \, d\mathbf{x} \\
w_h^p &\stackrel{\text{def}}{=} u_h^p + \delta \, \Delta t L_h(u_h^p)
\end{aligned}
\tag{7.11}
$$

where $\delta > 0$ is a parameter. Suppose that the operator L_h satisfies the following maximum principle:

$$
\bar{u}_K \in [a, b] \rightarrow \bar{w}_K \in [a - Bh_K^\alpha, b + Bh_K^\alpha] \tag{7.12}
$$

where α and B are non-negative parameters. Then the Runge-Kutta time discretization defined by (7.10) is Total Variation Bounded in the Mean, i.e.,

$$
\bar{u}_K^n \in [a_0 - snBh_K^\alpha, b_0 + snBh_K^\alpha] \tag{7.13}
$$

Proof: By induction. See Cockburn, Hou, and Shu [12] for the case when $\alpha = 2$. The case when α is arbitrary follows directly. ∎

Remarks:

(i) The second- and third-order schemes in Table 7.1 require little storage since at each stage there is only one non-zero parameter β.

(ii) The fourth-order scheme is the classical fourth-order Runge-Kutta method. For this and higher-order schemes, nearly all intermediate solutions must be stored since most of the parameters are non-zero.

∎

7.3 Enforcing the Maximum Principle

A crucial step in the proof of the TVBM property is the assumption that the spatial operator satisfies the maximum principle (7.12). The local projection, Π_h in (7.10), is designed to enforce the maximum principle by modifying the solution at each stage in the Runge-Kutta scheme. Cockburn, Hou, and Shu [12] derive conditions on the solution on the boundary of an element so that (7.12) is satisfied. These condition are expressed as limits on the deviation of the solution on an element boundary from its mean values based on the difference between the element mean and the mean values in neighboring elements. The "stencil" of elements used to define these limits includes neighboring elements as well as neighbors of neighboring elements. (See [12] or [6].) Note that (7.12) enforces the TVB property on solution mean values; it says nothing about the actual solution in an element. Moreover, values on the boundary of an element are insufficient to define a p-unisolvent element. Here we use a simple projection strategy which overcomes some of these difficulties.

The overall strategy for the local projection is as follows:(1) identify elements in the neighborhood of a shock as those where the jump in the solution along the element boundary $[\![u_h^p]\!] \geq h_K$; (2) If $p_K > 1$, perform an intermediate projection $P : Q^p(K) \to Q^1(K)$ (for $p_K = 1$, P is the identity operator); (3) perform a local projection, Π_K, on the result of step (2) to enforce the following condition:

$$\Pi_K P(u_h^p|_K) \in [\min(\bar{u}_K; \bar{u}_{K_e}, e \in \partial K), \max(\bar{u}_K; \bar{u}_{K_e}, e \in \partial K)] \ , \ \forall \mathbf{x} \in K \quad (7.14)$$

These conditions are the multi-dimensional extension of those used by Van Leer [51] in one space dimension and are identical to those used by Barth [5]

in reconstructing piecewise linear polynomials from mean values in his higher-order finite volume schemes.

The limits in (7.14) can also be written in terms of the deviation of the solution from its mean value. Denoting the deviation from the mean by $\tilde{u}_K$ where $u_h^p|_K = \bar{u}_K + \tilde{u}_K$, (7.14) becomes

$$\Pi_K \widetilde{P(u_h^p|_K)} \in [\min_{e\in\partial K}(0, \bar{u}_{K_e} - \bar{u}_K), \max_{e\in\partial K}(0, \bar{u}_{K_e} - \bar{u}_K)] \ , \ \forall \mathbf{x} \in K \tag{7.15}$$

In order to maintain conservation, the projection must also preserve the mean value,

$$\overline{\Pi_K P(u_h^p|_K)} = \bar{u}_K \tag{7.16}$$

7.3.1 The Projection $P : Q^p(K) \to Q^1(K)$

There are several choices for the projection of a higher-order solution onto the space of bilinear shape functions; the only requirement is that it preserve the mean value. A computationally efficient approach for the projection P is to simply truncate the higher-order terms in polynomial representation of $u_h^p|_K$. To enforce the conservativity condition (7.16), the bilinear part of $u_h^p|_K$ is augmented by the mean value of the truncated higher-order terms. To describe this procedure, the approximate solution is decomposed into its linear and higher-order contributions:

$$\begin{aligned} u_h^p|_K &= u_{linear} + u_{h.o.} \\ &= \sum_{i=1}^{4} u_i \phi_i(x,y) + \sum_{i=5}^{(p_K+1)^2} a_i \phi_i(x,y) \end{aligned} \tag{7.17}$$

where $\phi_i(x,y)$, $i = 1,\ldots,4$ are the standard bilinear shape functions and u_i, $i = 1,\ldots,4$ are the solution values at the nodes of the element. The

element mean value is thus

$$\begin{aligned}\bar{u}_K &= \bar{u}_{linear} + \bar{u}_{h.o.} \\ &= \sum_{i=1}^{4} u_i\bar{\phi}_i + \sum_{i=5}^{(p_K+1)^2} a_i\bar{\phi}_i \end{aligned} \tag{7.18}$$

Let u_i^{new} denote the degrees-of-freedom of $P(u_h|_K)$, then its mean value is

$$\overline{P(u_h^p|_K)} = \sum_{i=1}^{4} u_i^{new}\bar{\phi}_i \tag{7.19}$$

The conservativity condition (7.16) and the property of the bilinear shape functions that $\sum_{i=1}^{4}\bar{\phi}_i = 1$ imply that

$$\begin{aligned}\sum_{i=1}^{4} u_i^{new}\bar{\phi}_i &= \sum_{i=1}^{4} u_i\bar{\phi}_i + \bar{u}_{h.o.} \\ &= \sum_{i=1}^{4} u_i\bar{\phi}_i + (\sum_{i=1}^{4}\bar{\phi}_i)\bar{u}_{h.o.} \\ &= \sum_{i=1}^{4}(u_i + \bar{u}_{h.o.})\bar{\phi}_i \\ \Longrightarrow u_i^{new} &= u_i + \bar{u}_{h.o.},\ i = 1,\ldots,4 \end{aligned} \tag{7.20}$$

Combining the definition of $\bar{u}_{h.o.}$ in (7.18) with (7.20) results in the final definition for $P(u_h^p|_K)$:

$$P(u_h^p|_K) = \sum_{i=1}^{4}(u_i + \sum_{j=5}^{(p_K+1)^2} a_j\bar{\phi}_j)\phi_i(x,y) \tag{7.21}$$

7.3.2 The Local Projection $\Pi_K : Q^1(K) \to Q^1(K)$

Construction of a projection which results in a function satisfying (7.15) for every point in the element is straightforward for linear elements since the maximum solution values within the element occur at the nodes (vertices) of the element.

Let p_i, $i = 1, \cdots, 4$ denote the degrees of freedom associated with the projected solution,

$$\Pi_K P(u_h^p|_K) = \sum_{i=1}^{4} \phi_i(x,y) p_i \tag{7.22}$$

which can be expressed in terms of the mean value and the deviation from the mean,

$$\Pi_K P(u_h^p|_K) = \overline{\Pi_K P(u_h^p|_K)} + \Pi_K \widetilde{P(u_h^p|_K)} \tag{7.23}$$

Evaluating (7.23) at the nodes yields a direct expression for the degrees of freedom of the projected solution,

$$p_i = \overline{\Pi_K P(u_h^p|_K)} + \Pi_K \widetilde{P(u_h^p|_K)}(x_i^K, y_i^K) \ ; \quad i = 1, \ \cdots, 4 \tag{7.24}$$

where (x_i^K, y_i^K) , $i = 1, \cdots, 4$ are the coordinates of the element vertices. All that remains to define the local projection, Π_K, is to select values for

$$\Pi_K \widetilde{P(u_h^p|_K)}(x_i^K, y_i^K) \ i = 1, \cdots, 4$$

so that the monotonicity conditions (7.15) and the conservativity condition (7.16) are satisfied. To simplify the notation, let

$$\begin{aligned} \tilde{p}_i &= \Pi_K \widetilde{P(u_h^p|_K)}(x_i^K, y_i^K) = \Pi_K P(u_h^p|_K)(x_i^K, y_i^K) - \overline{\Pi_K P(u_h^p|_K)} \\ \tilde{u}_i &= \tilde{u}_K(x_i^K, y_i^K) = u_h^p|_K(x_i^K, y_i^K) - \bar{u}_K \ , \ i = 1, \cdots, 4 \end{aligned}$$

denote the deviation of the projected solution and the actual solution from the mean value, respectively. A strategy similar to Barth [5] is used to select $\tilde{p}_i$ so that (7.15) is satisfied:

$$\tilde{p}_i = \begin{cases} \min(\tilde{u}_i, \max(\bar{u}_K; \bar{u}_{K_e}, e \in \partial K)) & \text{if } \tilde{u}_i \geq 0 \\ \max(\tilde{u}_i, \min(\bar{u}_K; \bar{u}_{K_e}, e \in \partial K)) & \text{if } \tilde{u}_i < 0 \end{cases} \tag{7.25}$$

Note that (7.25) represents the minimum modification to $u_h^p|_K$ that satisfies (7.15) without regard for the conservativity condition.

The conservativity condition is enforced by appropriate scaling of $\tilde{p}_i$. From (7.23) we have

$$\begin{aligned}\overline{\Pi_K P(u_h^p|_K)} &= \sum_{i=1}^{4} \bar{\phi}_i \; p_i \\ &= \sum_{i=1}^{4} \bar{\phi}_i(\overline{\Pi_K P(u_h^p|_K)} + \tilde{p}_i) \text{ from (7.24)} \end{aligned} \tag{7.26}$$

and since $\overline{\Pi_K P(u_h^p|_K)}$ is a constant and $\sum_{i=1}^{4} \bar{\phi}_i = 1$, (7.26) becomes

$$\sum_{i=1}^{4} \bar{\phi}_i \; \tilde{p}_i = 0 \tag{7.27}$$

To enforce conservativity, the appropriate $\tilde{p}_i$ are scaled by a factor $\sigma < 1$ which is is a ratio of the positive and negative parts of (7.27). This scaling process is described by the following algorithm:

$$\begin{aligned} \text{Let } S^+ &= \{i : \tilde{p}_i \geq 0\} \\ S^- &= \{i : \tilde{p}_i < 0\} \\ P^+ &= \sum_{i \in S^+} \bar{\phi}_i \; \tilde{p}_i \\ P^- &= \sum_{i \in S^-} \bar{\phi}_i \; \tilde{p}_i \end{aligned}$$

$$\begin{aligned} &If \quad P^- < P^+, \text{ then } \sigma = \frac{P^-}{P^+} \text{ and } \tilde{p}_i \mapsto \sigma \tilde{p}_i \; ; \; \forall i \in S^+ \\ &If \quad P^- > P^+, \text{ then } \sigma = \frac{P^+}{P^-} \text{ and } \tilde{p}_i \mapsto \sigma \tilde{p}_i \; ; \; \forall i \in S^- \\ &If \quad P^- = 0 \text{ or } P^+ = 0, \text{ then } \tilde{p}_i = 0, i = 1, \ldots, 4 \end{aligned} \tag{7.28}$$

This completes the definition of the projection for $p = 1$ elements since from (7.24), (7.16), and (7.23) we get

$$\Pi_K P(u_h^p|_K) = \sum_{i=1}^{4} \phi_i(x, y) \; \bar{u}_K + \tilde{p}_i \tag{7.29}$$

7.4 Numerical Results for Burger's Equation

The performance of the discontinuous Galerkin method is investigated by solving the two-dimensional Burger's equation with periodic initial and boundary conditions:

$$\begin{aligned} u_t + f(u)_x + g(u)_y &= 0 \quad (x,y) \in (-1,1) \times (-1,1),\ t > 0 \\ \text{where } f(u) &= g(u) = \frac{u^2}{2} \\ u(x,y,0) &= \frac{1}{4} + \frac{1}{2}\sin \pi(x+y) \\ u(1,y) &= u(-1,y) \\ u(x,1) &= u(x,-1) \end{aligned} \tag{7.30}$$

The solution to (7.30) is smooth until the time $t = 0.45$ when two shocks form diagonally to the domain boundaries. The exact solution at $t = 0.1$ and $t = 0.45$ are shown in Figure 7.1 where a 40×40 mesh is used to generate the contours and 100 points are used to generate the distributions along the domain diagonal. The exact solution for $t > 0$ is computed using the method of characteristics.

The time accurate solutions presented in this chapter were obtained using the Godunov numerical flux function [23]

$$h_{K,e}(u_1,u_2) = \begin{cases} \min_{u\in[u_1,u_2]} q(u)\cdot \mathbf{n}_{K,e} & \text{for } u_1 < u_2 \\ \max_{u\in[u_2,u_1]} q(u)\cdot \mathbf{n}_{K,e} & \text{for } u_1 > u_2 \end{cases} \tag{7.31}$$

and the Runge-Kutta time marching schemes defined in Table 7.1 using $p+1$ intermediate steps for elements with a polynomial approximation of degree p. To assess the accuracy of the method, the error in the approximate solution, $e = u - u_h^p$, is computed in the L^1 and the L^∞ norms. The L^1 norm is a global

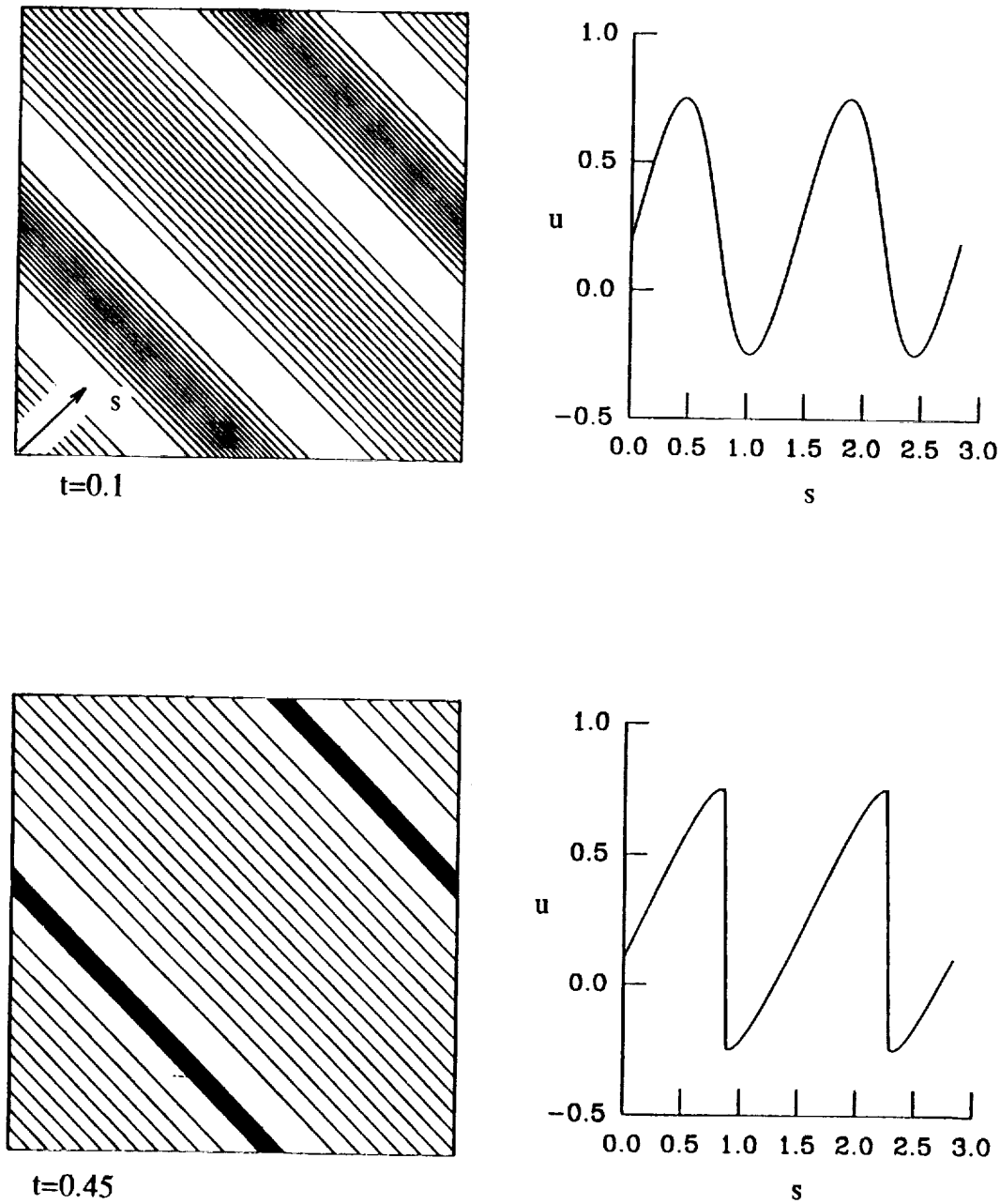

Figure 7.1: Evolution of the exact solution to (7.30).

measure of the error and is defined as

$$\begin{aligned} ||u - u_h^p||_{L_1(\Omega)} &= \int_\Omega |u - u_h^p| \; dx \; dy \\ &= \sum_{K \in \mathcal{P}_h} \int_K |u - u_h^p| \; dx \; dy \end{aligned} \tag{7.32}$$

The element integrals in (7.32) are evaluated using numerical quadrature with nine integration points in each local coordinate direction to accurately compute the error near discontinuities. The L^∞ norm is a local measure of the error and is defined as

$$\begin{aligned} ||u - u_h^p||_{L^\infty(\Omega)} &= \max_{(x,y)\in\Omega} |u - u_h^p| \\ &= \max_{K \in \mathcal{P}_h} \left[\max_{(x,y)\in K} |u - u_h^p|_K| \right] \\ &\approx \max_{\substack{(x_i,y_j)\in K \\ i,j=1,\ldots,9}} |u(x_i, y_j) - u_h^p|_K(x_i, y_j)| \end{aligned} \tag{7.33}$$

where $(x_i, y_j), i, j = 1, \ldots, 9$ are the coordinates of the integration points in element K.

Numerical results are shown in the form of distributions of the solution along the domain diagonal. The actual discontinuous solution is displayed by subdividing each element into 10 smaller elements, evaluating the approximate solution at the vertices of the sub-elements, and assuming a linear distribution of the solution in each sub-element. Discontinuities in the solution at element interfaces appear as vertical lines connecting two circles in the distribution plots. These circles represent the solution values at the vertices of an element. Since the solution is periodic, only one period is shown in the distribution plots.

To assess the accuracy of the Runge-Kutta discontinuous Galerkin method without the local projection, results are presented at $t = 0.1$ when the solution to (7.30) is smooth. The solution obtained on an 8×8 mesh of uniform

$p-$elements ($p = 1, \cdots, 4$) is shown in Figure 7.2. Note that the approximate solution is discontinuous at element interfaces even though the exact solution is smooth. These discontinuites are small, $O(h^{(p+1)})$, and thus decrease as the mesh is refined or as p_K is increased.

The rate of convergence of the error in the L^1-norm for a sequence of uniform mesh refinements is shown graphically in Figure 7.3. Each line on the graph represents a sequence of meshes with a fixed element polynomial degree p. The slope of the lines on the log-log scale is nearly $p+1$ indicating that the error decreases at the rate of h^{p+1} as the mesh size h decreases. In other words, the method is $(p+1)$-order accurate.

A graph of the error as a function of the total number of unknowns in the solution, Figure 7.4, shows that the number of unknowns required to achieve a certain level of accuracy decreases by an order of magnitude for each increase in p. Figure 7.4 also shows that for a fixed problem size, more accurate solutions are obtained using higher-order elements.

As the solution evolves, the local projection is required to control oscillations in the solution. To demonstrate the effectiveness of the projection at controlling oscillations, the solution obtained at $t = 0.45$ on a uniform 8×8 and 40×40 element mesh with $p = 1$ and $p = 2$ is shown in Figure 7.5. The solutions obtained for $p = 3$ elements in indistinguishable from the $p = 2$ solution, and is therefore, not shown. In all cases, the projection is extremely effective at controlling oscillations at the shock.

The error in the solution in smooth regions, computed on a subdomain which excludes the shock, is summarized in Figure 7.6. Each line on the graph represents a sequence of meshes with uniform p-elements. Note that the slope

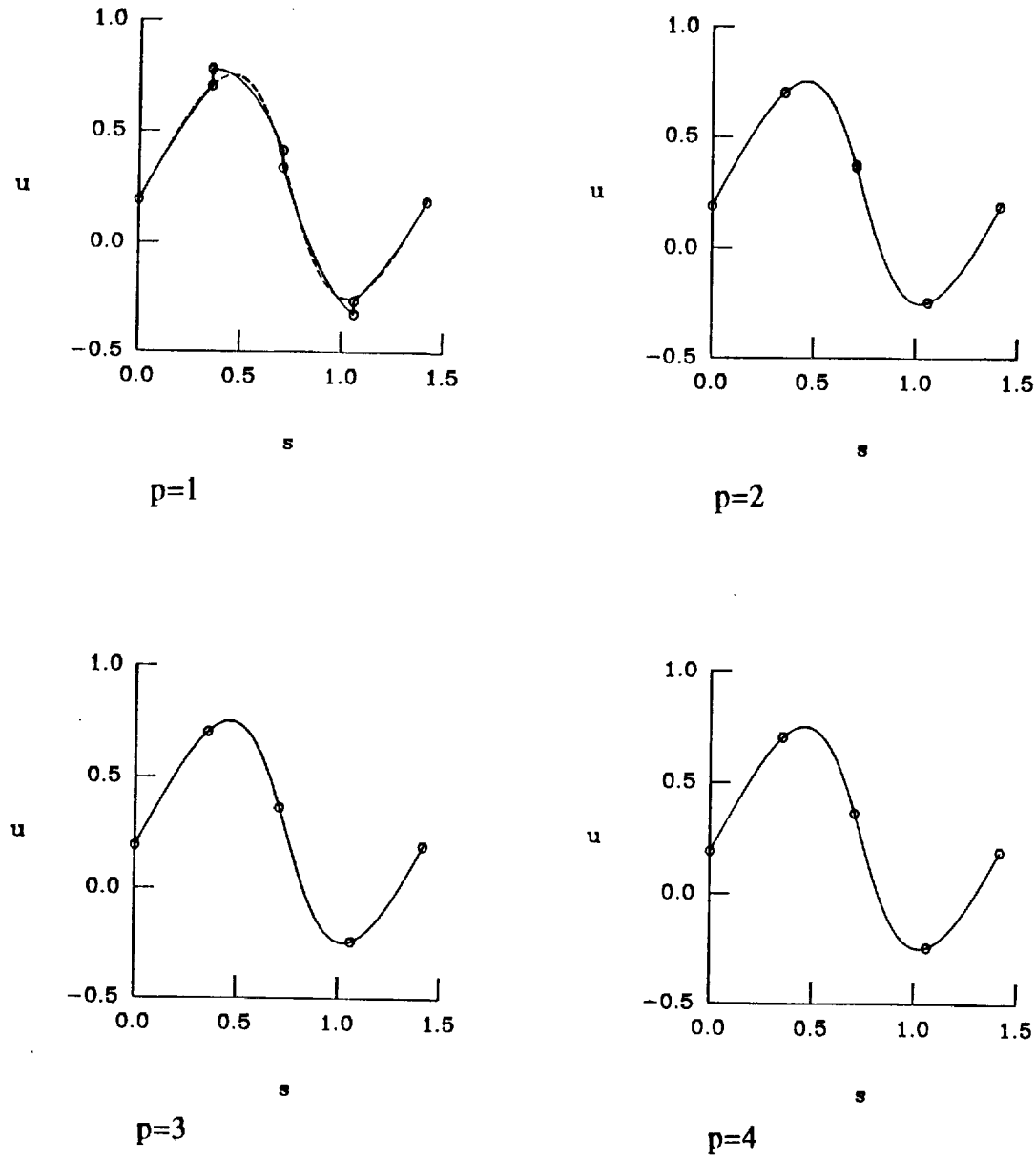

Figure 7.2: Discontinuous Galerkin solution to (7.30) at $t = 0.1$. Solutions obtained on an 8×8 mesh of uniform p-elements.

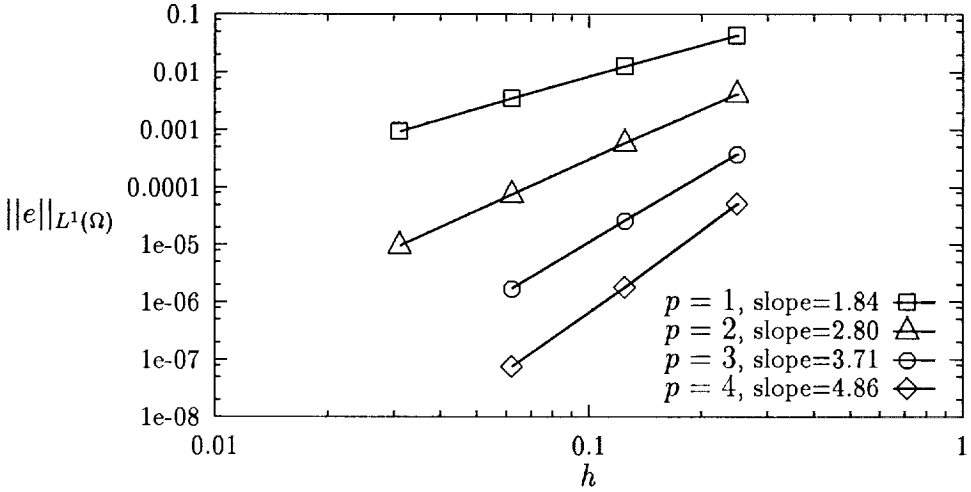

Figure 7.3: Rate of convergence of the error with h-refinements at $t = 0.1$.

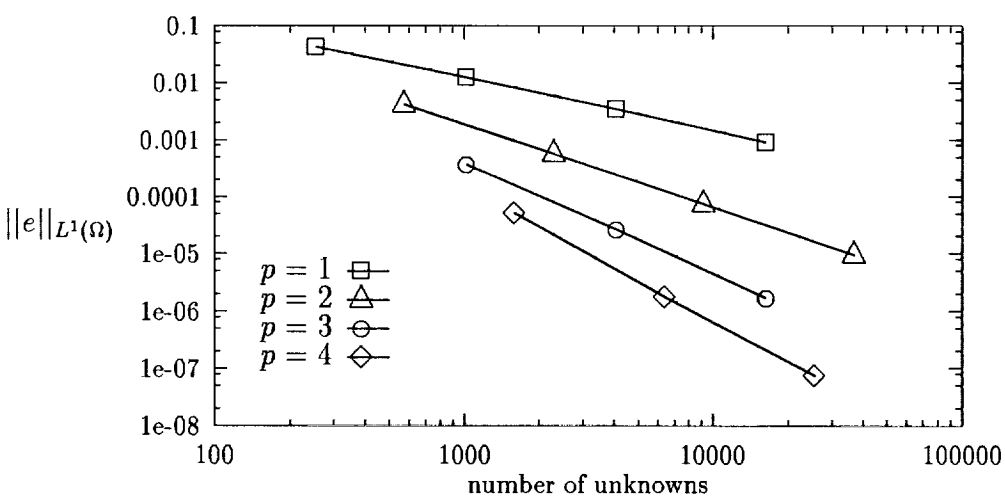

Figure 7.4: Rate of convergence of the error with the total number of unknowns at $t = 0.1$.

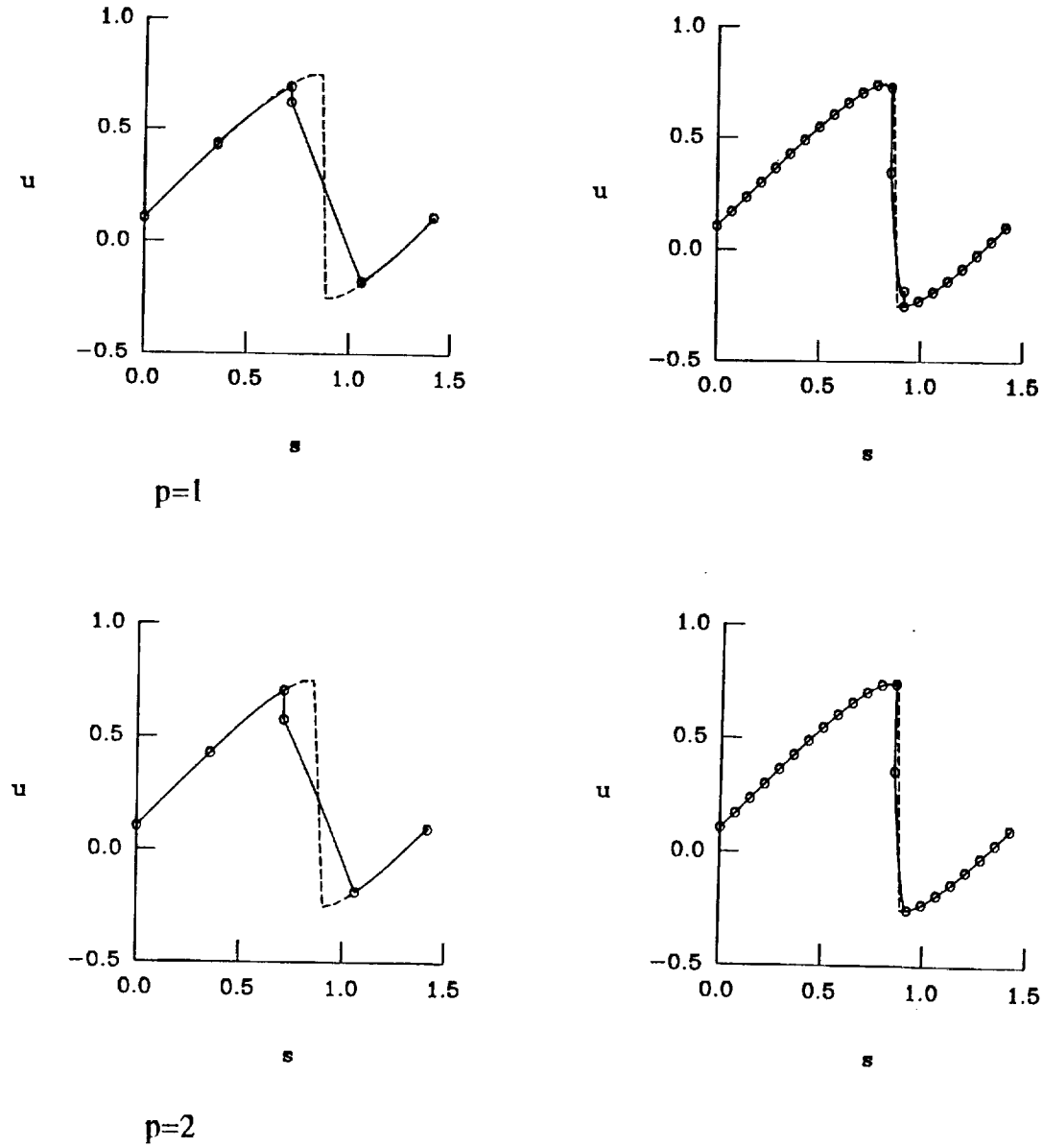

Figure 7.5: Discontinuous Galerkin solutions at $t = 0.45$.

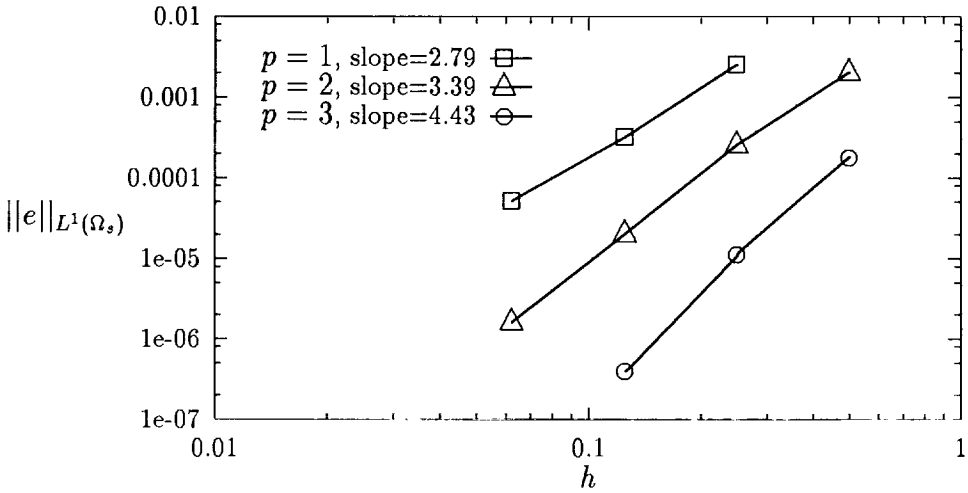

Figure 7.6: Rate of convergence of the error in smooth regions at $t = 0.45$. ($\Omega_s = [-0.2, 0.4] \times [-0.2, 0.4]$)

of the lines is $p + 1$ indicating that the order of accuracy of the method is preserved in smooth regions.

Chapter 8

Concluding Remarks

8.1 Summary

The development of a parallel *hp*-adaptive discontinuous Galerkin method for hyperbolic conservation laws is presented in this work. *A priori* error estimates are derived for a model class of linear hyperbolic conservation laws. These estimates are obtained using a new mesh-dependent norm that reflects the dependence of the approximate solution on the local element size and the local order of approximation. The results generalize and extend previous results on mesh-dependent norms to *hp*-version finite elements and to discontinuous Galerkin methods.

A posteriori error estimates which provide bounds on the actual error are developed in this work. The *a priori* and *a posteriori* estimates play an essential role in the development of an *hp*-adaptive strategy designed to deliver solutions to a specified error level in an efficient way. A generalization of the three-step *hp*-adaptive strategy is developed using the error estimates to provide for detection of discontinuities in the solution and local *h*-adaptivity when appropriate.

Numerical experiments verify the *a priori* estimates and demonstrate the effectiveness of the *a posteriori* estimates in providing reliable estimates of the

actual error in the numerical solution. The numerical examples also illustrate the ability of the hp-adaptive strategy to provide super-linear convergence rates with respect to the number of unknowns in the problem, even for discontinuous solutions.

A parallel implementation of the discontinuous Galerkin methods is presented which takes full advantage of the local character of the method and results in nearly optimal speedups on hp-meshes.

Extensions of the discontinuous Galerkin methods to nonlinear hyperbolic conservation laws are also presented. Numerical results illustrate the effectiveness of the method at delivering high-order accuracy in smooth regions. A local projection, designed to control nonlinear stability, is shown to eliminate oscillations and provide high resolution of discontinuities.

8.2 Conclusions and Future Work

The study reported in this dissertation represents a significant departure from conventional studies on the numerical solution of hyperbolic problems. The aim was to produce new schemes which deliver very high accuracies, were readily parallelizable, were based on rigorous mathematical foundations, and which were capable of delivering exponential rates of convergence. All of these goals were accomplished for a model class of linear hyperbolic conservation laws in two-dimensions, and encouraging results were obtained on extensions to model nonlinear problems.

Among the major conclusions drawn from this work are the following:

1. The machinery of elliptic approximation theory can be extended to hp-

finite element approximations of hyperbolic equations using the notion of discontinuous Galerkin methods; this is made possible by the introduction of special bilinear and linear forms which depend upon mesh parameters, the mesh size h_K of a cell K in the mesh and the spectral order p_K of the shape functions characterizing local approximations over the cell.

2. The use of the new mesh-dependent norms makes it possible to derive, for the first time, *a priori* error estimates for non-uniform *hp*-approximations of linear hyperbolic problems; these estimates are quasi-optimal, and the estimated rates of convergence are fully confirmed by numerous numerical experiments.

3. Exponential and/or super-linear rates of convergence are obtained, even for solutions with very low regularity; this justifies the use of *hp*-methods and demonstrates their superiority over conventional methods for a model class of problems.

4. Rigorous *a posteriori* error estimates are derived using a new version of the element residual method; these estimates provide computable measures of local (elementwise) error with remarkable accuracy and provide a reasonable basis for assessing solution quality and for adaptivity.

5. Equipped with both *a priori* and *a posteriori* estimates; an effective *hp*-adaptive strategy is developed which can be parallelized and generally gives a good *hp*-mesh in three or four steps; this work represents an extension and generalization of the three-step scheme for non-uniform *hp*-meshes; it exploits the unique feature of the *a priori* estimates for

hyperbolic problems, in particular, the loss of the rate of convergence in the vicinity of a discontinuity.

6. The adaptive scheme developed here is quite robust and effective for the example problems tested; results suggest that it is possible to specify target global error in an appropriate norm and to then reach that error quite accurately in three or four steps.

7. New versions of load-balancing schemes based on recursive bisection provide for a domain decomposition well-suited for *hp*-version disontinuous Galerkin methods; the schemes, which are in an early stage of development, still provide a reasonably balanced computation when implemented on a 16-processor Intel iPSC 860 computer. Near linear speedups were realized on a model problem.

8. Extensions of the methodologies to nonlinear problems appear to be possible; preliminary studies suggest that with a proper projection to control oscillations near discontinuities, very high accuracies can be obtained with *hp*-schemes using the discontinuous Galerkin method; while much work remains to be done in this area, the high convergence rates and accuracies observed in the numerical experiments on nonlinear problems suggest that further studies in this area may be very fruitful.

Bibliography

[1] Ainsworth, M. and Oden, J. T., "A Unified Approach to A Posteriori Error Estimation using Element Residual Methods," *Numerische Mathematik*, Vol. 65, pp. 23-50, 1993.

[2] Ainsworth, M. and Oden, J. T., "A Procedure for A Posteriori Error Estimation for h-p Finite Element Methods," *Computer Methods in Applied Mechanics and Engineering*, Vol. 101, pp.73-96, 1992.

[3] Babuška, I. and Suri, M., "The hp-Version of the Finite Element Method with Quasiuniform Meshes," *Mathematical Modeling and Numerical Analysis*, Vol. 21, pp. 199–238, 1987.

[4] Bank, R. E. and Weiser, A., "Some *A posteriori* Error Estimates for Elliptic Partial Differential Equations," *Mathematics of Computations*, Vol. 44, pp. 283-301, 1985.

[5] Barth, T. J. and Jespersen, D. C., "The Design and Application of Upwind Schemes on Unstructured Meshes,", AIAA Paper No. 89-0366, 1989.

[6] Bey, K. S. and Oden, J. T.,. "A Runge-Kutta Discontinuous Galerkin Method for High Speed Flows," In *Proceedings of the 10th AIAA Computational Fluid Dynamics Conference*, Honolulu, Hawaii, 1991.

[7] Biswas, R., Devine, K., and Flaherty, J., "Parallel, Adaptive Finite Element Methods for Conservation Laws," Department of Computer Science Technical Report No. 93-5, Rensselaer Polytechnic Institute, Troy, New York, February, 1993.

[8] Boris, J. P. and Book, D. L., " A Flux-Corrected Transport Algorithm that Works," *Journal of Computational Physics*, Vol. 11, pp. 38-69, 1970.

[9] Butcher, J. C., **The Numerical Analysis of Ordinary Differential Equations**, Jon Wiley and Sons, New York, 1987.

[10] Cai, W., Gottlieb, D., Harten, A., "Cell Averaging Chebyshev Methods for Hyperbolic Problems," Computers and Mathematics with Applications, Advances in Partial Differential Equations, Annual Issue, 1990.

[11] Ciarlet, P. G., **The Finite Element Method for Elliptic Problems**, North-Holland, 1978.

[12] Cockburn, B., Hou, S., and Shu, C. W., "The Runge-Kutta Local Projection Discontinuous Galerkin Method for Conservation Laws IV: The Multidimensional Case," *Mathematics of Computations*, Vol. 54, pp. 545–581, 1990.

[13] Cockburn, B. and Shu, C. W., "TVB Runge-Kutta Local Projection Discontinuous Galerkin Finite Element Methods for Conservation Laws II: General Framework," *Mathematics of Computations*, Vol. 52, pp. 411-435, 1989.

[14] Coquel, F. and LeFloch, F., "Convergence of Finite Difference Schemes for Conservation Laws in Several Space Dimensions: The Corrected An-

tidiffusive Flux Approach," *Mathematics of Computations*, Vol. 57, pp. 169-210, 1991.

[15] Crandall, M. and Majda, A., "Monotone Difference Approximations for Scalar Conservation Laws," *Mathematics of Computations*, Vol. 34, pp. 1-22, 1980.

[16] Demkowicz, L., Devloo, P., and Oden, J. T., "On an h-type Mesh Refinement Strategy based on Minimization of Interpolation Errors,", *Computer Methods in Applied Mechanics and Engineering*, Vol. 53, pp. 67-89, 1985.

[17] Enquist, B. and Oscher, S., "Stable and Entropy Satisfying Approximations for Transonic Flow Calculations," *Mathematics of Computations*, Vol. 34, pp. 45-75, 1980.

[18] Demkowicz, L., Oden, J.T., and Rachowicz, W., "An New Finite Element Method for Solving Compressible Navier-Stokes Equations Based on Operator Splitting and h-p Adaptivity,", *Computer Methods in Applied Mechanics and Engineering*, Vol. 84, pp. 275-326, 1990.

[19] Demkowicz, L., Oden, J. T., Rachowicz, W., and Hardy, O., "Toward a Universal h-p Adaptive Finite Element Strategy, Part 1. Constrained Approximation and Data Structure," *Computer Methods in Applied Mechanics and Engineering*, Vol. 77, pp. 79-112, 1989.

[20] DiPerna, R. J., "Measure-Valued Solutions to Conservation Laws," *Archive for Rational Mechanics and Analysis*, Vol. 88, pp. 221-270, 1985.

[21] Dorr, M. R., "The Approximation Theory for the p-Version of the Finite Element Method," *SIAM Journal of Numerical Analysis*, Vol. 21, pp. 1180–1207, 1984.

[22] Glimm, J., "Solutions in the Large for Nonlinear Hyperbolic Systems of Equations," *Communications on Pure and Applied Mathematics*, Vol. 18, pp. 697-715, 1965.

[23] Godunov, S. K., "A Finite Difference Method for the Numerical Computations of Discontinuous Solutions to the Equations of Fluid Dynamics," *Mathematik Sbornik*, Vol. 47, pp. 271-290, 1959.

[24] Goodman, J. B. and LeVeque, R. J., "On the Accuracy of Stable Schemes for 2D Conservation Laws," *Mathematics of Computations*, Vol. 45, pp. 15-21, 1985.

[25] Harten, A., "High Resolution Schemes for Hyperbolic Conservation Laws," *Journal of Computational Physics*, Vol. 49, pp. 357-393, 1983.

[26] Harten, A., Enquist, B., Osher, S., and Chakravarthy, S. R. , "Uniformly High Order Accurate Essentially non-Oscillatory Schemes, III," *Journal of Computational Physics*, Vol. 71, pp. 231-303, 1987.

[27] Hilbert, D., "Uber die Stetige Abbildung einer Linie auf ein Flachenstuck," *Math annalen*, Vol. 38, 1981.

[28] Jameson, A., Baker, T. J., and Weatherhill, N. P., "Calculation of Inviscid Transonic Flow Over a Complete Aircraft," AIAA Paper No. 84-0093, 22nd Aerospace Sciences Meeting, Reno, Nevada, 1984.

[29] Johnson, C., Navert, U., and Pitkaranta, J., "Finite Element Methods for Linear Hyperbolic Problems," *Computer Methods in Applied Mechanics and Engineering*, Vol. 45, pp. 285–312, 1984.

[30] Johnson, C. and Pitkaranta, J., "An Analysis of the Discontinuous Galerkin Method for a Scalar Hyperbolic Equation," *Mathematics of Computations*, Vol. 46, pp. 1–26, 1986.

[31] Johnson, C. and Szepessy, A., "On the Convergence of a Finite Element Method for a Nonlinear Hyperbolic Conservation Law," *Mathematics of Computations*, Vol. 49, pp. 427-444, 1987.

[32] Kružkov, S. N., "First-Order Quasilinear Equations in Several Independent Variables," Math. USSR Sbornik, Vol. 10, pp. 217-243, 1970.

[33] Lesaint, P. and Raviart, P.A., "On a Finite Element Method for Solving the Neutron Transport Equation," **Mathematical Aspects of Finite Elements in Partial Differential Equations**, Edited by C. de Boor, Academic Press, pp. 89–123, 1974.

[34] Löhner, R., Morgan, K., and Peraire, J., "A Simple Extension to Multidimensional Problems of the Artificial Viscosity Due to Lapidus," *Computers in Applied Numerical Methods*, Vol. 2, pp. 141-147, 1985.

[35] Löhner, R., Morgan, K., Peraire, J., and Vahdati, M., "Finite Element Flux-Corrected Transport for the Euler and Navier-Stokes Equations," *International Journal for Numerical Methods in Fluids*, Vol. 7, pp. 1093-1109, 1987.

[36] Löhner, R., Morgan, K., and Zienkiewicz, O. C., "Adaptive Grid Refinement for the Compressible Euler Equations," **Accuracy Estimates and Adaptive Refinements in Finite Element Computations**, Edited by I. Babuška, O. C. Zienkiewicz, J. Gago, and E. R. de A. Oliviera, John Wiley and Sons, Ltd., Chichester, pp. 281-297, 1986.

[37] Oden, J. T., Demkowicz, L., Rachowicz, W., and Westerman, T. A., "Toward a Universal *h-p* Adaptive Finite Element Strategy, Part 2: *A Posteriori* Error Estimation," *Computer Methods in Applied Mechanics and Engineering*, Vol. 77, pp. 113-180, 1989.

[38] Oden, J. T., Demkowicz, L., Strouboulis, T., and Devloo, P., "Adaptive Methods for Problems in Solid and Fluid Mechanics," **Accuracy Estimates and Adaptive Refinements in Finite Element Computations**, Edited by I. Babuška, O. C. Zienkiewicz, J. Gago, and E. R. de A. Oliviera, John Wiley and Sons, Ltd., Chichester, pp. 249-280, 1986.

[39] Oden, J. T., Patra, A., and Feng, Y. S., "An *hp* Adaptive Strategy", *Adaptive, Multilevel, and Hierarchical Computational Strategies*, A. K. Noor (ed.), AMD-Vol. 157, pp. 23-46, 1992.

[40] Patra, A. and Oden, J. T., "Problem Decomposition for Adaptive hp Finite Element Methods,", to appear.

[41] Patra, A., private communication.

[42] Peano, G., "Sur Une Courbe, que Remplit Toute une Aire Plane," *Math Annalen*, Vol. 36, pp. 157-160, 1980.

[43] Peraire, J., Vahdati, M., Morgan, K., and Zienkiewicz, O. C., "Adaptive Remeshing for Compressible Flow Computations," *Journal of Computational Physics*, Vol. 72, pp. 449-466, 1987.

[44] Peraire, J., Morgan, K., and Peiro, J., "Unstructured Finite Element Mesh Generation and Adaptive Procedures for Computational Fluid Dynamics," AGARD Conference Proceedings No. 464, pp. 18.1-18.12, 1990.

[45] Pothen, A., Simon, H., and Liou, K. P., "Partitioning Sparse Matrices with Eigenvectors of Graphs," *SIAM Journal of Matrix Analysis and Application*, Vol. 11, pp. 430-452, 1990.

[46] Roe, P. L., "Approximate Riemann SOlvers, Parameter Vectors, and Difference Schemes," *Journal of Computational Physics*, Vol. 43, pp.357-372, 1981.

[47] Sanders, R., "On the Convergence of Monotone Finite Difference Schemes with Variable Spatial Differencing," *Mathematics of Computations*, Vol. 40, pp.91-106, 1983.

[48] Shu, C. W., "TVD Time Discretizations," *SIAM Journal of Scientific and Statistical Computing*, Vol. 9, pp. 1073-1084, 1988.

[49] Tadmor, E., "Shock Capturing by the Spectral Vanishing Viscosity Method," ICASE Report No. 89-67, 1989.

[50] Vandeven, H., "Family of Spectral Filters for Discontinuous Problems," *Journal of Scientific Computing*, Vol. 6, pp. 159-192, 1991.

[51] Van Leer, B., "Towards the Ultimate Conservative Difference Schemes V: A Second Order Sequel to Godunov's Method," *Journal of Computational Physics*, Vol. 32, pp. 101-136, 1979.

[52] Vavasis, S. A., "Automatic Domain Partitioning in Three Dimensions," *SIAM Journal of Scientific and Statistical Computing*, Vol. 12, pp. 950-970, 1991.

Vita

Kim S. Bey, the daughter of Delas F. Strode and Glenda J. [redacted] was born in [redacted] on [redacted]. After graduating as valedictorian of the class of 1977 from Booker T. Washington High School in Norfolk, Virginia, she received a B.S. in Mechanical Engineering in 1982 from Old Dominion University in Norfolk. She began her career in the Aerothermal Loads Branch at the NASA Langley Research Center in Hampton, Virginia in 1982 and received an M.S. in Mechanical Engineering from Old Dominion University in 1986. Her work in the Aerothermal Loads Branch has focused on adaptive finite element methods for flow problems and she has authored several papers in that area. The desire for a more thorough understanding of the mathematical aspects of finite element methods led her to the University of Texas at Austin in 1987. On graduate study leave, she completed her course work in 1989 and returned to NASA to perform her research.

Permanent address: 2764 Console Avenue
Norfolk, Virginia 23518

This dissertation was typeset with LaTeX[‡] by the author.

[‡] LaTeX is a document preparation system developed by Leslie Lamport as a special version of Donald Knuth's TeX Program.